ABSTRACT

Title of Dissertation: **NMR STUDIES OF POLYUBIQUITIN CHAINS: INSIGHTS INTO STRUCTURAL BASIS OF FUNCTIONAL DIVERSITY**

Ranjani Varadan, Doctor of Philosophy, 2004

Dissertation Directed By: Prof. David Fushman
Department of Chemistry and Biochemistry

Signaling by polyubiquitin (polyUb) chains mediates numerous cellular processes. All these processes involve the covalent modification of the substrate protein with a polyubiquitin chain that is itself formed by isopeptide linkages between the C-terminus of one Ub and a specific Lys residue of the next Ub. Remarkably, the outcome of the signaling event depends on the specific Lys residue that is involved in the formation of the polyUb signal. In the current model of Ub-mediated signaling, diversity in signaling arises from the ability of differently linked polyUb chains to act as functionally distinct signals. Such a model predicts that the distinct structures adopted by alternatively linked polyUb chains modulate their recognition by various effector proteins. However, direct structural evidence in support of this view has been lacking. This work is aimed at elucidating structural differences (if any) between Lys^{48}- and Lys^{63}-linked polyUb chains, and to investigate the structural basis of the specific recognition of Lys^{48}-linked polyUb chains by UBA domains.

Using a combination of NMR methods, Lys^{48}-linked Ub_2 chains are shown to adopt a 'closed' conformation in solution under physiological conditions. A switch in the conformation of these chains, from 'closed' to 'open' states with decreasing pH is

described. The Ub_2 interface in the 'closed' conformation is shown to be dynamic, allowing functionally important hydrophobic residues sequestered at the interface to be accessible to Ub-recognition factors. In contrast, Lys^{63}-linked Ub_2 chains are shown to be characterized by an extended conformation, with no definitive interface between the Ub units. Such an extended conformation allows each Ub moiety to independently bind a UBA molecule, in a manner similar to the monoUb-UBA interaction. The results presented in this study suggest that the specific recognition of Lys^{48}-linked Ub_2, however, may not involve such a simple 'one-UBA-per-Ub' interaction. The interaction of UBA with Lys^{48}-linked Ub_2 appears to involve the primary association of the UBA domain with the proximal Ub in Ub_2. The relative positioning of the distal Ub in the chain allows its simultaneous association with the same UBA domain, leading to a higher affinity UBA-Ub_2 interaction. The results provide the first experimental evidence that alternately linked polyUb chains adopt distinct conformations, and suggest that specific recognition of these chains might indeed depend on differences in their structures.

NMR STUDIES OF POLYUBIQUITIN CHAINS: INSIGHTS INTO STRUCTURAL BASIS OF FUNCTIONAL DIVERSITY

By

Ranjani Varadan

Dissertation submitted to the Faculty of the Graduate School of the
University of Maryland, College Park, in partial fulfillment
of the requirements for the degree of
Doctor of Philosophy
2004

Advisory Committee:
Professor George Lorimer, Chair
Professor David Fushman (Advisor)
Professor Dorothy Beckett
Professor Jin Hu
Professor Neil Blough

Acknowledgements

It is to my advisor, Prof. David Fushman, that I owe my deepest appreciation for his guidance and encouragement throughout the duration of this work. My first introduction to NMR came from him, and I thank him for all the countless hours of patient teaching and insightful discussions.

Special thanks to Prof. Cecile Pickart, for helping set up synthesis of polyUb chains, and for plasmids for all the Ub constructs and enzymes used in this study. I thank her for her support and many stimulating discussions. Thanks also to Shahri Raasi for participating in the collaboration with Prof.Pickart's laboratory and in helpful discussions and support.

My thanks to all past and present members of the Fushman lab, for making the lab a very pleasant workplace, and especially to Dr. Olivier Walker and Dr. Michael Assfalg for their contributions to this work. Thanks also to Dr. Mariapina D'Onofrio and Aydin Haririnia for help with protein purifications.

Thanks to Prof. Fenselau for the use of the MALDI and ESI mass spectrometers, to Prof. Beckett for allowing me to explore analytical ultracentrifugation and ITC, and to Prof. Lorimer for the use of the HPLC and the preparative centrifuge.

I also wish to thank Dr. Yetrib Hathout and Patrick Brown for help with the use of the mass spectrometer and the calorimeter.

I thank faculty members and my fellow graduate students in the Department of Biochemistry for a memorable graduate experience through all my classes. Thanks

also to members on the dissertation committee, for their comments and helpful advice.

Finally, I also extend my appreciation to all my friends and to Kuldeep for constant cheer and all the help. My deepest thanks also to my family, especially to my mother for her endurance and support from across the miles.

Table of Contents

List of Figures

List of Tables

Chapter 1: Introduction and Specific Aims

Protein modifications via phosphorylation, acetylation, methylation and glycosylation are well recognized as biologically significant signals for mediating cellular response to external factors. However, biochemical research over the last two decades has revealed that in many signaling events, a myriad of proteins are also modified by Ubiquitin (Ub), itself a 76 amino acid protein highly conserved among all eukaryotes[1]. All Ub-mediated cellular events involve the covalent linkage of the C-terminal Gly (Gly76) of Ub to the ε-amine of a specific Lysine residue on the surface of the substrate protein. Because Ub itself possesses 7 surface Lys residues, it can undergo iterative ubiquitination to result in the formation of polyubiquitin chains (polyUb) of varying length and Lys linkages. Very remarkably, conjugation of substrates to polyUb chains of different length and linkages leads to distinct cellular outcomes[2]. Although first shown to target cellular proteins for selective degradation, ubiquitin conjugation now rivals the canonical protein modifications such as phosphorylation in the diversity of cellular events it regulates.

1.1 The Ubiquitination Cycle

The covalent attachment of Ubiquitin to the substrate protein is an obligatory step in all Ub-mediated events. The process of Ub conjugation (ubiquitination) occurs via tightly regulated enzymatic steps catalyzed by a series of Ub activating (E1), conjugating (E2) and ligase (E3) enzymes. [1, 3, 4] (figure 1.1). In the first step, the C-terminus of Ub is activated by adenylation and subsequent thioester formation with a Cys residue on E1. Activated Ub is then transferred to an active site Cys residue of a Ub-carrier protein, E2. In the last step, Ub is transferred to the substrate protein by a

substrate-specific E3. Different E3s may use either of two different mechanisms to transfer Ub to the substrate protein: (1) HECT domain E3s (*H*omologous to *E*6AP *C*-*t*erminus) bind E2s via the conserved HECT domain and Ub is transferred from the active site of E2 to the active site Cys of the E3. A different region of the same E3 binds the substrate protein, and the Ub is transferred to the substrate in a transthioesterification reaction. (2) RING-domain E3s (*R*eally *I*nteresting *N*ew *G*ene) do not form thiol esters with Ub. Since they bind both the E2 (via the RING domain) and the protein substrate, Ub is directly transferred from E2 to the substrate. The ubiquitinated proteins are in a dynamic state, and may be subject to further rounds of ubiquitination or Ub removal by deubiquitinating enzymes.

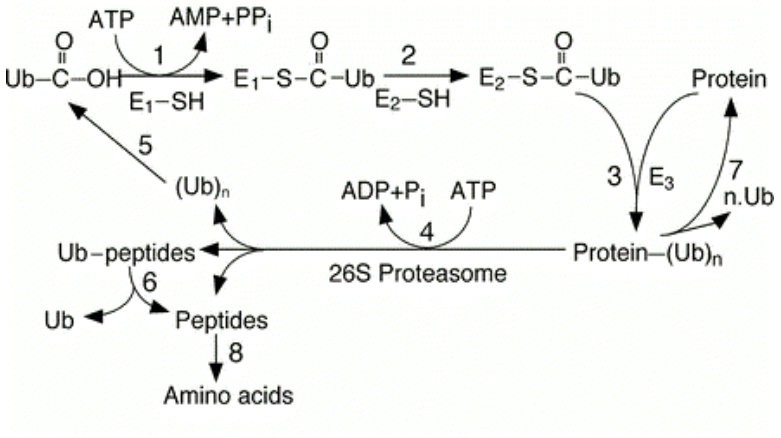

Figure 1.1 The ubiquitination cycle Ubiquitination of substrate proteins occurs in a series of transthioesterification reactions 1-3. Substrates modified with Lys^{48}-linked polyUb chains are targeted to the proteasome and degraded, and the Ub units in the polyUb chain are recycled (steps 4-8). Figure from [1].

Recent mass spectrometric analysis of ubiquitin conjugates in *S. cerevisiae* revealed that substrates were most frequently polyubiquitinated with Lys^{48}-linked polyUb chains[5]. PolyUb chains linked via other Lys were found in a relative abundance of Lys^{48}>Lys^{63}>Lys^{11}>>Lys^{33}, Lys^{27} and Lys^{6}. In addition, substrates

conjugated with Ub on multiple sites were also detected, with members of the same protein family showing identical sites of ubiquitination. Thus, substrate proteins in the cell may be conjugated to polyUb chains of varying lengths and linkages: the diversity in Ub-mediated signaling arises from the ability of differently linked chains to function as distinct signals in the cell.

1.2 Cellular outcomes of ubiquitination

1.2.1 Proteolytic roles of Ub

In their most well characterized form, polyUb chains linked via Lys48 target the substrate protein to degradation by the 26S proteasome, a large multicatalytic proteinase complex. The eukaryotic 26S proteasome is a 2.5 MDa complex comprising a 20S proteasome complex and two 19S regulatory complexes (reviewed in [5]). The 20S complex is a cylindrical stack of four 7-membered rings, two distal α-rings that control the passage of substrates and degradation products into and out of the proteasome and two central β-rings that each harbor 3 catalytic sites. The ends of the 26S proteasome are capped by the 19S complex, a 900 kDa complex that comprises of at least 17 different subunits that form 2 major subcomplexes- a base with 6 ATPases and 2 non ATPases that is placed adjacent to the α-rings of the 20S particle, and a lid subcomplex that sits above the base subcomplex. Deubiquitinating enzymes and Ub-ligases have been shown to be part of the 19S lid subcomplex, suggesting that a dynamic equilibrium between ubiquitination and deubiquitination of substrates on the proteasome helps regulate the turnover rates of various substrates degraded by the Ub-proteasome pathway. The 19S particle specifically recognizes

substrates that are tagged by Lys^{48}-linked polyUb chains comprising four or more Ubs. The Rpn10 (regulatory particle non ATPase 10 in the lid subcomplex in yeast /S5a in mammals) has been implicated in polyUb chain recognition by the proteasome, however, it is unlikely to be the sole Ub recognition factor in the proteasome[6]. Certain proteins of the UBL-UBA family (with Ubiquitin-like and Ubiquitin-associated domains) that simultaneously bind both the Rpn10/S5a subunit and polyUb chains have been proposed to function as adaptor proteins that deliver ubiquitinated substrates to the proteasome [7, 8]. There are also some instances of direct binding of the proteasome to the substrate that have been reported; however, it is still unclear if the targeting is ubiquitin-independent [9]. In the current model of protein degradation by the 26S proteasome, substrate degradation proceeds via its processive unfolding starting at unstructured regions by one or more ATPase subunits in the base subcomplex. The unfolded region is threaded through a pore in the base subcomplex and translocated by ATP hydrolysis to the proteolytic chamber in the 20S particle where it is degraded to short peptides. Deubiquitinating enzymes in the lid subcomplex release the polyUb chain from the substrate that is subsequently disassembled by non-proteasomal deubiquitinating enzymes such that the free Ubs are re-used in the cell. Thus, the ubiquitin-proteasome machinery negatively regulates intracellular levels of many proteins in the cell and thereby is important in cellular processes such as cell cycle progression, transcription, DNA repair, apoptosis and antigen processing.

C*ell-Cycle Regulation* Ubiquitin-mediated degradation of positive and negative regulators of the cell cycle, such as cyclins, inhibitors of cyclin-dependent

kinases (Ckis) and anaphase inhibitors is important for several cell cycle transitions [1]. Progress through the eukaryotic cell cycle is driven by oscillations in the activities of cyclin-dependent kinases (Cdks). Cdk activity is controlled by periodic synthesis and degradation of positive and negative regulatory subunits (cyclins and Ckis respectively) and by reversible phosphorylation. Different cyclins, specific for the G1, S or M phases of the cell cycle accumulate and activate Cdks at appropriate times during the cell cycle and are then targeted to degradation by E3 ligases. Although the mechanisms of targeting of all regulators is not known, two major types of E3 ligase complexes that ubiquitylate cell cycle regulators have been identified. The anaphase-promoting complex or the cyclosome (APC/C) ligase complex targets mitotic cyclins containing a 'destruction box' motif (R (A/T) (A) L (G) x (I/V) (G/T) (N)) to the proteasome. Other cell cycle regulators that lack the 'destruction box' are phosphorylated and subsequently ubiquitinated by E3s belonging to another family of SCF (Skp-Cullin-Fbox protein) ubiquitin ligases.

Endoplasmic Reticulum Associated Degradation (ERAD) (reviewed in [10]). The endoplasmic reticulum is the site of folding and modification of nascent polypeptide chains and assembly of multi-subunit protein complexes. As part of the "ER quality control" aberrant or mutated proteins that fail to fold or oligomerize are selected for degradation by their association with chaperones in the ER. The substrate proteins are ubiquitylated with a Lys^{48}-linked polyUb chain, and retro-translocated back into the cytosol through the translocation channels by the action of ATPases of the 19S complex of the proteasome. In addition, normal proteins such as HMG-CoA reductase that reside in the ER are also degraded via this pathway in response to

levels of metabolites of sterol synthesis. As is apparent from its importance in maintaining protein quality control, defects in the ERAD pathway have been associated with various diseased states such as cystic fibrosis, heart diseases and Parkinson's disease.

Transcriptional Control (reviewed in [11]) The Ub-proteasome system regulates transcription at multiple levels, in both degradative and non-degradative ways. Despite the seemingly disparate nature of transcription and proteasomal degradation, recent studies have revealed that the two processes are mechanistically connected. Ubiquitin (and ubiquitin family members such as SUMO: small Ub like modifier) controls transcription by regulating the nuclear localization and levels of transcriptional activators such as NF-κB and p53. Ubiquitination also influences the activity of transcriptional activators by regulating their association with co-activators. Some instances of transcriptional activators requiring ubiquitination have been reported in yeast, suggesting that ubiquitination regulates the amount of time an activator is available before it is destroyed by the proteasome. ATPase components of the 19S complex of the proteasome have also been found to act as transcriptional activators, and at least five of the 19S subunits have been found to be recruited to transcriptionally active genes in yeast. However, it still remains unclear if the entire 19S complex is recruited to an active gene and what its possible roles might be. It has been suggested that the ATPase activity of the 19S complex might play a role in chromatin remodeling or converting RNA pol II to an elongation-competent form. Interestingly, ubiquitination of RNA pol II itself is important in repair of DNA lesions (see also below).

1.2.2 Non-proteolytic roles of Ub

The canonical role of Ub involves the degradation of proteins by the proteasome. The Ub-proteasome pathway is associated with a variety of different cellular events as discussed above. Recently however, several new non-proteolytic roles of Ub have been reported. These non-canonical roles of Ub involve modification of the substrate by a single Ub or Lys^{63}-linked polyUb chains suggesting that the nature of the polyUb chain dictates the fate of the substrate protein.

Protein trafficking (reviewed in [12]) Ub participates in the membrane protein trafficking system by targeting proteins from the plasma membrane and the trans-Golgi network to the endosomal compartments. It is also involved in sorting proteins to multivesicular bodies and the lysosomal/vacuolar compartments. Several plasma membrane proteins such as the G-protein coupled receptors and the epidermal growth factor receptor require ubqiuitination for internalization. In some cases, such as the internalization of the growth hormone receptor, the associated endocytotic machinery but not the receptor itself requires ubiquitination. The role of Ub in the endocytic pathway is not completely understood, however, it has been suggested that the ubiquitinated cargo proteins recruit other ubiquitin-binding proteins such as epsins via their UIM (Ub-interacting motif) and UBA (Ub-associated) domains. These Ub-binding proteins could subsequently associate with other components of the endocytic pathway such as clathrins leading to the formation of multi-protein complexes that are required for efficient internalization of the membrane receptors.

Histone modification (reviewed in [13]) Although the first eukaryotic protein found to be ubiquitylated was histone2A (H2A), other core histone and linker

histones have been found to be modified by monoUb. The recent finding that H2B is the only ubiquitinated histone in yeast has made genetic studies on histone ubiquitination more tractable. The H2B C-terminus that protrudes from the nucloesome core and is accessible for interactions with DNA and regulatory factors has been found to be monoubiquitinated. The ubiquitination of H2B regulates selective methylation of H3 that defines transcriptionally active domains of euchromatin. It is still to be seen what factors affect the histone modification and how H2B ubiquitination regulates H3 methylation.

DNA repair (reviewed in [14]) Most DNA lesions are removed by base excision repair and nucleotide excision repair mechanisms prior to DNA replication. If however, these pathways do not remove the lesion before the S phase, replication forks accumulate at the sites of DNA damage and initiate post-replicative DNA repair. Post-replicative repair can occur via either 'error free bypass' that proceeds by template switching involving the sister chromatid, or by 'translesion synthesis' ('error prone repair') that involves recruitment of specialized DNA polymerases that read through the DNA lesion. RAD6 is an E3-ubiquitin ligase that has been implicated in the regulation of post-replicative DNA repair by ubiquitination of the proliferating cell nuclear antigen (PCNA, a processivity factor for DNA polymerases) in response to DNA damage. Recent studies have shown that while ubiquitination of PCNA by Lys^{63}-linked polyUb initiates 'error-free' repair, monoubiquitination of PCNA targets the replication fork to 'error-prone' mode of DNA repair.

Possible role in protein stabilization A recent study showed that Lys^{6}-linked polyUb chains are recognized by the proteasome, but processed differently from the

canonical Lys^{48}-linked chains [15]. It was shown that the ovarian tumor suppressor, BRCA1, in complex with its partner BARD1, has E3-like activity and assembles Lys^{6}-linked polyUb chains. Lys^{6}-linked autoubiquitinated BRCA1 was shown to be de-ubiquitinated, but not degraded in vitro suggesting that these chains might be distinctly edited by the proteasome. However, *bona fide* substrates for Lys^{6}-polyubiquitination will have to be identified to determine if Lys^{6}-linked polyUb chains will signal for their stabilization, rather than degradation.

1.3 Molecular recognition of (poly)ubiquitin

The variety of cellular events that involve Ub-mediated regulation suggests the existence of several proteins in the cell that interact with polyUb chains. Indeed, a number of different ubiquitin interacting proteins that possess both an ubiquitin binding domain and a variable effector domain have been found. The various ubiquitin binding motifs include the UBA (ubiquitin associated), UIM (ubiquitin interacting motif), CUE (coupling of ubiquitin conjugation to endoplasmic reticulum degradation) or NZF (Np14 Zinc finger) domains, PLIC (protein linking integrin associated protein to cytoskeleton) and UEV (ubiquitin E2 variant) domains.

The UBA domain (~40 residues) was originally identified by sequence analysis as a domain present in enzymes of the Ub-proteasomal pathway and has been subsequently found in several other proteins involved in Ub-mediated signaling pathways [16]. At least 15 proteins in fission yeast have been found to contain putative UBA domains [17]. Biochemical studies by immunoprecipitation and surface plasmon resonance have shown that several of these UBA containing proteins bind polyUb chains (K_d ~ 30nM), and some bind monoUb, supporting their discovery as

potential Ub binding domains. Some UBA containing proteins have been found to dimerize via the UBA domain [18]. The solution structures of UBA domains from hHR23a (human homolog A of yeast protein Rad23 involved in DNA repair) reveals that the UBA domain is a compact 3-helix bundle with an exposed hydrophobic surface [19]. NMR and modeling studies have shown that the UBA-monoUb interaction is predominantly hydrophobic and occurs via the exposed hydrophobic surface on UBA [20](a more detailed structural description of the UBA-Ub interaction is presented in the following chapter). However, the mode of interaction of UBA domains with polyUb chains still remains to be elucidated. The molecular basis of how UBA domains recognize and differentiate between monoUb and polyUb and between various polyUb chains still needs to be elucidated.

The UIM is an ubiquitin-binding motif of ~20 amino acids that form a single helix. It was first identified in the proteasomal subunit S5a and a recent homology search revealed the presence of UIM domains, often in tandem repeats, in many proteins involved in ubiquitination and endocytosis. Although the S5a UIM (UIM-2) preferentially binds polyUb, UIMs found in many endocytic proteins have been proposed to bind monoUb. ([16, 21-23]

The latest addition to the family of ubiquitin binding motifs is the CUE domain, another helical domain ~40 amino acids in length. CUE domains have so far been identified in about 50 different proteins that are involved in protein degradation at the endoplasmic reticulum and endocytosis of receptors at the cell surface [24]. Studies on the CUE domain from Vps9p, a protein that regulates endocytosis of monoubiquitinated mating receptors in yeast, have shown that the domain is a domain

swapped dimer similar to the UBA domain [25]. The crystal structure of CUE-monoUb complex shows the CUE dimer binds one ubiquitin molecule. However, the NMR structure of a complex of monoUb with a CUE domain from the yeast protein Cue2 shows that CUE2-1 domain binds Ub in a 1:1 complex without any domain swapping mechanism [26]. It still remains to be seen how other CUE domains bind Ub and how these domains interact with polyUb chains.

1.4 Scope of present work

The above discussion provides an overview of the ubiquitin system: the diverse processes (poly)ubiquitin regulates and the ubiquitin-binding proteins that tie the (poly)ubiquitin signal to various downstream events in these cellular pathways. While the focus of many biochemical research groups has been to identify novel pathways regulated by Ub-mediated signaling and to discover novel ubiquitin binding proteins, many fundamental issues pertaining to the diversity of Ub-mediated signaling remain unresolved. For example, it is known that conjugation of differently linked polyUb chains commits the substrate to distinct fates in the cell - while Lys^{48}-linked polyUb chains target substrate proteins to proteasomal degradation, Lys^{63}-linked polyUb chains are involved in post-replicative DNA repair and monoubiquitination regulates other processes such as endocytosis and gene expression. However, it is still not known what properties of different polyUb chains are responsible for their ability to function as distinct signals in the cell. Because the only chemical difference between the various polyUb is in the specific Lys residue involved in the extension of the chains, it is possible that different linkages bestow unique conformational features to different polyUb chains. Different chains would

then be able to function as distinct signals if the difference in conformations/quaternary structures modulates their interaction with various cellular proteins. In an alternative model, direct recognition of the specific isopeptide bond could be responsible for the ability of differently linked chains to represent distinct signals[4]. However, direct structural evidence that would establish differences in conformations, if any, between alternatively linked chains, remains lacking. In addition, structural information elucidating how different ubiquitin-binding proteins bind monoUb is only just emerging. It still remains to be seen how different polyUb chains recognize the various ubiquitin-binding motifs, and how a difference in the chain linkage might modulate these interactions.

1.4.1 Specific Aims

This work is aimed at exploring the structural basis of the functional diversity of differently linked polyUb chains. The structural properties of the biochemically characterized Lys^{48}- and Lys^{63}-linked polyUb chains, are investigated. The molecular basis of the linkage-specific recognition of these chains was investigated using the UBA(2) domain of hHR23a. Because biochemical studies (pull down assays and surface plasmon resonance) have shown that this UBA(2) domain recognizes Lys^{48}-linked polyUb preferentially over Lys^{63}-linked chains [27], it potentially serves as a suitable polyUb-binding protein for these studies. Specifically, the present work addresses the following questions:

(i) What is the physiological conformation of Lys^{48}-linked Ub_2 and Ub_4 chains?

(ii) What is the physiological conformation of Lys^{63}-linked Ub_2 chains? How is it different from Lys^{48}-linked Ub_2?

(iii) What is the mode of interaction of the UBA(2) domain with both Lys^{48}- and Lys^{63}-linked Ub_2 chains? How does a difference in linkage in Ub_2 modulate this interaction?

Chapter 2: Review of structures of polyUb and Ub complexes

2.1 Crystal structures of Lys^{48}-linked polyUb

Ubiquitin is a compact globular protein characterized by a five-stranded β-sheet, an α-helix and an unstructured C-terminal tail comprising the last four residues 73-76. Perhaps the most important structural feature of ubiquitin is an extended hydrophobic surface flanked by basic residues on the β-sheet (figure 2.1). Alanine mutational screening studies have shown that residues on this hydrophobic surface and the C-terminal tail of ubiquitin are essential for cell viability in yeast [28]. The hydrophobic patch comprises residues Leu^{8}, Ile^{44} and Val^{70}, which are essential in the context of polyUb chains for proteasomal recognition. In addition, a small pocket formed by Phe^{4} has been implicated to be important in endocytosis [29].

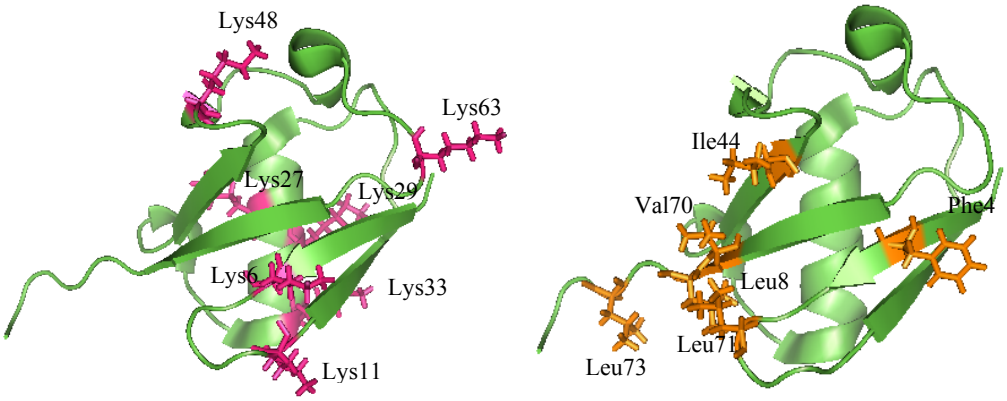

Figure 2.1 Structure of monoUb Ribbon representation of ubiquitin showing (a) surface lysine residues in magenta and (b) surface hydrophobic residues in orange (coordinates from 1D3Z.pdb)

The present repertoire of polyubiquitin chain structures includes the crystal structures of Lys^{48}-linked Ub_2 and Ub_4. Recently, structures of monoUb bound to various Ub- binding domains have also been solved. A brief summary of these structures highlighting important features is presented in the following sections.

2.1.1 Crystal structure of Lys^{48}-linked Ub_2

The crystal structure of Lys^{48}-linked Ub_2 [29] (figure 2.2) is an approximately 2 fold symmetric structure with the Ub_2 interface formed by the hydrophobic surface of each Ub. The structure shows the side chains of the functionally important Leu^8, Ile^{44} and Val^{70} to be buried at the interface, and hence not accessible for direct interactions with recognition factors in the cell. A subsequent NMR study that investigated the solvent accessibility of the hydrophobic residues at the Ub_2 interface showed that their side chains were solvent exposed just as in monoUb. If the crystal conformation was preserved in solution, the side chains of Leu^8, Ile^{44} and Val^{70} should have been solvent protected. Therefore, it was concluded that the crystal conformer did not predominate in solution [30].

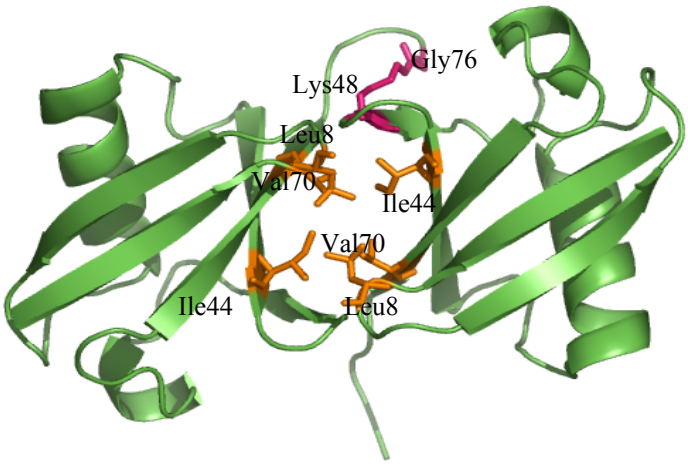

Figure 2.2 Crystal structure of Lys^{48}-linked Ub_2 Functionally important hydrophobic residues sequestered at the interface are shown in orange, and the Gly^{76}-Lys^{48} linkage is shown in magenta. (coordinates from 1AAR.pdb)

2.1.2 Crystal structures of Lys^{48}-linked Ub_4

The symmetry of the Ub_2 crystal structure predicted that the third Ub might not be able to utilize the same interactions in the extension of the chain. It was therefore not clear if and how the Ub_2 conformation would propagate through longer Ub chains.

The first crystal structure of Ub_4 ([31], figure 2.3(a)) showed that the chain is a compact molecule with both translational and 2-fold rotational symmetry. The 2-fold symmetry in each pair of Ub units is different from the 2-fold symmetry observed in the Ub_2 crystals. The hydrophobic surfaces on the Ub molecules that were buried at the Ub_2 interface are exposed just as in monoUb.

A later attempt to co-crystallize Ub_4 with a peptide derived from the ubiquitin-interacting motif (UIM) of the proteasomal subunit S5a resulted in crystals that excluded the peptide and were composed entirely of Ub_4 [32]. The crystals revealed Ub_4 in 2 possible conformations, both of which were different from the previously solved Ub_4 structure. In the first conformation, the Ub_4 molecule is extended, with no inter-Ub non-covalent contacts in the chain. Close packing of antiparallel pairs of Ub_4 chains in the crystal buries the hydrophobic surfaces on the Ub molecules. In the second conformation, the Ub_4 adopts a closed circular conformation that buries the same hydrophobic surfaces (figure 2.3b). It seemed therefore, that the non-covalent inter-Ub interactions were relatively weak, and crystal conformations were perhaps defined by stronger lattice interactions. The study put forth the important conclusion that the Lys^{48}-linked polyUb chains were inherently flexible, and hence a wide range of other inter-Ub orientations could also be accessible in solution.

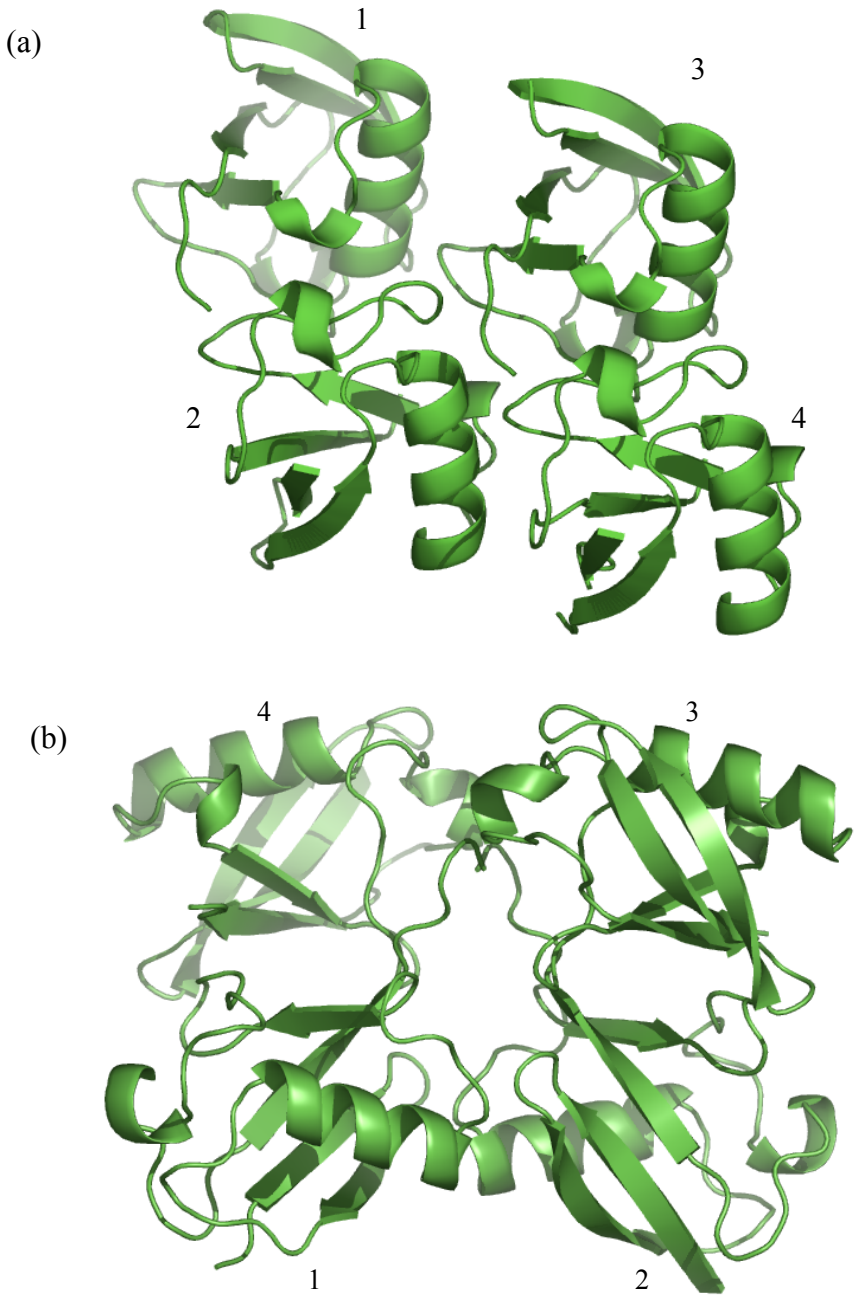

Figure 2.3 Crystal structures of Lys^{48}-linked Ub$_4$ showing different relative orientations of Ub units labeled 1 through 4, starting from the proximal Ub. Coordinates from (a) 1TBE.pdb and (b) 1F9J.pdb

2.2 Ubiquitin complexes with Ub binding proteins

2.2.1 Ub-CUE complexes

CUE domains are compact 3-helix bundles found in ubiquitin-binding proteins at the plasma membrane. The NMR structure of the N-terminal CUE domain of the yeast protein Cue2 complex with monoUb shows that the CUE 2-1 domain binds Ub through hydrophobic side chains on helices 1 and 3, as in the UBA-Ub complex [26](figure 2.4(a)). The binding surface on Ub is formed by the hydrophobic surface on the β-sheet. Two highly conserved sequence motifs among CUE domains- a Met-Phe-Pro motif in the loop connecting helices 1 and 2, and a Leu-Leu motif at the end of helix 3, make hydrophobic contacts with Ub. In addition, the complex is stabilized by electrostatic interactions between acidic side chains of CUE (Asp) and basic residues (Lys and Arg) of Ub and a hydrogen bond at the periphery of the hydrophobic pocket. The closest structural homolog of the CUE 2-1 domain is the UBA(2) domain from hHR23A. Based on the structural homology of the UBA domain with the CUE2-1 domain, it was predicted that the UBA domain would bind Ub through similar hydrophobic and electrostatic interactions mediated by residues at comparable positions in the sequences of the two domains.

Another CUE domain from Vps9p, a yeast protein involved in sorting at membranes, was found to exist as a domain swapped dimer in solution. This CUE domain binds tighter to monoUb (K_d~20μM) compared to the CUE2-1 domain (K_d~155 μM for binding Ub). The crystal structure of the CUE-Ub complex shows that one CUE dimer binds the hydrophobic patch of one Ub molecule [25] (figure 2.4(b)). The conserved Met-Phe-Pro and C-terminal Leu-Leu motifs bind Ub at the

region surrounding Ile^{44}. In addition, a third region on helix 2 (a less well conserved Ile/Leu/ValxxxLeu motif) also makes contacts with the region around Leu^{8} on Ub. Since the Vps9p CUE domain contains two Ub binding surfaces, a monomer CUE domain cannot bind one Ub such that both surfaces are utilized simultaneously. However, dimerization of the CUE domain allows it to bind Ub such that both surfaces contact Ub, providing a higher affinity mechanism of binding. It has been observed that CUE domains can bind polyUb chains in vitro. It still remains to be seen if the principles of oligomerization and domain swapping will apply to the CUE-polyUb interactions as well.

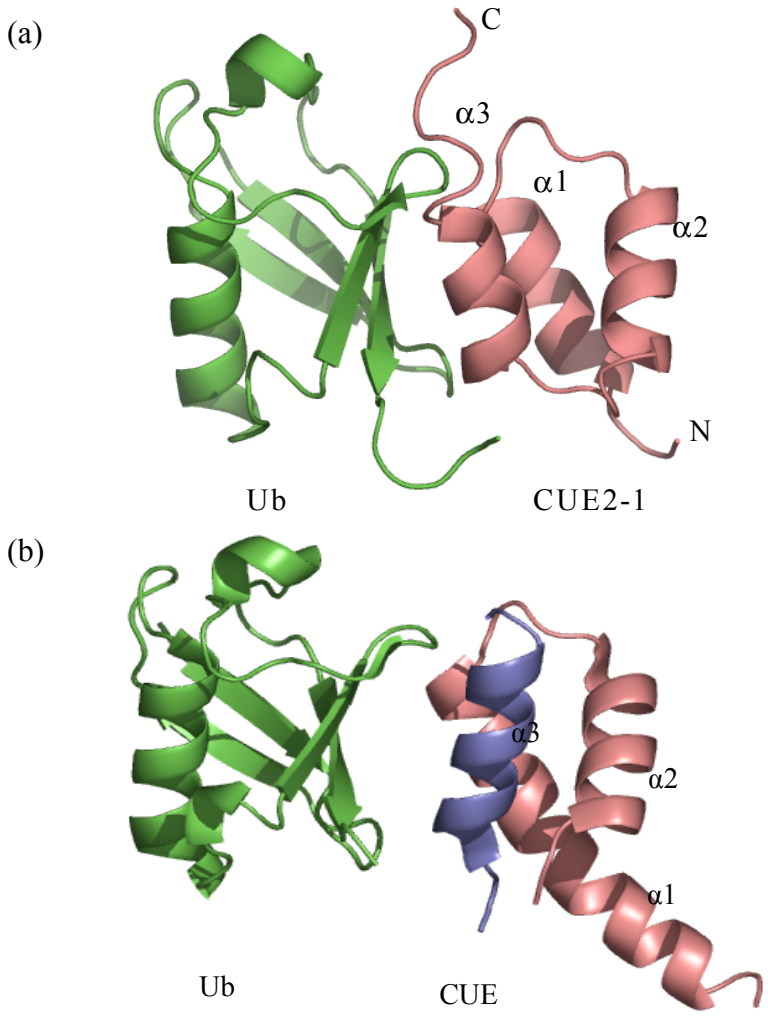

Figure 2.4 Structures of the Ub-CUE complexes (a) CUE domain from yeast protein Cue2 with helices 1 and 3 binding Ub (coordinates 1OTR.pdb) (b) part of the domain swapped CUE dimer from Vps9p binding the hydrophobic surface on Ub. Helices 1 and 2 in pink are from one CUE monomer, and helix 3 is the domain swapped segment from the second CUE monomer in the complex (coordinates from 1P3Q.pdb)

2.2.2 Ub-UBA complexes

UBA domains are compact 3-helix bundles found in a number of proteins that are involved in protein degradation. hHR23a is a protein belonging to the UBL/UBA family, with a UBL (ubiquitin-like) domain that binds the proteasomal subunit S5a, and two UBA domains that bind ubiquitin [33-35]. The UBL-UBA proteins have

been proposed to function as adaptor proteins that deliver polyubiquitinated substrates to the proteasome[7, 8]. However, whether these proteins indeed function as adaptor proteins in the cell is not clear, because in experiments with purified proteasomes, hHR23A has been shown to inhibit degradation of substrates by competing with the proteasome for binding substrate-linked polyUb chains [36].

Recent NMR studies have revealed that isolated UBA domains bind monoUb in a 1:1 (UBA:Ub) complex via a predominantly hydrophobic surface formed by helices 1 and 3 [35]. The binding of monoUb to isolated UBA domains of hHR23A is a weak interaction with reported binding constants in the range 300-600 μM, while binding to full-length hHR23A has been reported to be tighter with K_d~10 μM ([37]). The interaction surface on ubiquitin, as might be expected, involves the Leu^{8}-Ile^{44}-Val^{70} hydrophobic surface on the β-sheet. Although both UBA domains bind the identical surface on Ub, modeling the UBA-monoUb interaction based on structural homology between the UBA and CUE domains, and de novo docking of UBA-Ub complexes suggest that the two UBA domains are oriented differently on Ub [20]. Homology modeling of the UBA-Ub interaction based on the NMR structure of CUE2-1 (from Cue2) complex with Ub reveals slight differences between the orientations of the two UBA domains with respect to Ub. Surprisingly, de novo docking of the UBA molecules on Ub revealed completely different complex structures from those obtained by homology modeling. For the UBA(1)-Ub complex, the homology model differs from the de novo docked model by a 90^{o} rotation of the UBA(1) domain. In the case of the UBA(2)-Ub complex, the homology model can be transformed into the docked model by a 45^{o} rotation of the UBA domain in the

clockwise direction (figure 2.5). The authors showed that docking the Cue2 CUE domain on Ub reproduced the experimental NMR structure, and hence argued the differences between the structures of the complexes were unlikely to be an artifact of the docking procedure. Nevertheless, further experimental data will be required to verify how the UBA domains actually bind monoUb.

It is interesting to note that Ub mutants with single amino acid substitutions L8A, R42A, K48A, H68A or R72A do not show a significant decrease in binding affinity to UBA(1) and UBA(2) domains (less than 2-fold decrease). Consistently, Ub mutants K48A or L8A do not show a significant change in the binding affinity to the CUE2-1 domain [20]. In addition, the lack of hydrogen bonding at the interface suggests that the binding does not require the maintenance of geometries of hydrogen bond donors and acceptors, and would be governed by geometrical restrictions for the interacting hydrophobic side chains. Specificity in Ub binding might be defined by the overall topology of the binding partner. The hydrophobic surface of Ub could therefore allow binding of different helical bundle geometries.

(a)

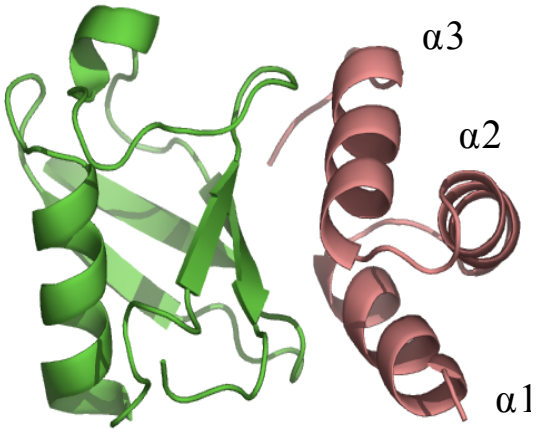

(b)

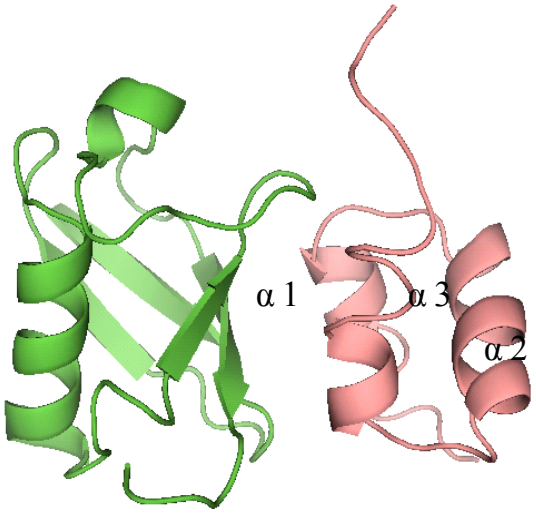

Figure 2.5 Models of the UBA(2)-Ub complex (a) structure from docking of UBA(2) on Ub (b) structure based on homology of UBA with CUE domains. Ub is shown in green and UBA(2) is shown in pink. The docked structure can be transformed into the the homology-modeled structure by rotating UBA(2) by 45^{o} in the counter clockewise direction. Both structures show UBA(2) binding Ub via helices 1 and 3.

Chapter 3: Methods

3.1 Protein expression and purification

3.1.1 Growth media and conditions

Plasmid DNA constructs for all proteins used in this study were cloned into *E.coli* BL21(DE3)pLysS cells and provided by Prof. Cecile Pickart (Johns Hopkins University). Starter cultures were grown for 6-8 hours at 37^{o}C to an OD_{600} ~0.6 using isolated colonies from a fresh plate. Cell cultures for unlabelled proteins were grown in the auto-inducing ZYP-5052 medium (composition from Dr. William Studier, Brookhaven National Laboratory) supplemented with ampicillin and chloramphenicol (at 100mg and 50 mg per liter culture respectively) at 37^{o}C in a shaker incubator with continuous agitation at 200rpm.

For uniform ^{15}N isotope incorporation in proteins, cell cultures were grown in ZYP-5052 medium replacing $(NH_4)_2SO_4$ with $^{15}NH_4Cl$ (1g/liter culture) and Na_2SO_4, such that $^{15}NH_4Cl$ provided the sole source of Nitrogen in the medium. ^{2}H labeled ubiquitin was expressed first by growing cells in 1liter M9 medium (in H_2O). The cells were grown at 30^{o}C overnight to an OD_{600} ~1.3. The cells were harvested and gently re-suspended into 500ml M9 medium (in D_2O) such that OD_{600} ~0.4-0.6. The cells were grown in the deuterated M9 medium at 37^{o}C till OD_{600}~1.2 (usually 6-8 hours), and then induced overnight with 0.4mM IPTG. Expression of ^{2}H labeled UBA required additional steps in the procedure to allow the bacteria to adapt to D_2O. Cells from the 1l M9 medium (in H_2O) were first re-suspended into 125ml M9 in 33% D_2O

such that OD_{600} ~0.6. After allowing for one cell division cycle (usually ~6 hours) at 37°C, the cells were harvested and re-suspended into 250 ml M9 medium in 66% D_2O to give OD_{600}~0.6. Finally, after the culture reached OD_{600}~1.2, the cells were harvested and re-suspended into 500ml M9 in 100% D_2O to an OD_{600} ~0.6. At OD_{600} ~1.2, the cells were induced with 1mM IPTG overnight and then harvested.

3.1.2 Purification of Ubiquitin

All cell pellets were frozen at –80°C for at least 30 minutes prior to lysis. Cells were resuspended in lysis buffer (50mM Tris pH 7.6, 0.02% Triton x100, 0.4 mg/ml lysozyme, protease inhibitors: 1mM PMSF, 50 µM TLCK, 5 µg/ml soyabean trypsin inhibitor, 2.5 µg/ml leupeptin). DNase1 (to 20 µg/ml) and $MgCl_2$ (to 10mM) were added to breakdown DNA. The cell suspension was centrifuged at 25000rpm for 25 minutes in a preparative ultracentrifuge 45Ti rotor. The soluble extract was transferred to a 50ml beaker. The extract was stirred and kept on ice, and ~300 µl undiluted perchloric acid was added drop-wise. Most proteins except ubiquitin precipitated at this step. The extract was ultracentrifuged again at 25000rpm for 25 minutes in a 45Ti rotor. The supernatant was filtered (0.22 µm) and dialyzed overnight at 4°C in 3.5 kDa cutoff dialysis tubing against 2 liters 50mM ammonium acetate buffer at pH 4.5.

The dialyzed sample was purified by cation exchange chromatography on a 5ml SP Sepharose Fast Flow column (GE Healthcare). The column was equilibrated with 50mM ammonium acetate, pH 4.5, and ubiquitin was purified using a salt gradient. Ubiquitin eluted at approximately 0.25M NaCl. The purified protein was

checked on a 15% SDS gel, concentrated using Amicon UF-4 filtration or ultrafiltration devices and exchanged into the desired buffer (50mM Tris pH 8 for polyUb synthesis, 20mM sodium phosphate pH 6.8 for most NMR experiments). Protein concentrations were determined using absorbance at 280 nm (ε=0.16 for 1mg/ml solution).

3.1.3 Purification of UBA, E2-25k and Ubc13

E2-25k, Ubc13 and the UBA(2) domain of hHR23A were expressed as GST-fused proteins in the medium described above. Cell lysis was performed in PBS buffer, pH 7.4 complete with protease inhibitors, lysozyme and Dnase1. The lysate was centrifuged and the soluble extract was filtered and loaded onto Glutathione Sepharose beads (Molecular Probes, 10 ml bead suspension per liter culture) pre-equilibrated with PBS buffer, pH 7.4. The suspension was incubated for 2 hours at 4^{o}C with mixing on a shaker. The unbound proteins were washed out with 6-8 bed volumes of PBS buffer, and the fusion protein was eluted with 50mM Tris pH 8, 10mM glutathione. GST-E2 was used as a fusion protein; however, the GST tags of Ubc13 and UBA2 were cleaved using thrombin. The purity of the proteins was checked on 15% SDS polyacrylamide gels; proteins were concentrated in the Amicon UF-4 filtration devices and exchanged into the appropriate buffer (50mM Tris pH 8 for GST-E2 and Ubc13, 20mM phosphate pH 6.8 for UBA(2)). The protein concentrations were determined by absorbance at 280nm (for 1mg/ml concentrations, for UBA ε=0.198, ε=1.7 for GST-E2-25k and ε=1.4 for GST cleaved Ubc13).

3.1.4 Purification of YUH-1

The yeast C-terminal hydrolase, also called UCH-L3 was purified by anion exchange and hydrophobic interaction chromatography. The crude lysate was first partially purified on a DEAE Sepharose column (GE Healthcare) using a salt gradient. YUH-1 was eluted at approx 0.4M NaCl. Fractions containing the protein were pooled and dialyzed against 50mM Tris pH 8. Solid $(NH_4)_2SO_4$ was added to a final concentration of 11% (w/v) and the suspension was filtered. The sample was then applied to a Phenyl Sepharose Hi-Load column equilibrated in 50mM Tris pH 8 + 11% $(NH_4)_2SO_4$. The protein was eluted with a linear gradient to 50mM Tris pH 8. YUH-1 eluted at approx 8% $(NH_4)_2SO_4$. Fractions containing YUH-1 were pooled and dialyzed against 50mM Tris pH 7.5, and applied to a MonoQ anion exchange column. A salt gradient caused the YUH-1 to elute at ~0.3M NaCl. After buffer exchange into 50mM Tris pH 8, the concentration was estimated by absorbance at 280nm (ε=1.035 for a concentration of 1mg/ml).

3.2 Synthesis of polyUb chains

3.2.1 Notation and design of segmentally isotope-enriched polyUb chains

To overcome the spectroscopic equivalence of all ubiquitin monomers comprising the polyUb chain, chains with only one Ub unit isotope labeled (^{15}N and/or ^{2}H) in a given sample were synthesized (figure 3.1). The following notations are used throughout to refer to Ub_2 and Ub_4 isotope labeled at different Ub units. Ub_2s are referred to as 'Ub_2-P' and 'Ub_2-D' for Ub_2 samples isotope labeled at the proximal and distal positions (with respect to a possible substrate) respectively. Ub_2-P

chains were synthesized using isotope labeled D77 Ub (proximal Ub) and unlabelled K48C, K48R, K63C or K63R Ub (distal Ub), and Ub_2-D chains were synthesized using unlabeled D77 Ub and isotope labeled K48C, K48R, K63C or K63R Ub. Ub_4 chains are referred to as Ub_4-1, Ub_4-2, Ub_4-3 and Ub_4-4 starting from the proximal end of the chain. Ub_4-1 and Ub_4-3 chains were assembled using Ub_2-P and unlabeled Ub_2 chains, and Ub_4-2 and Ub_4-4 were assembled using Ub_2-D and unlabeled Ub_2 chains as described in the next section.

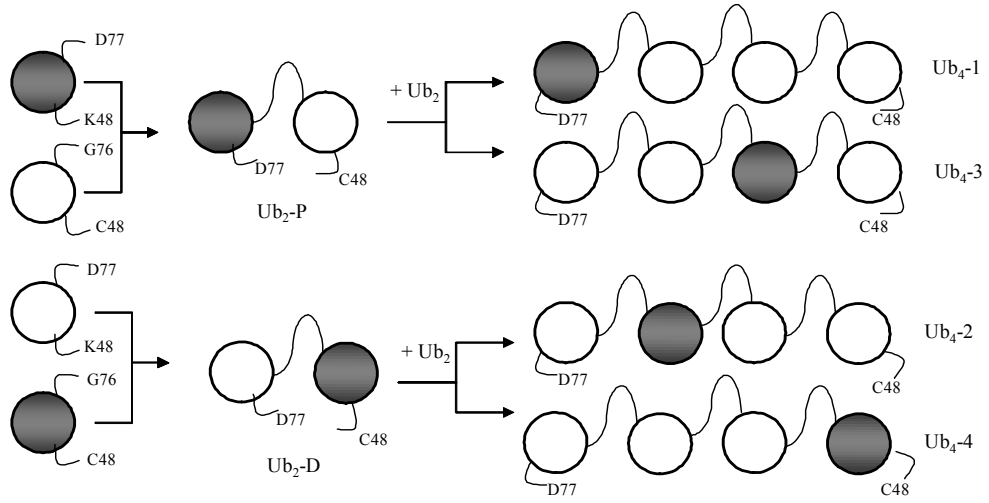

Figure 3.1 Design and synthesis of segmentally isotope labeled polyUb chains Open circles represent unlabeled Ub, and grey colored circles represent isotope labeled Ub. Lys^{48}-linked chains were assembled from Ub constructs D77 and K48C using enzymes E1 and E2. Use of D77 and K48C mutant Ub instead of wt Ub allowed controlled synthesis of Lys^{48}-linked polyUb chains of desired length. Lys^{63}-linked chains were synthesized using a similar strategy with D77 and K63R (or K63C) mutants of Ub.

3.2.2 Synthesis of Ub_2 chains

Lys^{48}- and Lys^{63}-linked Ub_2 were synthesized as described in [38]. All chemicals were from Sigma. E1 was obtained from Boston Biochemicals. The reactions were assembled in 50mM Tris pH 8, 5mM $MgCl_2$, 10mM creatine

phosphate, 0.6U/ml inorganic phosphatase and creatine phosphokinase, 2mM ATP, 0.5mM DTT, 7.5 mg/ml each of Ub (D77 and K48C or K48R Ub for synthesis of Lys^{48}-linked chains and D77 and K63C or K63R Ub for synthesis of Lys^{63}-linked chains), 30μM E2 (GST-E2-25k for Lys^{48}-linked Ub_2 and an equimolar mixture of Ubc13 and Mms2 for Lys^{63}-linked Ub_2) and 0.1 μM E1. Typically, 2ml reactions with a total of 30mg Ub were set up and incubated overnight at 37°C. The formation of Ub_2 was confirmed by SDS polyacrylamide gel electrophoresis and the Ub_2 was separated from unreacted monoUb and other components of the reaction mixture using cation exchange chromatography as follows. The reaction was first quenched by addition of DTT to a final concentration of 4 mM. After letting the mixture stand at room temperature for ~20 minutes to reduce any disulfide linked oligomers of Ub, the pH of the mixture was dropped to ~4 by the addition of 2-3 drops of undiluted acetic acid. The reaction mixture was then applied to a SP Sepharose Fast Flow column (1ml) pre-equilibrated in 50mM ammonium acetate, pH 4.5. Components of the reaction mixture such as E1 and E2, did not bind the column, and the Ub_2 was separated from monoUb using a salt gradient over 40 column volumes to a final salt concentration of 0.4M. 1-1.2 ml fractions were collected and checked on a 15% SDS gel. The fractions corresponding to Ub_2 were pooled, concentrated in Amicon UF-4 filtration units and exchanged into the desired buffer. Further purification of Ub_2 from monoUb, if required, was carried out using size exclusion chromatography on a Hi Load Sephadex 16/60 column in 50mM sodium phosphate buffer, pH 5.5, 2mM DTT. Typically, approximately 10 mg of Ub_2 was obtained after purification from a 30 mg initial reaction.

3.2.3 Synthesis of Lys^{48}-linked Ub_4

Ub_4 chains were assembled from 2 deblocked Ub_2 molecules. Synthesis of Ub_4-1 and Ub_4-3 required deblocking unlabeled Ub_2 molecules at the distal terminus (Cys^{48}) and deblocking proximal isotope labeled (Ub_2-P) molecules at the proximal terminus (Asp^{77}). Synthesis of Ub_4-2 and Ub_4-4 required deblocking Ub_2-D chains at the distal ends (Cys^{48}) and deblocking of unlabeled Ub_2 chains at the proximal terminus (Asp^{77}). Ub_2 molecules were deblocked at the distal end by alkylation of Cys^{48} with ethyleneimine (from Chemservice). The alkylation reaction was carried out in 200mM Tris, pH 8, 1mM EDTA and 55mM ethyleneimine. The reaction was incubated for 1 hr at 37 ^{o}C, and the Ub_2 was exchanged into 50mM Tris pH 8 to remove excess ethyleneimine. Deblocking at the proximal terminus was performed using the enzyme YUH-1 that removes the C-terminal Asp^{77} from Ub, such that Gly^{76} becomes available at the new C-terminus of Ub_2. The reaction was carried out in 50mM Tris pH 7.6, 1mM EDTA, 1mM DTT with ~15mg Ub_2 and 16 μg/ml YUH-1. After the mixture was incubated for 1 hr at 37 ^{o}C, DTT was added to a final concentration of 2mM. The mixture was then applied to an anion exchange column (Hi Load Q Sepharose Fast Flow, 1ml, GE Healthcare) to remove the YUH-1. The Ub_2 did not bind the resin, and was concentrated to ~300-500 μl volume and exchanged into 50mM Tris pH 8 buffer. Reactions for synthesis of Ub_4 were assembled similarly to that described for Ub_2 synthesis, except that deblocked Ub_2s were used instead of the monomeric Ubs. Purification of the final product was achieved using cation exchange chromatography, as before, with a longer salt gradient to 0.7M. Ub_4 typically eluted at 0.6M NaCl.

3.3 Determination of conformation of Ub_2

3.3.1 Challenges in structure determination

Conventional high-resolution methods used to determine structures of multidomain proteins include X-ray crystallography and determination of distance constraints from NOEs observed by NMR. In the first chapter, structures of Ub_2 and Ub_4 obtained from X-ray crystallography were presented. The multiple conformations of Ub_4 chains observed in crystal structures suggested that polyUb chains are inherently flexible, so that conformations observed in crystals could represent some bias due to lattice forces. In addition, the conformations observed in the crystal structures could represent only a subset of all the conformations that the chains could adopt in solution. Direct structure determination of polyUb by obtaining NOEs also presents a challenge for large systems like Ub_4 chains. The fairly large size of the molecule (~36 kDa) would result in broadening of resonance linewidths. In addition, due to interdomain dynamics in the chain, any observable NOEs will represent only an average distance between the interacting nuclei. Thus, the alternate approaches were required to address the problem.

3.3.2 Approaches to determining interdomain orientation

Recently, at least two NMR approaches have been developed to provide long-range orientational information in large systems. The first utilizes the orientation dependence of spin-relaxation parameters to describe the overall rotational diffusion of the molecule, and the second is based on measurement of residual dipolar couplings (RDCs) in anisotropic solutions[39, 40]. The general idea of deriving

interdomain orientation involves, first, the determination of rotational diffusion tensor (from relaxation parameters) or the alignment tensor (from RDCs) of the individual Ub domains in the context of the whole molecule (figure 3.2). If all the domains reorient together in solution, the individual tensors represent the property of the whole molecule as 'seen' by that domain. Therefore, alignment of the domains by rigid body rotation, such that the tensors are collinear will result in proper positioning of the domains with respect to each other, in terms of interdomain orientation. This approach of determining interdomain orientation is based on the premise that the structure of the individual domains (here, Ub) is known, and is not perturbed in the context of the whole molecule. Also, as alluded to above, it assumes that the domains reorient together as a single entity rather than as independent 'beads-on-a-string'. It should also be pointed out that the resulting conformation of the molecule represents a time-averaged orientation of the different domains because the domains may not be rigidly locked together in the molecule. Also, since only orientation dependent parameters are utilized, the approaches do not provide inter-domain distances.

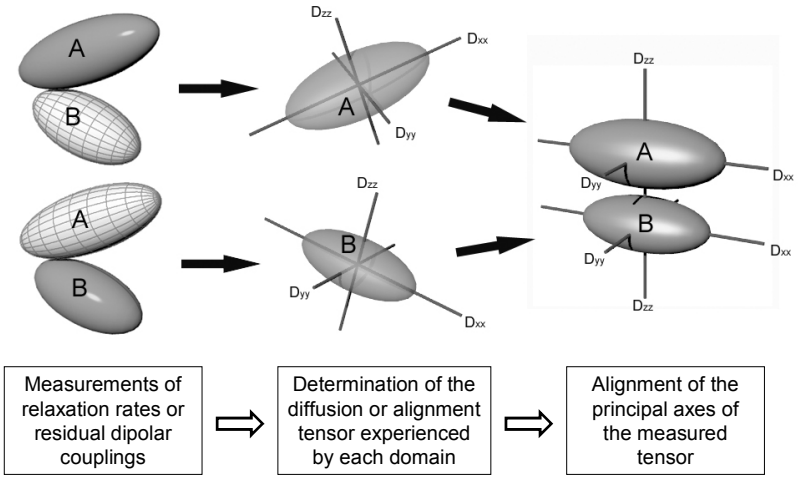

Figure 3.2 Concept of determining interdomain orientation from measurement of rotational diffusion or alignment tensors

3.3.3 Determination of alignment tensor

The internuclear dipolar interaction between two nuclei in an external magnetic field depends on the angle of the internuclear vector with respect to the external field. In isotropic liquids, the molecule samples all orientations with equal probability, and hence the dipolar interaction is averaged to zero. If, however, the sampling of orientations is not isotropic (for example, in paramagnetic proteins, or in liquid crystals) and molecules have some preferred orientations, a non-zero average dipolar coupling can be observed [40, 41]. Dipolar couplings can be large (~20kHz), rendering NMR spectra intractable; however, in dilute liquid crystalline media, the tendency for the preferred orientation is very small (10^{-3}), resulting in measurable residual dipolar couplings (RDCs) of the order of 20Hz. The partial alignment of molecules in liquid crystals usually results from steric or electrostatic interactions between the molecules and the medium.

For a given internuclear vector with polar coordinates [12], the residual dipolar coupling between 2 nuclei, i and j, is given by

$$d_{ij} = \frac{3}{4} d_{ij}^{0} \left[A_{zz} \left(3\cos^2 \theta - 1 \right) + \left(A_{xx} - A_{yy} \right) \sin^2 \theta \cos 2\phi \right] \qquad (1)$$

where $d_{ij}^{0} = -(\mu_o/4\pi)(\gamma_i\gamma_j h/2\pi^2 r_{ij}^{3})$ is the strength of the static dipolar coupling between the two nuclei, μ_o is the magnetic permeability of vacuum, γ_i and γ_j are the gyromagnetic ratios of the nuclei, r_{ij} is the internuclear distance and A_{ii} are the principal components of the alignment tensor. This tensor is traceless ($A_{xx}+A_{yy}+A_{zz}= 0$) and symmetric ($A_{ij}=A_{ji}$). Therefore, if at least 5 independent RDCs are available, the alignment tensor for the molecule (or domain) can be determined.

In the present study, RDCs were measured in a weakly aligned liquid crystalline phase. The medium was composed of n-alkyl-poly(ethylene glycol) (C12E5) (5% by wt) and n-hexanol (molar ratio 0.85) as described [42].Typically, aliquots of 2x concentrated hexanol-C12E5 mixtures were prepared beforehand, and stored at 4^{o}C. Ub2 samples were added to this mixture in a 1:1 ratio (by volume) such that the final medium was a 5% C12E5 with 0.85 molar equivalents of n-hexanol. As judged by the HSQC spectra, there is no direct interaction between Ub and the medium. The ^{1}H-^{15}N couplings were measured using IPAP ^{1}H-^{15}N HSQC experiments [43] and extracted using the approximation of contour levels as ellipses [44]. Typically, 256 t1 increments were used. The RDCs were obtained from the difference in the ^{1}H-^{15}N couplings observed in the oriented (25^{o}C) and isotropic phase (35^{o}C). Derivation of the tensor using singular value decomposition was implemented in MATLAB [45].

3.3.4 Determination of rotational diffusion tensor

Anisotropic rotational diffusion of molecules, resulting from their intrinsic shape (for example, a symmetric or asymmetric ellipsoid), results in faster reorientation of the molecules around some directions than others. Hence, different nuclei (here ^{15}N) experience different spin-relaxation rates depending on the average orientation of the bond vector (here NH) with respect to the principal axis frame of the rotational diffusion tensor. Thus, the spin-relaxation rates contain information about the overall rotational diffusion and the structure of the molecules. One of the methods that has been described [39, 46] to derive the rotational diffusion tensor from ^{15}N relaxation rates uses the orientational dependence of the ratio of relaxation rates

$$\rho = \left(\frac{2R_2'}{R_1'} - 1 \right)^{-1} = \frac{3}{4} \frac{J(\omega_N)}{J(0)} \tag{2}$$

where R_1' and R_2' are the longitudinal and transverse relaxation rates modified to remove the high frequency components of the spectral density such that

$$R_1' = 3\left(c^2 + d^2\right) J(\omega_N) = R_1 \left[1 - 1.249 \left|\gamma_N / \gamma_H\right| (1 - NOE)\right] \tag{3}$$

$$\text{and } R_2' = 0.5\left(c^2 + d^2\right)\left[4J(0) + 3J(\omega_N)\right] = R_2 - 1.079 \left|\gamma_N / \gamma_H\right| R_1 (1 - NOE) \tag{4}$$

where *c* and *d* represent contributions from chemical shift anisotropy and dipolar couplings, and ω_N and ω_H are Larmor frequencies of the ^{15}N and ^{1}H nuclei respectively. *J(ω)* represent the spectral density functions, and contain information about the motions involving the NH group under observation.

For a fully anisotropic model of rotational diffusion, the overall correlation function is described by [47]

$$C_{ovrl}(t) = \frac{1}{5} \sum_{i=1}^{5} a_i \, \mathrm{e}^{-tD_i} \tag{6}$$

where the coefficients a_i depend on the coordinates of the NH vector in the tensor frame and the rate constants D_i are related to the principal components of the diffusion tensor D

$$D_1 = 4D_{xx} + D_{yy} + D_{zz}; \quad D_2 = D_{xx} + 4D_{yy} + D_{zz}; \quad D_3 = D_{xx} + D_{yy} + 4D_{zz}; \quad D_4 = 6D_{iso} + 6\left(D_{iso}^2 - D^2\right)^{\frac{1}{2}};$$
$$D_5 = 6D_{iso} - 6\left(D_{iso}^2 - D^2\right)^{\frac{1}{2}}; \quad D^2 = \left(D_{xx}D_{yy} + D_{yy}D_{zz} + D_{xx}D_{zz}\right)/3; \quad D_{iso} = tr\left(\underline{\underline{D}}\right)/3 = \left(D_{xx} + D_{yy} + D_{zz}\right)/3 . \tag{7}$$

The corresponding spectral density function *J(ω)* is given by

$$J(\omega) = \frac{2}{5} \sum_{i=1}^{5} \frac{a_i D_i}{D_i^2 + \omega^2} \tag{8}$$

and the expected value of the relaxation rates can be calculated by substituting equation (8) into equations (3) and (4).

The parameters describing the rotational diffusion tensor were determined by minimizing the target function

$$\chi^2 = \sum_{i=1}^{N_r} \left(\frac{\rho_i^{\exp} - \rho_i^{calc}}{\sigma_i} \right)^2 \qquad (9)$$

where N_r is the total number of residues used in the analysis, ρ^{exp} is determined using equations (2)-(4) from experimentally measured relaxation parameters and ρ^{calc} is calculated using equations (2)-(8), and σ_i is the experimental error in ρ_i for residue i.

^{15}N transverse (R_2) and longitudinal (R_1) relaxation rates and the ^{15}N steady state NOE were measured using standard pulse sequences described in [48,49].The R_1 and R_2 rates were derived from a single exponential fit of the signal decay measured in a series of 2D HSQC planes. The 2D planes for these ^{15}N relaxation experiments were acquired with 7.2 kHz and 2 kHz in the ^1H and ^{15}N dimensions, respectively. For each 2D plane, 128 t_1 increments were collected, each consisting of 1024 complex points. Steady-state NOEs were derived from the ratio of signal intensities in the 2D NOE and NONOE experiments. Minimization of the target function (equation (9)) was performed in a 6 dimensional space of the principal values of the diffusion tensor and the Euler angles using the Levenberg-Marquardt algorithm implemented in MATLAB [45].

3.3.5 Alignment of Ub moieties based on NMR data

For determination of the rotational diffusion and the alignment tensors, the coordinates for the backbone NH groups for Ub were obtained from the NMR

structure 1D3Z.pdb. Residues in the loop regions and the flexible C-terminus of Ub were excluded from the analysis due to uncertainty in their orientations. The use of these coordinates of monoUb for derivation of the Ub_2 conformation was justified by the excellent agreement between measured and back-calculated RDCs from the derived structures (see Chapter 4). Details of the analyses are presented in the relevant chapters. Once the tensors of both the Ub domains in Ub_2 were determined, the relative orientation of the two domains was determined by aligning the principal axes, using the method of [46, 50]. The derived principal axes of these tensors have no directionality, i.e. both –x and +x, -z and +z orientations are possible, resulting in four possible relative orientations of the two domains. The degeneracy was reduced by applying chemical link requirements (Gly^{76}-Lys^{48} or Gly^{76}-Lys^{63} isopeptide bond) and considerations based on chemical shift perturbation data.

3.4 Chemical shift perturbation mapping

The approach of chemical shift perturbation mapping was used to identify interfaces between Ub domains in Ub_2 and Ub_4. Backbone amide resonances in monomeric Ub, and individual Ub domains in Ub_2 and Ub_4 were observed using ^1H-^{15}N HSQC (for Ub_2-D and Ub_2-P) or TROSY experiments (for Ub_4). The combined amide chemical shift perturbation was calculated as $\Delta\delta=[(\Delta\delta_H)^2 + (\Delta\delta_N/5)^2]^{½}$, where $\Delta\delta_H$ and $\Delta\delta_N$ are the chemical shift changes for ^1H and ^{15}N, respectively. Residues showing chemical shift perturbations were most likely to be involved in the formation of the interdomain interfaces in Ub_2 or Ub_4.

The same approach was also used to identify interaction surfaces between the UBA(2) domain of hHR23A and Ub (monomeric Ub, Ub_2 and Ub_4).

3.5 Estimation of molecular weight from ^{15}N relaxation rates

^{15}N longitudinal relaxation rates were used to estimate molecular weights of the Ub-UBA(2) complexes. ^{15}N relaxation rates are sensitive to the overall tumbling rate, which is in turn proportional to the molecular weight of the molecule under observation. The theoretical dependence of ^{15}N R_1 on the molecular weight was calculated from

$$R_1=3d^2J(\omega_N) \qquad (10)$$

where the spectral density function is given by $J(\omega)= S^2\tau_c/(1+ \omega^2 \tau_c^2)$. Here, S^2 represents the Lipari-Szabo order parameter (taken as 0.85 for the simulation of the theoretical dependence) and d^2 is the dipolar contribution to R_1. τ_c is the overall tumbling time of the molecule given by the Stokes-Einstein-Debye relationship $\tau_c= \eta V/kT$, where η is the viscosity of the medium and V is the specific volume (taken as 0.735 cm^3/g), proportional to the molecular weight (M_w) of the molecule. A R_1-M_w calibration curve was plotted by scaling the values of τ_c obtained from the Stokes-Einstein-Debye equation by a factor of 1.55 to represent the effect of a hydration shell on the molecule, so that the experimental and calculated values of τ_c for protein GB3, monoUb, Ub_2 and Ub_4 agreed. The molecular weights of the UBA-Ub complexes were determined from their measured ^{15}N longitudinal relaxation rates using this calibration curve.

3.6 NMR titration experiments

Binding of UBA to Ub_x (monoUb, Ub_2 and Ub_4) was monitored in NMR titration experiments performed as a series of ^1H-^{15}N HSQCs. 0.6-0.9 mM ^{15}N labeled

Ub_2 samples (Ub_2-D and Ub_2-P) were titrated with increasing amounts of an unlabelled UBA(2) solution. Binding was monitored through changes in the peak positions in the ^{1}H-^{15}N HSQC spectra and titrations were continued until no or very little chemical shift changes were observed (usually at a 5:1 UBA/Ub_2 molar ratio). Combined amide chemical shift differences were computed as described in section 3.4. Changes in NMR signal intensities due to line broadening were measured by uniformly scaling the spectra obtained upon titration of UBA (or Ub_2) to compensate for higher molecular weight of the complex. The signal attenuation for each residue was then calculated as the ratio of peak intensities in HSQC spectra of the free and bound protein. Reverse titrations with ^{15}N labeled UBA and unlabeled Ub_x were also performed.

For binding interactions in the fast-exchange regime on the NMR timescale, affinities of UBA-Ub_x interactions were estimated from titration curves assuming that the observed chemical shift perturbation, $\Delta\delta$, at each step in the titration was weighted by the population of free (p_A) and bound states of the protein(p_B), such that

$$p_A + p_B = 1 \text{ and } \Delta\delta = \delta_A.p_A + \delta_B.p_B \qquad (11)$$

where δ_A and δ_B are the chemical shifts corresponding to free and bound states of the protein respectively.

In a 1:1 (UBA:Ub) model,

$$p_B = \left([P_t] + [L_t] + K_d - \sqrt{\left([P_t] + [L_t] + K_d\right)^2 - 4[P_t][L_t]} \right) \Big/ \left(2[P_t]\right) \qquad (12)$$

where P_t and L_t are the total molar concentrations of Ub (or UBA) and ligand UBA (or Ub) and K_d is the apparent dissociation constant.

For analysis of the UBA-Ub_2 (Lys^{63}-linked) titration data, both a 1:1 (UBA:Ub_2) and 2:1 (UBA:Ub_2) were used. A 1:1 model allows one UBA molecule bound per Ub_2 such that one UBA molecule can bind to either of the two Ub domains but not both. A 2:1 model allows up to two UBA molecules bound to Ub_2, one per Ub unit. For the measurements on the distal or proximal domain in Ub_2, the 1:1 model gives

$$p_B = \left([P_t] + [L_t] + \tfrac{1}{2}K_d - \sqrt{\left([P_t] + [L_t] + \tfrac{1}{2}K_d\right)^2 - 4[P_t][L_t]} \right) \Big/ \left(4[P_t]\right) \quad (13)$$

Here, $[P_t]$ and $[L_t]$ are the total molar concentrations of Ub_2 and UBA. For a 2:1 model,

$$p_B = \left(2[P_t] + [L_t] + K_d - \sqrt{\left(2[P_t] + [L_t] + K_d\right)^2 - 8[P_t][L_t]} \right) \Big/ \left(4[P_t]\right). \quad (14)$$

Perturbations observed in UBA upon Ub_2 titration do not discriminate between the two Ub domains, therefore the 1:1 model gives the same equation as for UBA-monoUb binding (where Pt and Lt correspond to UBA and Ub2 respectively). The 2:1 binding model gives

$$p_B = \left([P_t] + 2[L_t] + K_d - \sqrt{\left([P_t] + 2[L_t] + K_d\right)^2 - 8[P_t][L_t]} \right) \Big/ \left(2[P_t]\right) \quad (15)$$

Titration curves were fit to the above models using the method of least squares in MATLAB.

For binding interactions in the slow-exchange regime on the NMR timescale, the dissociation constant was determined using the ratio of the peak volumes representing 'free' (P_f) and 'bound' (P_b) states. The dissociation constant, K_d is given by $K_d = [L_f].R$ where $R = [P_f]/[P_b]$ is the ratio of the peak volumes of the 'free' and

'bound' resonances respectively. The 'free' ligand, L_f is given by $[L_t] - ([Pt]/(1+R))$ for a 1:1 stoichiometry of interaction, and $[Lt]-2([Pt]/(1+R))$ for a 2:1 (L:P) interaction. The apparent dissociation constant was obtained by substituting for L_f in the expression $K_d = [L_f].R$ at different points of the titration, and averaging the values thus obtained.

3.7 Site-directed spin labeling

The spin label (1-oxyl-2,2,5,5-tetramethyl-3-pyrroline-3-methyl)methane sulfonate (MTSL, Toronto Research Chemicals, Inc) was covalently linked to the side chain of Cys of the protein. Spin labeling reactions were performed in 50mM Tris, pH 8, in 1.5 molar excess of MTSL. MTSL was dissolved at 40mM concentration in acetonitrile. The reaction tube was flushed with N_2 and incubated in the dark for 1h. Unreacted MTSL was then removed from the protein solution and the buffer was exchanged into the desired buffer (20mM sodium phosphate, pH 6.8, 7% D_2O and 0.02% NaN_3 for spin-labeling experiments in this study).

The paramagnetic relaxation enhancement rate is dependent on the electron-nucleus distance, and therefore can be used to derive distance information. The increase in the ^1H transverse relaxation rate due to the presence of a paramagnetic spin S at a distance r from the nucleus under observation is given by [51]

$$\Delta R_{2para} = K[4\tau_c + 3\,\tau_c/(1+ \omega_H^2\,\tau_c^2)]/r^6 \qquad (16)$$

where $K= (1/15)S(S+1)\gamma_H^2\beta_e^2 g_e^2$. Here g_e is the electronic g-factor, and β_e is the Bohr magneton.

The ^1H paramagnetic relaxation rate enhancement ΔR_{2para} for the NH groups were calculated from the ratio of the signal intensities in ^{15}N-^1H HSQC spectra

acquired with the spin-label in oxidized (paramagnetic) and reduced states, I_{ox} and I_{red} respectively using [52]

$$\Delta R_{2para} = R_{2ox} - R_{2red} = \ln(I_{ox}/I_{red})/t \quad (17)$$

where t is the experimental time during which the 1H magnetization is in the transverse plane undergoing paramagnetic relaxation. The electron-nucleus distances were then derived from equation (15), and used as distance constraints to calculate the position of the unpaired electron with respect to the protein using optimization implemented in MATLAB.

Chapter 4: Conformation of Lys^{48}-linked polyUb chains

4.1 Objective

To determine the solution conformation of Lys^{48}-linked Ub_2 and Ub_4 chains and compare them with their crystal structures.

4.2 Conformation of Lys^{48}-linked Ub_2

4.2.1 Mapping the interdomain interface in Ub_2

Segmentally isotope labeled Lys^{48}-linked Ub_2 chains were synthesized as described in Section 3.2.2. Chemical shift perturbation mapping was used to identify the interdomain interface in Lys^{48}-linked Ub_2. Since chemical shifts are extremely sensitive indicators of the electronic environments of the nuclei, changes in chemical shifts between monoUb and polyUb observed under identical experimental conditions would indicate a change in the microenvironment of the nuclei as a result (direct or indirect) of interdomain interactions.

The crystal structure of Lys^{48}-linked Ub_2 has been described in Section 2.1.1. In order to determine if the crystal structure represented the solution conformation of the Ub_2 chains, experiments were first performed under acidic buffer conditions (50mM ammonium acetate, pH 4.5), in which crystals were grown. Changes in chemical shifts in ^{15}N-^{1}H HSQC spectra of Ub_2-P and Ub_2-D in comparison with the corresponding monoUb (D77 and K48C Ub constructs respectively) are plotted in figure 4.1 (a-b). Perturbations in the C-terminus (residues 74-76) of the distal Ub

(observed in Ub_2-D), and in residues (45-49) adjacent to Lys^{48} in the proximal Ub (observed in Ub_2-P) are expected due to the formation of the Gly^{76}-Lys^{48} isopeptide bond, and thus confirm the formation of the correct Gly-Lys linkage. Small perturbations (<0.05 ppm) were also observed in residues Leu^{50} to Asn^{60} in the proximal Ub. However, these residues are located on a surface of Ub that is relatively far from the inter-Ub interface in Ub_2. In addition, given that no systematic perturbations are observed in the distal Ub, it is unlikely that these perturbations are related to interdomain interactions in Ub_2. Thus, under these conditions, there is no indication of a formation of an interface between the proximal and distal Ub moieties in Ub_2.

However, a similar analysis performed under neutral pH conditions (20mM sodium phosphate, pH 6.8) shows dramatic changes in chemical shifts between Ub_2 and corresponding monomeric Ubs (figure 4.1 (c-d)). In addition to the perturbations observed in residues close to the site of the isopeptide linkage, significant backbone amide perturbations were observed in several residues: 7-13, 42-44, 68-74 in both domains and 46-48 in the distal Ub. As these symmetric perturbations are likely to reflect formation of an interface in Ub_2, they were mapped onto the crystal structure of Ub_2. Although chemical shift data alone do not allow pair wise identification of interacting residues in Ub2, figure 4.1(e) shows the distribution of chemical shifts is generally consistent with the 2-fold symmetry of crystal structure of Ub_2, with residues on the hydrophobic surfaces of the individual Ub domains forming the Ub_2 interface. Thus, although under acidic conditions, there appears to be no well-defined

interface between the two Ub domains in Ub2, an interface that is generally consistent with that of the crystal structure is formed under neutral pH conditions.

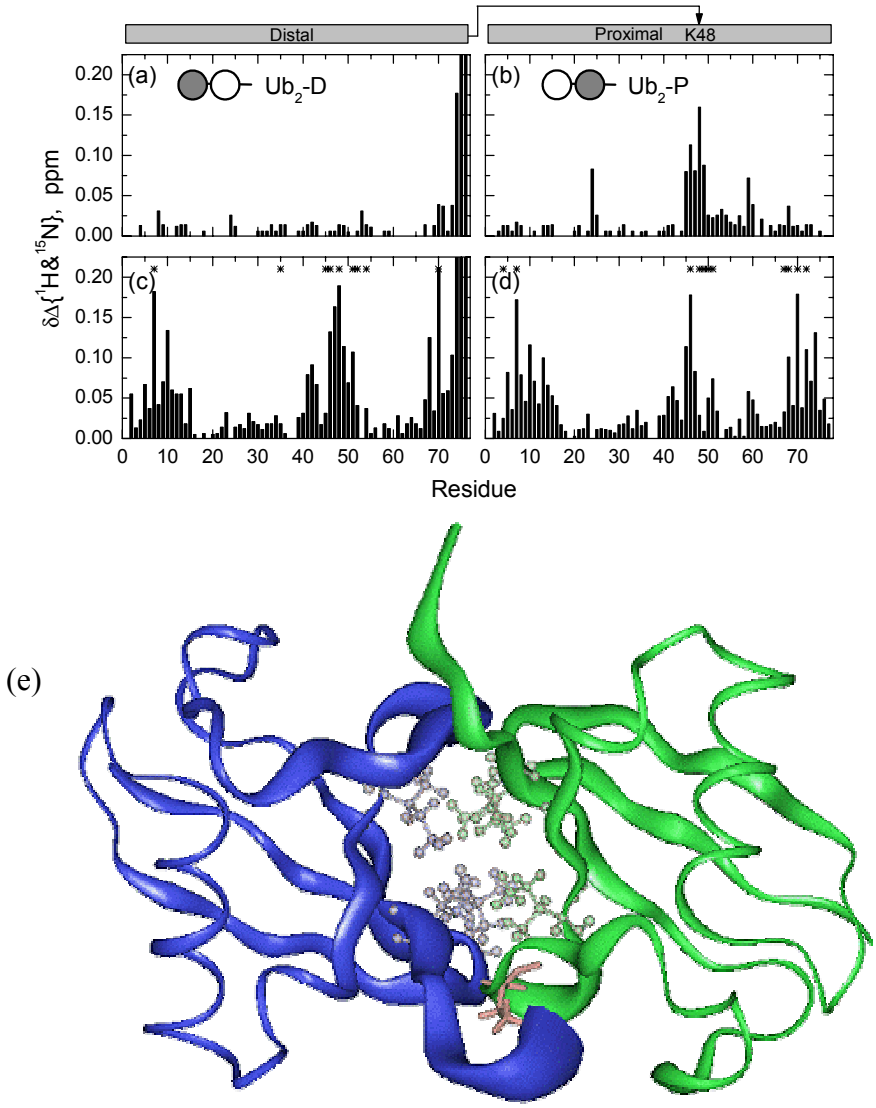

Figure 4.1 Mapping the Ub_2 interface Chemical shift perturbations in Ub_2 compared to monoUb at pH 4.5 (a,b) and pH 6.8 (c,d). Residues marked with asterisks in c,d represent those showing elevated R_2 levels (see sections 4.1.2 and 4.1.5). Panel (e) shows the chemical shift perturbations at pH 6.8 mapped on the crystal structure of Ub_2 (1AAR.pdb), with ribbon widths proportional to the magnitude of the observed perturbations. Hydrophobic residues at the interface are represented in ball-and-stick format, and the Gly^{76}-Lys^{48} linkage is shown as sticks.

4.2.2 pH dependent switch in Ub_2 conformation

The differences in the chemical shift perturbation maps of Ub_2 under acidic and neutral buffer conditions suggested that the equilibrium conformation of Ub_2 might be pH-dependent. Therefore, a detailed chemical shift mapping analysis was performed in a series of experiments at pH 4.5 to pH 8. Figure 4.2 shows that although at pH 4.5, no chemical shift perturbations are observed, well defined perturbations appear under conditions of higher pH. The results suggest that, under acidic conditions, Ub_2 can exist in one or more "open" conformations, with no definitive interface between the two Ub domains. Under neutral and alkaline solutions, Ub_2 molecules adopt a "closed" conformation, characterized by a well-defined interface. The "closed" conformation is likely to be stabilized by the hydrophobic contacts at the interface involving Leu^{8}, Ile^{44} and Val^{70} from both Ub domains. Several basic residues (Lys^{6}, Lys^{11}, Arg^{42}, Arg^{72} and His^{68}), which would acquire positive charges under acidic conditions, are located in regions flanking the Ub_2 interface. The switch to "open" conformations under acidic conditions could, therefore, be caused by increased electrostatic repulsion between the two Ub domains, upon titration of their bulk charges (the pI for both the Ub domains is ~5.8).

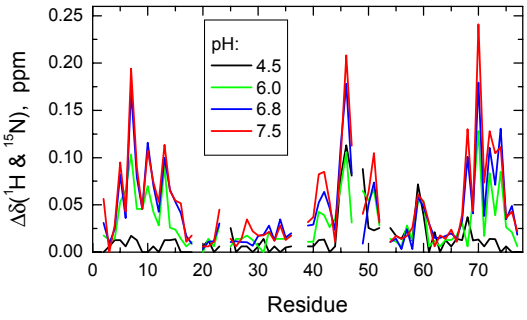

Figure 4.2 pH dependence of chemical shift perturbations Data are plotted for chemical shift perturbations observed in the proximal domain (Ub_2 vs monoUb) at different pHs

The broadening of resonances and elevated R_2 values for residues at the inter-Ub interface (marked by asterisks in figure 4.1) suggested the presence of conformation exchange in these residues. Since only one resonance is observed for every residue, the "open" and "closed" states are in fast exchange on the NMR timescale, such that the positions of the observed signals in the NMR spectra are a weighted average of those corresponding to fully "open" and "closed" states. Therefore, if the chemical shifts corresponding to the limits of "open" and "closed" conformations are known, the equilibrium populations of these states can be estimated for any given intermediate pH. Figure 4.2 shows that the chemical shift perturbations (Ub_2 versus monoUb) saturate at pH 7.5, with very little difference between the perturbations observed at pH 6.8 and 7.5. The titration data therefore suggest that Ub_2 molecules are "open" at pH 4.5, and almost fully populate the "closed" state at pH 7.5. Thus, at pH 6.8, the estimate of the population of the "open" conformation for individual amide groups ranged from 1% to 25%, with a mean value of 15%.

4.2.3 Solution structure of Lys^{48}-linked Ub_2

Determination of the Ub_2 structure using conventional NOE based approaches requires the detection of NOEs representing direct short-range contacts between the two Ub domains. Ub_2 (^{15}N, ^{2}H Ub_2-P), with ^{2}H incorporated in the ^{15}N-labeled proximal Ub was used to detect direct contacts between the side chains of the distal Ub and the backbone amides of the proximal Ub. In such an experiment, perdeuteration of the ^{15}N-labeled Ub domain causes only inter-Ub NOEs to be observed. However, no side chain-to-backbone amide NOEs were observed between

the two Ub domains. It is possible that the interdomain dynamics in Ub_2 renders these NOEs unobservable, and more extensive experiments with ^{13}C labeled Ub domains will be required to detect side chain-side chain contacts between the domains. In the absence of any interdomain NOEs, the relative orientation of the two Ub domains in Ub_2 was determined using methods based on the measurement of relaxation parameters to obtain the rotational diffusion tensor, and the measurement of residual dipolar couplings (RDCs) in liquid crystalline media to obtain the alignment tensor of Ub_2 (described in section 3.3).

In the first method, ^{15}N longitudinal and transverse relaxation rates, R_1 and R_2, and [48]-^{15}N heteronuclear NOEs, were measured for both Ub domains, and used to determine the rotational diffusion tensor of Ub_2 as "seen" by each domain. Since the rotational diffusion tensor as "seen" by each Ub domain essentially represents the same overall diffusion tensor, the relative orientation of the two domains was determined by their rigid body rotation that aligns the principal axes of these two tensors. Relaxation parameters were measured in segmentally ^{15}N-enriched samples, Ub_2-P and Ub_2-D, at concentrations ranging from 250 μM-1mM. The measured relaxation parameters showed weak concentration dependence, possibly due to aggregation of Ub_2 molecules. To avoid artifacts due to these intermolecular interactions, the concentrations of the samples were decreased until no further change in relaxation rates was observed. The final concentration of Ub_2 samples used in this study was 250 μM.

The measured ^{15}N relaxation parameters for Ub_2 and monoUb (for comparison) are plotted in figure 4.3. Several features of the data should be noted

here. First, residues in Ub_2 show a larger variation in ρ-values in comparison with monoUb, indicating a larger degree of rotational anisotropy in Ub_2 than in monoUb. This variation illustrates the orientational dependence of relaxation parameters described in section 3.2.2: due to the asymmetric shape of Ub_2, ^{15}N nuclei in different parts of the molecule experience different apparent rates of overall rotational motion depending on the average orientation of the NH bond with respect to the overall rotational diffusion tensor, and therefore show different relaxation rates. Second, the average ^{15}N T_2 value is approximately two-fold shorter in Ub_2 than in monoUb, that is, the ^{15}N T_2 scales inversely with molecular weight. The measured ^1H T_2 values for monoUb (50ms) and Ub_2 (22-23 ms at pH6.8, and 25-26 ms at pH 4.5) also show a similar dependence on molecular weight. This inverse dependence of T_2 on molecular weight is in accordance with $T_2 \alpha 1/\tau_{ovrl}$, where $\tau_{ovrl} = \eta V/kT$ (Stokes-Einstein-Debye relationship) is the overall tumbling time, η is the viscosity, and V is the molar volume (hence, proportional to molecular weight). In addition, the overall correlation times derived from the relaxation data (see table 4.1) are two fold greater for Ub_2 than for monoUb. These relaxation rates therefore indicate that the two Ub domains in Ub_2 (open and closed states) re-orient in solution as one compact molecule, rather than as independent beads on a string, and validate the method of determining the interdomain orientation used here.

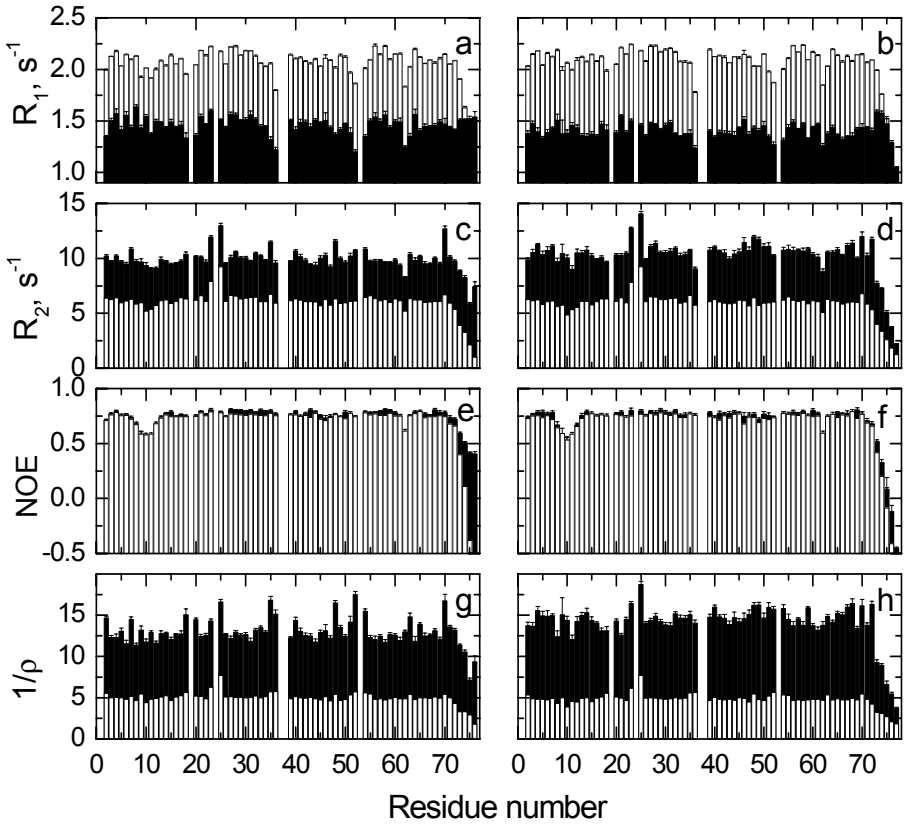

Figure 4.3 ^{15}N Relaxation data for Ub_2 Experimental values of R_1 (a,b), R_2 (c,d) and NOEs (e,f) measured for both the proximal (left panels) and distal (right panels) domains at pH 6.8 in solid bars. Open bars represent data for monoUb (for comparison). The derived values of 1/ρ are plotted in panels g and h.

The rotational diffusion tensors of both the proximal and distal domains in Ub2 were derived from the relaxation data using the method described in 3.2.2. Since the magnitude of chemical shift perturbations in Ub_2 compared to monoUb is small, it is reasonable to assume that the structures of the individual Ub domains in Ub_2 are the same as monoUb. Therefore, NH bond coordinates from the published structures of monoUb (solution structure 1D3Z and crystal structure 1UBQ) and Ub_2 (crystal structure 1AAR) were used in the determination of the diffusion tensors. A representative example of the data analysis is shown in figure 4.4 for the proximal domain at pH 6.8. The data were fit to both, axially symmetric and fully anisotropic

models of the rotational diffusion tensor. Fitting the orientation dependence of ρ using the axially symmetric model of rotational diffusion results in a large vertical spread in the ρ values around the fitting curve, most pronounced in the region where $\theta = 90^{o}$. However, using the fully anisotropic model of rotational diffusion results in much better agreement between experimental and calculated values of ρ. The ρ values now depend on both angles θ and ϕ, that define the orientation of the NH bond with respect to the principal axes frame (PAF) of the rotational diffusion tensor. The data is therefore fit to a curved surface, rather than a curve, as shown in figure 4.4 (a)-(b). The vertical spread in ρ values in the axially symmetric model (figure 4.4(a)) now fits the "hills" and "valleys" of the curved surface (figure 4.4(b)). The characteristics of the derived rotational diffusion tensors are presented in table 4.1.

The rotational diffusion tensors as 'seen' by each domain were used to determine the relative orientation of the two Ub domains in Ub_2. The resulting solution structures of Ub_2, under acidic and neutral conditions are shown in figure 4.6. It should be noted that since only orientational information is used to derive the structures, they represent a time-averaged orientation of the two Ub domains with respect to each other, and not actual distances between the two domains. A comparison of figures 4.6(a) and (b) shows that, consistent with the chemical shift perturbation data, Ub_2 adopts different conformations under different pH conditions. Under acidic conditions, Ub_2 adopts "open" conformations, represented by figure 4.6(a), with no contact between the hydrophobic surfaces on the Ub domains. As seen in chemical shift mapping, Under neutral conditions, the closed conformation of Ub_2 is represented by figure 4.6(b). The conformation is in agreement with the chemical

shift perturbation data, and hydrophobic residues showing chemical shift perturbations at pH 6.8 are located at the interface of the two Ub domains.

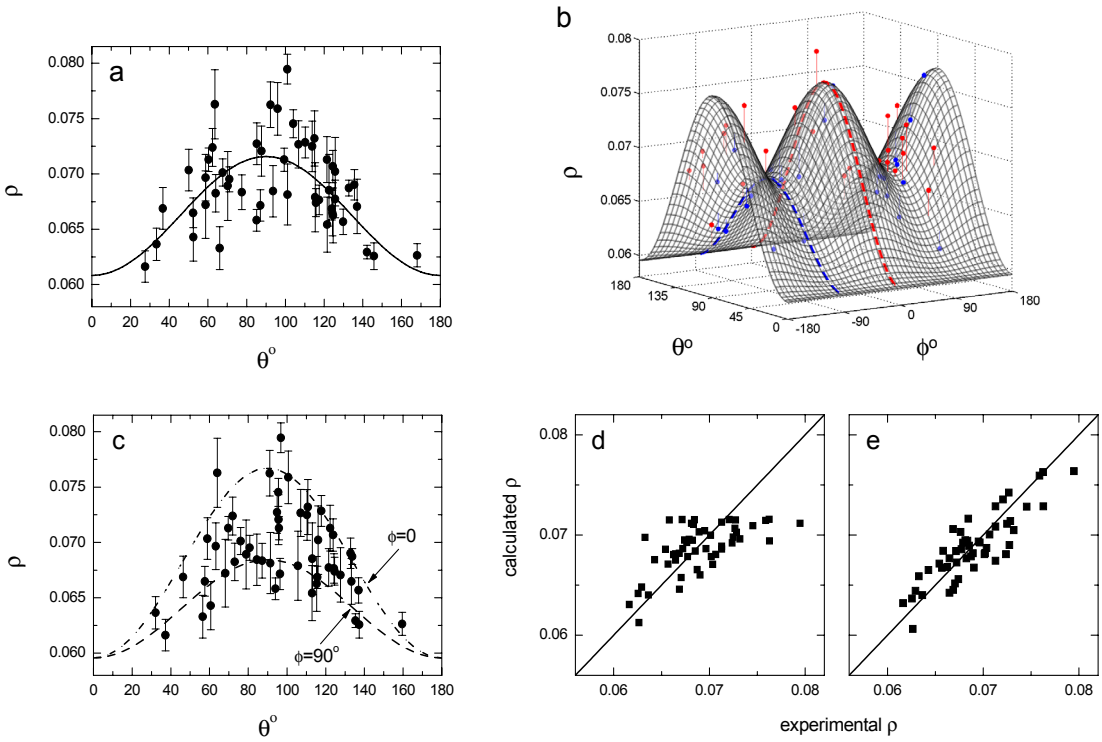

Figure 4.4 Relaxation data analysis Details of analysis of data obtained at pH 6.8 for the proximal Ub: orientation dependence of ρ obtained using axially symmetric (a) and fully anisotropic (b and c) models for the diffusion tensor. Panel (c) is a projection of the surface in panel (b) onto the ρ-θ plane. The dashed lines in (b) and (c) represent the upper and lower boundaries of ρ(θ) corresponding to $\varphi=0^{o}$ and 90^{o} respectively. Agreement between calculated and experimental values of ρ for the axially symmetric and fully anisotropic models is shown in panels (d) and (e) respectively.

Table 4.1 Characteristics of the overall rotational diffusion tensor of Ub_2 at neutral and acidic pH, determined from ^{15}N relaxation data for the Ub domains

Ub unit	D_{xx}	D_{yy}	D_{zz}	τ_c (ns)	α	β	γ
Ub_2-P pH 6.8	1.75 (0.08)	2.05 (0.08)	2.27 (0.08)	8.23 (0.19)	83 (13)	81 (8)	172 (11)
Ub_2-D pH 6.8	1.75 (0.09)	1.88 (0.08)	2.75 (0.14)	7.85 (0.23)	115 (5)	76 (5)	117 (30)
Ub_2-P pH 4.5	1.80 (0.06)	1.98 (0.07)	2.16 (0.07)	8.43 (0.32)	159 (14)	101 (7)	11 (17)
Ub_2-D pH 4.5	1.72 (0.09)	1.79 (0.07)	2.45 (0.14)	8.36 (0.32)	131 (5)	74 (5)	108 (40)

NH vector coordinates for each Ub domain were from 1AAR.pdb. Numbers in parantheses represent standard deviations. The principal values of the diffusion tensor (D_{xx}, D_{yy}, D_{zz}) are in 10^7 rad^2s^{-1}. The overall correlation time, $\tau_c = 1/(2\ tr(D))$. The Euler angles characterize the orientation of the diffusion tensor of Ub_2 as 'seen' by each of the Ub domains. These angles (in degrees) are determined with respect to the particular PDB coordinate frame for each domain.

As an independent verification of the structures derived from the ^{15}N relaxation data, the solution conformation of Ub_2 was also determined using alignment tensors derived from RDCs. RDCs were measured in both Ub domains in the ordered phase of n-alkyl-poly(ethyleneglycol)/n-hexanol mixtures at pH 6.8. The observed ^2H quadrupolar splitting in ^2H_2O was ~21 Hz in the ordered phase of the medium. The measured RDC values for both Ub domains are shown in figure 4.5(a-b). The excellent agreement between measured and back-calculated RDCs (figure 4.5 c,d) indicates the structure of the individual Ub domains is preserved in Ub_2, and validates the use of NH coordinates from the PDB structures of monoUb to derive the alignment tensor. The PAFs of the alignment tensors derived from RDCs were

aligned to obtain the relative orientation of the two Ub domains. Table 4.2 shows the characteristics of the derived alignment tensors, and the structure of Ub_2 obtained from these is shown in figure 4.6(c).

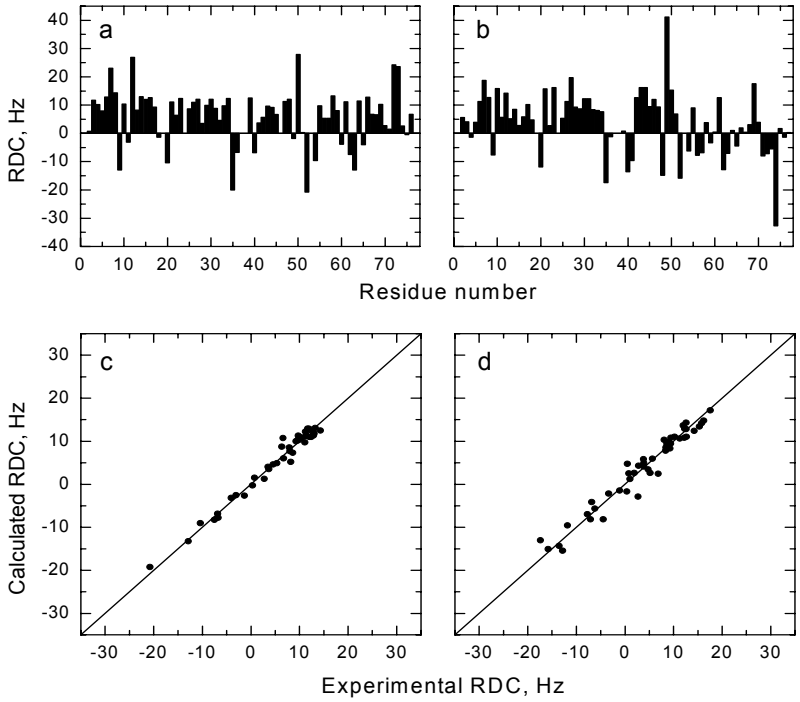

Figure 4.5 Alignment tensor analysis in Ub_2 Residual dipolar couplings (RDCs) measured at pH 6.8 are shown for the distal (panel a) and proximal (panel b) domains. The agreement between calculated and experimental values of RDCs for residues belonging to the Ub core is shown in panels c and d, the corresponding correlation coefficients were 0.99 and 0.98 respectively.

Table 4.2 Characteristics of the alignment tensor for Lys^{48}-linked Ub_2 at pH 6.8, determined from the RDCs for the two Ub domains

Ub unit	S_{xx}	S_{yy}	S_{zz}	α	β	γ
Ub_2-P	6.9	18.2	-25.1	87	83	228
	(0.7)	(0.8)	(0.9)	(1)	(1)	(3)
Ub_2-D	10.8	13.1	-24.0	105	79	208
	(0.5)	(0.7)	(0.8)	(1)	(1)	(16)

The principal values of the alignment tensor (in Hz) were ordered assuming $|S_{zz}| > |S_{yy}| > |S_{xx}|$. The Euler angles $\{\alpha,\beta,\gamma\}$ characterize the orientation of the principal axes frames of the alignment tensor of Ub_2 with respect to the PDB coordinate frame for each domain. A simultaneous reduction by 65^o of the γ angles for both the domains (corresponding to a rotation of the whole Ub_2 molecule about the *z*-axis) results in γ values of $163(\pm 3)$ for Ub_2-P and $143(\pm 16)$ for Ub_2-D, in agreement within experimental precision with those obtained from the diffusion tensor (table 4.1). This has no effect on the relative orientations of the Ub domains, and represents the difference in orientation of the *x* and *y* axes of the diffusion and alignment tensors for Ub_2.

The structures of Ub_2 derived from both rotational diffusion and alignment tensors at pH 6.8 agree with each other within experimental errors. If the distal Ubs from both the structures are aligned, the proximal domains can be superimposed by a rotation of the proximal domain in the diffusion-derived structure by 18^o around the z-axis and 10^o and 4^o about the other orthogonal axes. These differences could arise from different averaging of structural information by RDC and relaxation measurements in the presence of exchange between "open" and "closed" conformations. Additionally, the difference could also reflect intrinsic dynamic properties of Ub_2 that depend on how the two Ubs are linked. Both the alignment and diffusion tensors for the distal Ub appear more axially symmetric (Dxx~ Dyy, Sxx~Syy) than for the proximal Ub, and hence a larger uncertainty is obtained in the γ angle. This could reflect greater conformational freedom for the distal domain about the z-axis, and is more pronounced under acidic conditions where the open

conformations are more populated. Further studies will be required to understand the difference in dynamic properties of the two Ub domains. Nevertheless, the good agreement between the structures derived from independent methods (RDCs and relaxation) strongly supports the derived conformation of Ub_2.

4.2.4 Comparison of NMR derived structures with Ub_2 crystal structure

The "closed" conformation of Ub_2 observed in solution is, in general, consistent with the crystal structure of Ub_2, with the Leu^8-Ile^{44}-Val^{70} hydrophobic patch forming the interUb interface. However, the interface in the solution conformations appears more open than in the crystal structure: the α-helices of the two Ub domains are at an angle of 161^o and 145^o in the diffusion and alignment tensor derived solution structures respectively, compared to an angle of 128^o in the crystal structure. The crystals for the X-ray studies were grown under acidic conditions, where Ub_2 molecules are observed to adopt "open" conformations in solution. It is, therefore, likely that the conformation observed in the crystals is a result of packing forces that force the Ub_2 molecules to adopt a "closed" conformation. It is also relevant to point out here that the "closed" conformation derived from the NMR methods described here represents an average conformation of Ub_2 molecules in dynamic equilibrium between predominantly "closed" and lesser-populated "open" states (see also below).

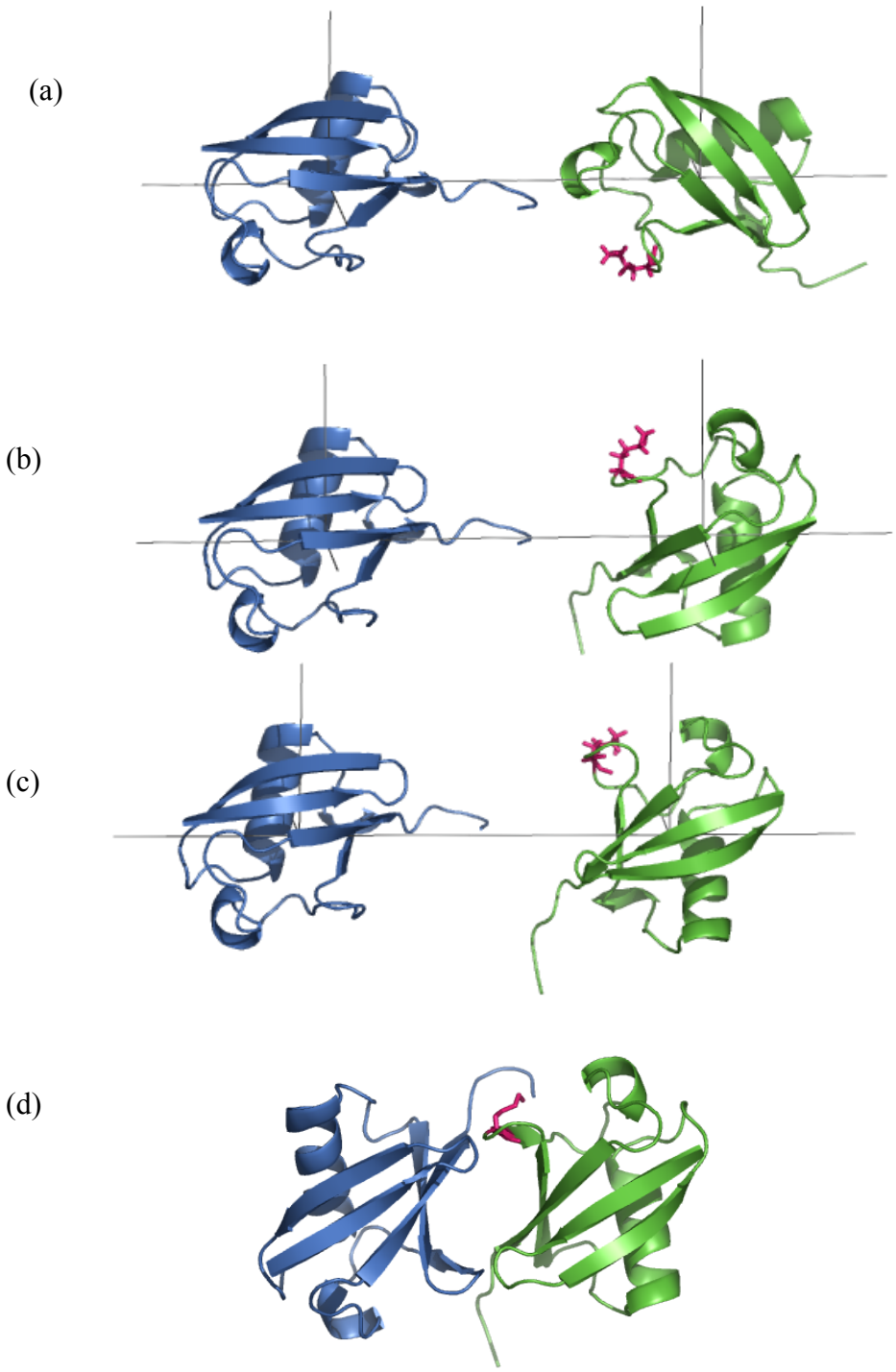

Figure 4.6 Solution conformations of Lys^{48}-linked Ub$_2$ Structures of Ub_2 under (a) acidic conditions and ((b) and (c)) neutral pH. Structures in (a) and (b) were derived from ^{15}N relaxation measurements (rotational diffusion tensor), while that in (c) was derived from RDCs (alignment tensor). For comparison, panel (d) shows the crystal structure of Lys^{48}-linked Ub_2 (1AAR.pdb). The distal Ub and the proximal Ubs are shown in blue and green respectively. Residue Lys^{48} on the proximal Ub is shown in magenta.The orientation of the PAFs of the tensors, as seen by the individual Ub domains are shown as black lines, with the z-axes oriented in the horizontal direction. The distance between the two domains is arbitrary. Since the C-terminus of Ub is flexible, it should readily adopt a conformation that accommodates the Gly^{76}-Lys^{48} linkage.

4.2.5 Inter-domain dynamics in Ub_2

The "closed" conformation of Ub_2 at neutral and higher pH conditions (close to physiological) shows residues Leu^8, Ile^{44} and Val^{70} to be buried at the interdomain interface. However, if these residues are to be involved in recognition of polyUb chains by various proteins in the cell, it is important to determine if these residues can be exposed to solvent, and potentially to Ub-recognizing proteins in the cell.

A previous NMR study [30], employed the soluble nitroxide, HyTEMPO, to address the solvent accessibility in Ub_2 chains. HyTEMPO causes paramagnetic relaxation rate enhancement that selectively broadens signals arising from solvent accessible hydrophobic residues. It was observed that, at pH 6, proton NMR signals from Leu^8, Ile^{44} and Val^{70} were strongly attenuated in the presence of HyTEMPO, suggesting that these residues were exposed, and not buried at the interface as observed in the crystal structure. However, chemical shift data presented in this study suggest that at pH 6, the closed conformation is significantly, although not fully, populated.

To address this apparent contradiction, experiments were performed to compare solvent accessibility in Ub_2 as a function of pH. ^{15}N-^{1}H HSQC spectra of Ub_2 were recorded with and without the presence of 20mM HyTEMPO in solution, and signal intensities were compared to identify residues that were solvent exposed. A comparison of the signal intensities in the spectra at pH 4.5 and 6.8 is shown in figure 4.7. At acidic pH, the HyTEMPO-induced attenuation in NMR signals is very similar to that observed in monoUb, consistent with the model that Ub_2 chains adopt "open" conformations under these conditions. Surprisingly, however, at neutral pH

also, signals corresponding to residues at the interface were attenuated by HyTEMPO. In order for these residues to both, participate in the formation of the Ub_2 interface and be solvent accessible, the "closed" Ub_2 conformation must be mobile. Figure 4.7 also shows that more residues are attenuated at neutral pH, than in monoUb, or in Ub_2 under acidic conditions (wider "valleys" around Leu^8, Ile^{44} and Val^{70} in figure 4.7(d) than in figure 4.7(b), (c)). This pattern could be explained if the HyTEMPO is transiently trapped at the hydrophobic interface in the closed conformation resulting in an increased residence time that causes attenuation in a larger number of residues at the interface. Consistent with this model, all residues at the Ub_2 interface, both hydrophilic and hydrophobic, that show chemical shift perturbations in Ub_2, experience signal attenuation on addition of HyTEMPO.

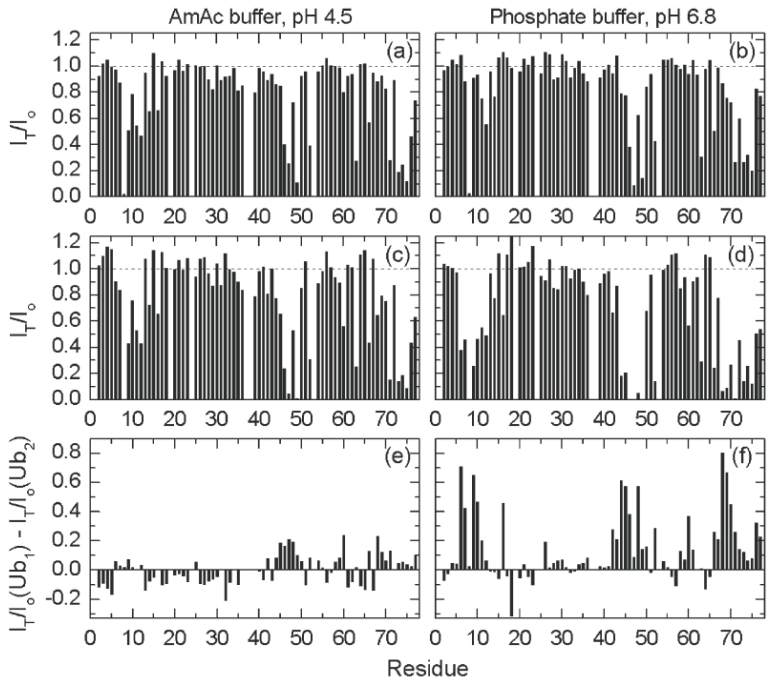

Figure 4.7 Solvent accessibility data Signal attenuation caused by HyTEMPO, calculated as a ratio of signal intensities in the presence and absence of HyTEMPO, is plotted for monoUb at (a) pH 4.5 and (b) pH 6.8. Panels c and d show attenuation observed in the proximal domain in Ub_2. Panels e and f show differences in attenuation factors between monoUb and Ub_2.

Thus, the data suggest that the "closed" conformation is not a rigidly locked structure. Rather, the Ub_2 interface is dynamic, and allows functionally important residues such as Leu^8, Ile^{44} and Val^{70} located at the interface to be solvent accessible. The dynamic nature of the "closed" conformation is also supported by ^{15}N relaxation data. Several residues (marked by asterisks in figure 4.1 c-d) located at the interface in Ub_2 show significantly elevated levels of ^{15}N transverse relaxation (R_2) at pH 6.8, indicative of conformational exchange (R_{ex}) type of motions in the μs-ms timescale. Most of these conformational exchange contributions to R_2 are absent at pH 4.5, suggesting they are specific to the "closed" conformation, and hence likely to arise from exchange between "open" and "closed" states of Ub_2. From the R_{ex} contributions to R_2 values, the characteristic time scale of the exchange process can be estimated using

$$\tau_{ex} = R_{ex}/(p_{op}.p_{cl}.\Delta\omega^2)$$

where p_{op} and p_{cl} are the relative populations of the open and closed states respectively (0.85 and 0.15 respectively at pH 6.8), and $\Delta\omega$ is the frequency difference between open and closed states (estimated from chemical shift difference between monoUb and Ub_2 at pH 7.5). The derived values of τ_{ex} (table 4.3) range from 50μs-1ms, providing an estimate of the timescale for the motions associated with opening and closing of the Ub_2 interface. Interestingly, the presence of interdomain mobility in Ub_2 is also reflected in the observed anisotropy of the diffusion tensor. The measured anisotropy of the diffusion tensor (ξ ~1.2-1.5) is smaller than that expected for an ellipsoid with a 2:1 axial ratio (ξ=1.87), or for a system of two rigidly

attached spheres (ξ=2.3). The reduced value of measured anisotropy suggests its averaging by interdomain dynamics/mobility in Ub_2.

Table 4.3 Characteristic time constants for conformational exchange observed in residues at the interface in Lys^{48}-linked Ub_2

Residue	R_{ex}, s^{-1}	$\Delta\delta(^{15}N)$, ppm	τ_{ex}, μs
Distal Ub			
Q2	0.62 ± 0.14	0.26	497 ± 261
V5	0.46 0.21	0.39	166 ± 96
T7	1.22 ± 0.18	-0.97	70 ± 23
Q41	0.61 0.23	-0.39	216 ± 117
K48	0.81 ± 0.18	-0.91	53 ± 19
H68	0.52 0.16	-0.58	83 ± 36
V70	2.58 ± 1.56	-0.91	169 ± 114
Proximal Ub			
T7	1.21 ± 0.20	-0.97	37 ± 14
Q41	0.75 ± 0.17	-0.39	271 ± 118
R42	1.29 ± 0.32	-0.39	429 ± 197
K48	1.21 ± 0.20	-0.26	973 ± 491
E51	1.19 ±0.35	-0.52	240 ± 107
Y59	0.40 ±0.10	-0.19	564 ± 359
H68	1.42 ±0.33	-0.58	249 ± 90
V70	2.08 ±0.50	-1.10	93 ± 35

Thus, the residues at the interface of Ub_2 are not rigidly buried between the two Ub domains. The solvent accessibility studies with HyTEMPO indicate that the interface 'opens' to allow hydrophobic residues to be exposed. The amplitude of 'opening' allows HyTEMPO to transiently enter and be trapped at the interface. From the R_{ex} values, the timescale of this 'opening' and 'closing' of the interface is estimated to be 50 μs-1ms. These motions could therefore allow the functionally important hydrophobic residues sequestered at the interface to be available for recognition by various cellular proteins. Alternatively, these motions may also

modulate specific recognition of these chains, positively, by helping present specific residues, and negatively, by sequestering them.

4.3 Conformation of Lys^{48}-linked Ub_4

4.3.1 Chemical shift perturbation mapping

Lys^{48}-linked Ub_4 chains have been shown to be the minimal efficient signals for targeting proteins to the proteasome *in vitro*. The X-ray crystallographic studies of Lys^{48}-linked Ub_4 have yielded different conformations of the chains (section 2.1.2), highlighting their inherent interdomain flexibility, and raising the question of whether these chains are structured at all in solution. This issue was addressed by chemical shift perturbation mapping studies on the Ub_4 chains. Segmentally ^{15}N labeled Ub_4 chains were synthesized as described in section 3.2.3. Chemical shift perturbations (Ub_4 vs monoUb, top panels in figure 4.8 a-d) were used to map interfaces between Ub units. At neutral pH, all four Ub domains show perturbations in regions similar to that observed in Ub_2. Although the magnitude of perturbations is smaller at the proximal than at the distal end of the chain, the presence of chemical shift perturbations indicates that the Ub domains are interacting in Ub_4. Hence, Ub_4 chains are structured in solution. In addition, the ^1H T_2 value for Ub_4 (13ms) is twice and four times shorter than that for Ub_2 (23-25 ms) and monoUb (50ms), confirming that Ub_4 chains adopt a relatively compact conformation in solution at neutral pH.

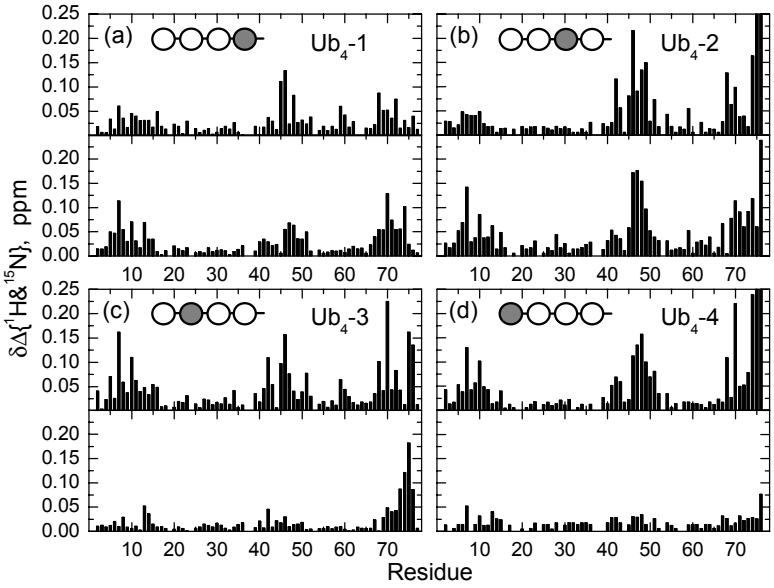

Figure 4.8 Chemical shift perturbations in Ub_4 observed between the four Ub domains in Ub_4 compared to monoUb (top panels in a-d), and corresponding Ub constructs in Ub_2 (lower panels in a-d).

Although the chemical shift data do not provide information about interacting partners in Ub_4, a comparison of chemical shifts in Ub_4 with those observed in Ub_2 provides some insights into the conformation adopted by these chains (lower panels figure 4.8 (a)-(d)). The distal two Ub domains (observed in Ub_4-3 and Ub_4-4), behave very similarly to the corresponding domains in Ub_2. Therefore, in a working model of the conformation of Ub_4, it seems possible that the distal two Ub domains adopt a conformation similar to the closed conformation of Ub_2. The proximal two Ubs show perturbations that are smaller and in a somewhat different pattern than the distal end of the chain. Therefore, it is likely that the proximal two Ub domains form an interface that is less well defined and somewhat different from that formed between the distal Ub domains.

In order to characterize the conformation of Ub_4 chains, attempts were made to measure RDCs in dilute liquid crystalline medium (polyethylene glycol/hexanol

mixture as in the case of Ub_2). However, RDCs could not be measured in the experiments due to very weak alignment of the Ub_4 molecules in the ordered phase. Therefore, alternative experiments that will provide information about either directly interacting residues (NOEs) or long-range orientational information (for example, RDCs from other liquid crystalline media or use of paramagnetic tags to measure anisotropic magnetic susceptibility tensors) will be required to completely characterize the conformation of Ub_4 chains.

4.4 Summary

The results presented in this chapter address the first objective of the present study: to elucidate the solution conformation of Lys^{48}-linked Ub_2 and Ub_4 chains. Under near-physiological conditions, Lys^{48}-linked Ub_2 was shown to adopt a 'closed' conformation that is characterized by an interface similar to, but distinguishable from, the crystal structure of Ub_2. The results also suggest a switch in the conformation of Ub_2, from 'closed' to 'open' states, with decreasing pH of the solution. The interface between the two Ub domains, was shown to be dynamic, with 'opening' and 'closing' motions in the 50 μs-1ms timescale, allowing important hydrophobic residues sequestered at the interface to be potentially available for recognition by various cellular factors. Studies with Ub_4 chains indicate that the distal two Ubs in the chain might adopt a 'closed' Ub_2-like conformation. However, further experiments will be required to determine the conformation of Ub_4 chains.

Chapter 5: Conformation of Lys^{63}-linked Ub_2 chains

5.1 Objective

In the current view of Ub-mediated signaling, diversity in polyUb chain function has been ascribed to the ability of differently linked chains to bind differentially to various effector proteins in the cell[53]. In such a model, it seems reasonable to expect that the differential recognition of different chains arises from linkage-specific differences in polyUb chain conformation. In order to directly test this hypothesis, this chapter is aimed at elucidating the solution conformation of Lys^{63}-linked polyUb chains. The positioning of Lys^{63} on the surface of Ub, almost directly across Gly^{76} at the C-terminus (see figure 2.1) suggests that a Gly^{76}-Lys^{63} linkage between two Ubs should result in an extended chain. Such a conformation would be in contrast with the conformation of Lys^{48}-linked chains determined in the previous chapter. Furthermore, because Lys^{48}- and Lys^{63}-linked chains have been shown to signal for distinct processes in the cell, it is of interest to determine if these chains do adopt distinct conformations in solution.

5.2 Search for interdomain interface in Ub_2 using chemical shift mapping

Segmentally isotope labeled Lys^{63}-linked Ub_2 chains were synthesized and purified as described in Chapter 3. The molecular mass of the purified product was confirmed by MALDI-TOF mass spectrometry (17,304 Da versus 17,307 Da expected). In the first step of characterization of the conformation of Lys^{63}-linked Ub_2 chains, the chemical shift mapping approach was used to identify the interdomain interface in these chains. Chemical shift perturbations observed in the backbone

amide groups between monoUb and Ub_2 in ^{15}N-^{1}H HSQC spectra recorded under identical conditions (20mM Sodium phosphate, pH 6.8) are shown in figure 5.1. No significant perturbations were observed in Ub_2, except in the residues close to the Gly^{76}-Lys^{63} linkage: C-terminal residues of the distal Ub (observed in Ub_2-D) and Lys^{63} and adjacent residues in the proximal Ub (observed in Ub_2-P). This suggests that there is no specific interaction between the two Ub domains in Lys^{63}-linked Ub_2. The lack of inter-domain interactions in Lys^{63}-linked Ub_2 is strikingly different from the results of studies on Lys^{48}-linked chains, where a well-defined interface is observed between the two Ub domains under identical experimental conditions.

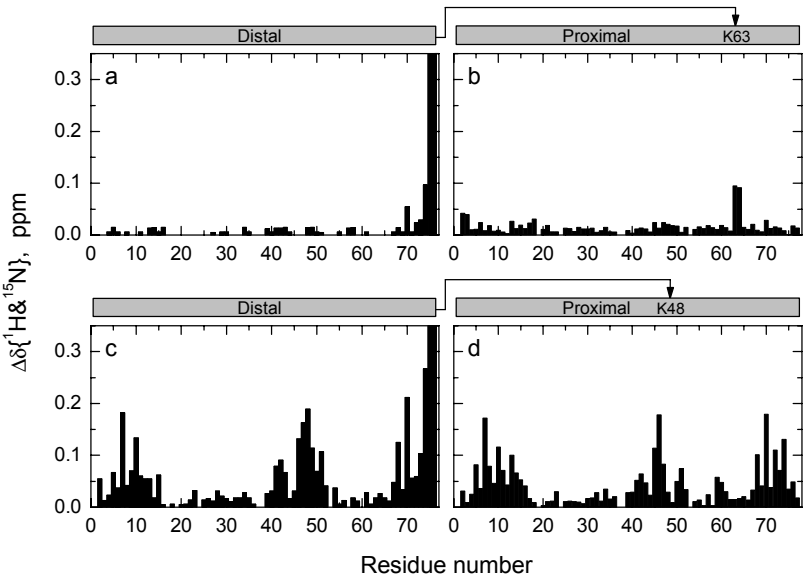

Figure 5.1 Mapping the interface in Lys^{63}-linked Ub_2 Chemical shift perturbations in (a) the distal and (b) the proximal Ub domains in Lys^{63}-linked Ub_2 with respect to monoUb. Panels (c) and (d) show chemical shift perturbations in the same residues in Lys^{48}-linked Ub_2 for comparison. Data is shown for pH 6.8

5.3 Solution structure of Lys^{63}-linked Ub_2

The chemical shift data indicates no interface between the two Ub domains in Lys^{63}-linked Ub_2. However, NMR relaxation parameters measured on Lys^{63}-linked

Ub_2 suggest that despite the absence of a clear interface, the two Ub domains do re-orient together as one entity in solution. The measured ^1H T_2 values for Lys^{63}-linked Ub_2 (26ms) and monoUb (50ms), vary inversely with molecular weight. Similarly, the average ^{15}N T_2 values in Ub_2 (88 ± 6 ms for Ub_2-D and 83 ± 7 ms for Ub_2-P) are approximately twice that measured in monoUb (166 ± 10 ms). Also, the overall correlation times derived for each Ub domain (8.5 ns in Ub_2-D and 8.9 ns in Ub_2-P) suggest a two-fold slower molecular tumbling time compared to monoUb (4.2 ns), in accordance with the molecular weight dependence of the overall tumbling time predicted from Stokes-Einstein-Debye equation. Thus, the two Ub domains reorient together in solution, and their relative orientation can be determined using methods based on the alignment of rotational diffusion and alignment tensors.

The relative orientation of the Ub domains in Lys^{63}-linked Ub_2 chains was determined from molecular alignment in dilute liquid crystalline medium as described in section 3.3. The characteristics of the alignment tensors obtained for the two domains from the measured residual dipolar couplings (RDCs) are shown in table 5.1. The structure of the Lys^{63}-linked Ub_2 obtained by aligning the principal axes frames (PAFs) of the alignment tensors is shown in figure 5.2(a). The structures represent a time-averaged relative orientation of the two Ub domains with respect to each other, and because the method does not provide distance information, the interdomain distance is chosen arbitrarily in the representation shown. Consistent with the chemical shift perturbation data, the structure shows no interactions between the hydrophobic surfaces of the two Ubs.

In order to verify that the conformation derived from the measured RDCs is not biased by interactions with the alignment medium, the relative orientation of the two Ub domains was also determined from the rotational diffusion tensors derived from ^{15}N relaxation parameters. In the absence of any alignment medium, the ^{15}N relaxation parameters (R_1, R_2 and $\{^1H\}$-^{15}N NOE) were measured for both Ub domains, and used to derive their rotational diffusion tensors (table 5.2). The PAFs of these tensors were aligned by rigid body rotation of the two domains to determine their relative orientation. The resulting solution structure representing the average orientation of the two Ub domains is shown in figure 5.2. The structure is in good agreement with that obtained from RDCs, therefore suggesting that the alignment medium does not significantly perturb the conformation of the chains, and confirming the accuracy of the derived structure.

Table 5.1 Characteristics of the alignment tensor for Lys^{63}-linked Ub_2, determined from the residual dipolar couplings measured in each of the two Ub units.

Ub unit	S_{xx}	S_{yy}	S_{zz}	α	β	γ	R
Ub_2-D	-5.5 (0.6)	-7.7 (0.5)	13.3 (0.7)	233 (4)	28 (2)	233 (3)	0.09
Ub_2-P	-4.1 (0.5)	-6.7 (0.7)	10.8 (0.7)	272 (3)	38 (2)	148(11)	0.11

The principal values of the alignment tensor (in Hz) were ordered assuming $|S_{zz}| > |S_{yy}| > |S_{xx}|$. The Euler angles {α,β,γ} (in degrees) characterize the orientation of the principal axes frame of the alignment tensor of Ub_2 with respect to the PDB coordinate frame for each domain. Quality factor R was used to assess the quality of the derived alignment tensor. The validity of the structural data obtained here is justified by the low values of R indicating good agreement between the measured RDCs and those predicted from the structure. The correlation coefficient between the measured and predicted RDCs was 0.982 (distal) and 0.979 (proximal).

Table 5.2 Characteristics of the rotational diffusion tensor for Lys^{63}-linked Ub_2, determined from the ^{15}N relaxation rates measured in each of the two Ub units.

Ub unit	D_x	D_y	D_z	α	β	γ	γ*	τ_c
Ub_2-P	1.49 (0.08)	1.58 (0.09)	2.53 (0.20)	248 (12)	24 (4)	199 (26)	239 (26)	8.92 (0.37)
Ub_2-D	1.72 (0.15)	1.73 (0.14)	2.46 (0.35)	278 (9)	33 (5)	272 (88)	132 (88)	8.46 (0.58)

The principal values of the diffusion tensor (D_x, D_y, D_z) are in 10^7 s^{-1}. Numbers in the parentheses represent standard deviations. The Euler angles {α,β,γ} (in degrees) characterize the orientation of the principal axes frame of the diffusion tensor of Ub_2 reported by each of Ub domains. The angle $\gamma^* = \gamma + 40^o$ is a result of a rotation of the whole Ub_2 molecule by 40^o about the z-axis, which brings the γ values in agreement, within the experimental precision, with those from the RDC data (Table 5.1). This transformation has no effect on the relative orientation of Ub units and merely represents the difference in the orientation of the x,y axes of the alignment and diffusion tensors for Ub_2. The overall rotational correlation time of the molecule, τ_c is in nanoseconds.

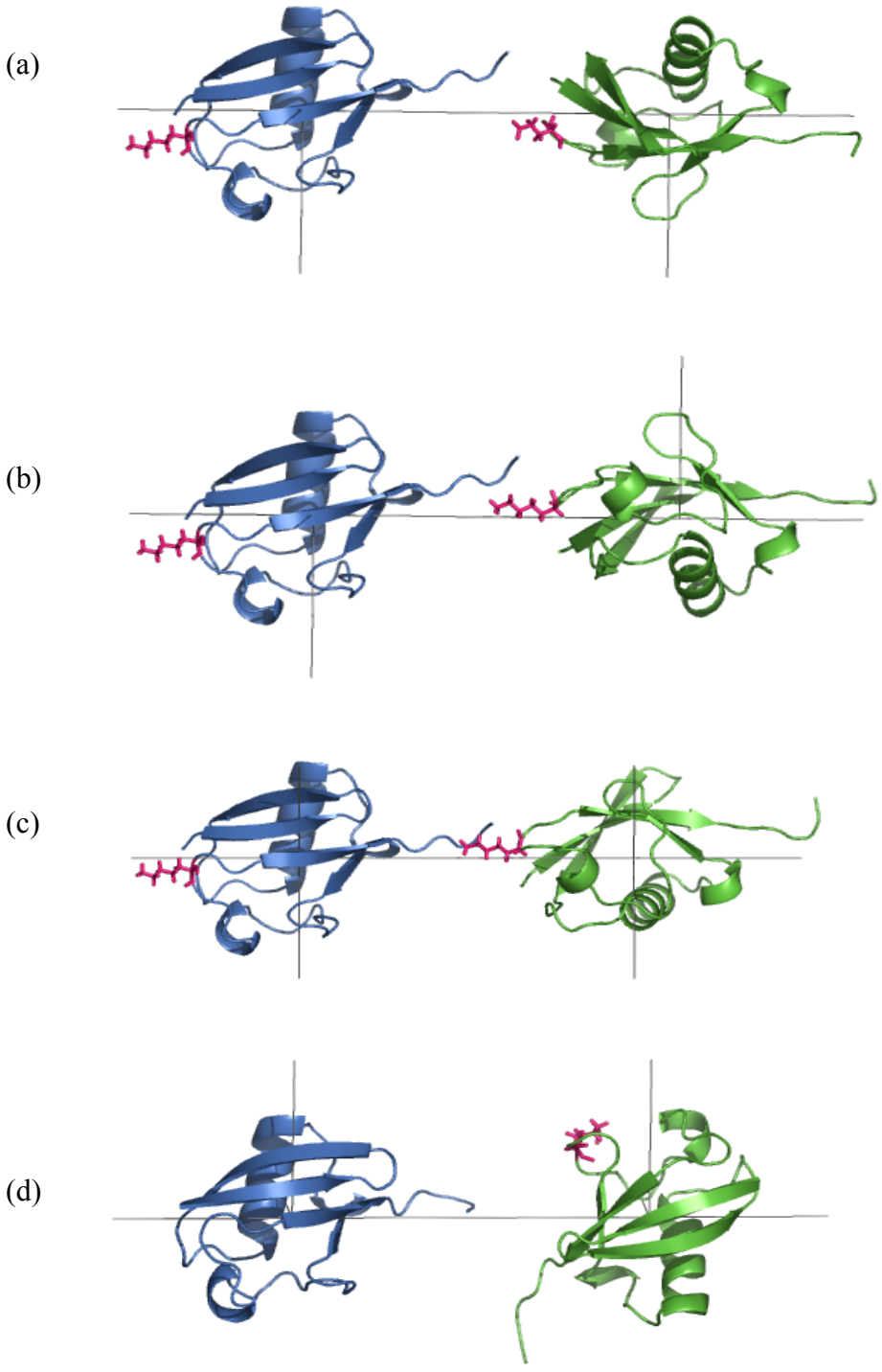

Figure 5.2 Solution conformations of Lys^{63}-linked Ub$_2$ Structures of Lys^{63}-linked Ub$_2$ obtained from RDCs (a and b), and ^{15}N relaxation measurements (c). Panel (d) shows the conformation of Lys^{48}-linked Ub$_2$ derived from RDC measurements for comparison. The distal and the proximal Ubs are shown in blue and green respectively. Residue Lys^{63} on the Ubs is shown in magenta

The flexibility in the Lys^{63}-linked Ub_2 chains is apparent from the measured relaxation parameters. The relaxation data show a decrease in the R_1 and R_2 values in the inter-domain linker in Ub_2 (the four C-terminal residues in Ub_2-D), suggesting the region is flexible, although to a lesser extent than the free C-terminus of Ub_2-P. It is interesting to note that, as in the case of Lys^{48}-linked Ub_2, the diffusion tensor for the distal Ub appears more axially symmetric than that for the proximal domain (hence larger uncertainty in γ angle), suggesting a "twisting" type of motion of the distal domain about the z-axis of the diffusion tensor (that would average the x- and the y-components, and hence make the tensor appear more axially symmetric). The difference in the hydrodynamic behavior of the two domains might be a consequence of the dynamics of the system associated with the nature of the Gly^{76}-Lys^{63} linkage.

Given that the Lys^{63}-linked Ub_2 displays a considerable degree of conformational flexibility, it is relevant to determine if it can adopt a conformation that would allow the two hydrophobic surfaces to come close enough to form a "closed" structure. This issue was addressed by attaching a spin label to one end of the Ub_2 and monitoring its effect in NMR spectra. The presence of an unpaired electron spin on the spin label causes paramagnetic relaxation rate enhancement (and hence signal attenuation) in nearby nuclei without significantly affecting their chemical shifts. The paramagnetic spin relaxation enhancement agent, MTSL (1-Oxyl-2,2,5,5-tetramethyl-3-pyrroline-3-methyl methanesulfonate) was selectively attached to a single Cys in Ub_2 (Cys^{63} in Ub_2 synthesized with K63C Ub used as the distal Ub) and its attachment was confirmed by an increase in the mass of Ub_2 by 183 Da (185 Da expected) by MALDI-TOF mass spectrometry. Also, residues around

Cys^{63} in Ub_2-D showed attenuation in signal intensities, indicating the correct positioning of the MTSL moiety. If the Lys^{63}-linked Ub_2 molecules adopt a conformation, such as in figure 5.2 (a-c), residues in the proximal Ub will come in close proximity of the modified Cys and experience signal attenuation due to paramagnetic relaxation rate enhancement. However, no such effect was observed in spin-labeled Ub_2-P samples (figure 5.3a). In a control experiment, attachment of MTSL to the distal Ub (K48C mutant) in Lys^{48}-linked Ub_2 resulted in strong attenuation of NMR signals in the proximal Ub (figure 5.3b). Thus, the Lys^{63}-linked Ub_2 chains do not adopt a conformation that allows the proximal Ub to come in close proximity of Cys^{63}. The results also support the extended conformation of the chains determined above.

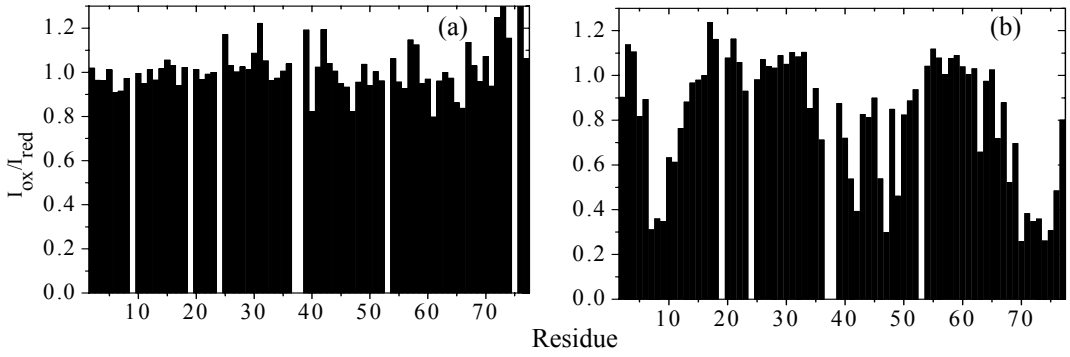

Figure 5.3 Effect of spin-labeling the distal Ub in Ub_2 Signal attenuation observed in the proximal Ub in (a) Lys^{63}-linked Ub_2 and (b) Lys^{48}-linked Ub_2. The attenuation is calculated as the ratio of signal intensities in the presence of oxidized and reduced MTSL. The MTSL moiety was attached to a single Cys residue in the Ub_2 constructs, Cys^{63} and Cys^{48} in the distal Ubs of Lys^{63}- and Lys^{48}-linked Ub_2 respectively.

5.4 Comparison with Lys^{48}-linked Ub_2 chains

In the previous chapter, Lys^{48}-linked Ub_2 chains were shown to predominantly adopt a closed conformation under near-physiological conditions. In this closed conformation, hydrophobic residues (Leu^8, Ile^{44} and Val^{70}) implicated in the

proteasomal recognition of polyUb chains, are sequestered at the interface between the Ub domains. However, the conformation of the Lys^{63}-linked Ub_2 chains determined here is in striking contrast with that of Lys^{48}-linked Ub_2. The results discussed in this chapter show that under identical experimental conditions, Lys^{63}-linked Ub_2 chains adopt an extended conformation, fully exposing the hydrophobic patch on the surface of both Ub domains. This result provides the first experimental evidence that alternatively linked polyUb chains adopt distinct conformations in solution.

In Lys^{63}-linked chains, the hydrophobic surfaces on the Ub domains should be readily accessible for interacting with Ub-binding proteins. To a first approximation, the two Ubs in Lys^{63}-linked Ub_2 should be able to independently interact with all proteins that recognize the hydrophobic surface of Ub. On the other hand, in Lys^{48}-linked Ub_2, such an interaction with hydrophobic residues would require an 'opening' of the interface. The next chapter explores how these linkage-specific differences in conformation could modulate specific recognition of polyUb chains.

Chapter 6: Interactions of polyUb chains with UBA domains

6.1 Background and objectives

The hypothesis being tested in this dissertation postulates that functional diversity in polyUb signaling arises from the ability of differently linked polyUb chains to bind differentially to various effector proteins in the cell. In this model, alternatively linked polyUb chains are recognized differentially due to linkage-specific differences in their conformations. The results presented in the two preceding chapters strongly argue in favor of this view: under identical experimental conditions at near-physiological pH, Lys^{48}- and Lys^{63}-linked chains adopt distinct conformations. It is then crucial to understand exactly how these alternate conformations are differentially recognized by Ub-binding proteins. For example, it is still unknown if linkage-specific recognition of polyUb chains arises from differential display of the hydrophobic surfaces, or from the recognition of linkage-specific conformational features (in addition to/or the hydrophobic surfaces).

A number of Ub-binding proteins that transmit the regulatory information conferred by (poly)ubiqutination have been identified. Most of these effector proteins are characterized by modular architecture comprising one or more ubiquitin-binding domains and other domains that mediate specific functions. Several recent studies that have elucidated the mode of interaction of UBA and other Ub binding domains with monoUb were reviewed in Chapter 2. In all these interactions, ubiquitin associates via its hydrophobic patch (comprising Leu^{8}-Ile^{44}-Val^{70}), with a corresponding conserved

hydrophobic surface on the binding partner. With polyUb chains potentially presenting a multiplicity of such hydrophobic surfaces for binding, the interactions could presumably involve cooperative mechanisms that will need to be elucidated before the molecular basis of linkage-specific signaling by polyUb chains is understood.

A prominent member of ubiquitin-binding domains is the UBA (Ub-associated domain), a small domain ~40 residues that form a 3-helix bundle. The structure of the two UBA domains from hHR23A (the human homolog of yeast Rad23A, a protein involved in the *Rad6* pathway for DNA repair), and their mode of interactions with monoUb have been shown by other groups, and were described in Chapter 2. Recent biochemical binding studies (GST-pull down assays and surface plasmon resonance) have shown that the UBA(2) domain from hHR23a binds Lys^{48}-linked polyUb chains in strong preference to Lys^{63}- and Lys^{29}-linked chains[27, 54]. Therefore, determination of the mode of interaction of this UBA(2) domain with Lys^{48}- and Lys^{63}-linked polyUb chains will provide insights into how the conformation of different polyUb chains modulates their recognition.

6.2 Interaction of UBA domain with monoUb

The UBA(2) construct used in this study (GST-fused clone obtained from CP), carries an N-terminal linker sequence (Gly-Ser-Ala-Ala-Ala-Gln-Val) absent in the UBA domains that have been used in previously reported studies. Ryu et al mapped the interacting surfaces on monoUb and UBA(2) domain from hHR23B [37], and Mueller and coworkers modeled the UBA2 (from hHR23A) with yeast Ub [20].

Therefore, prior to the analysis of UBA(2) binding to Ub_2 and Ub_4 chains in this study, the monoUb-UBA(2) interaction was characterized.

6.2.1 Interacting surfaces on monoUb and UBA(2)

The binding sites on both UBA(2) and monoUb were mapped by monitoring backbone amide chemical shifts in NMR titrations performed as a series of ^{15}N-^{1}H HSQC experiments. The protein under observation (UBA(2) or monoUb) was ^{15}N labeled and the corresponding unlabeled binding partner was titrated into solution. Typically, starting protein concentrations were 0.8-1mM, and the titration was continued until a saturation of spectral changes was observed (at ligand:protein ratios > 3:1).

Significant chemical shift perturbations were observed in both UBA(2) and monoUb (figure 6.1), indicating the formation of a well-defined interface between the two proteins. A single set of resonances was observed for each of the proteins in the HSQC spectra with no attenuation in signal intensities, suggesting the bound and free protein states were in fast exchange on the NMR timescale. Observation of fast exchange indicates the complex was rapidly dissociating and re-associating. As seen in figure 6.1, the binding epitope on monoUb is formed by the hydrophobic patch comprising Ile^{8}, Leu^{44}, and Val^{70} and the nearby sites on the Ub surface. On the UBA2 domain, the major perturbations are located in residues comprising the loops 1 and 2 connecting the helices, helix3 and the C-terminal region. In addition, Gln^{339} and Phe^{342} (helix2) display combined chemical shifts changes greater than 0.1 ppm at saturation. Based on comparison with the modeled structure of the UBA-Ub complex [20], description in section 2.2.2), and the UBA(2)-Ubl (Ub-like domain from Rad23)

interaction, the latter effect is likely caused by a binding-induced rearrangement of the hydrophobic core of UBA. The UBA-monoUb binding interface observed here is consistent with that reported for related protein constructs [37, 55].

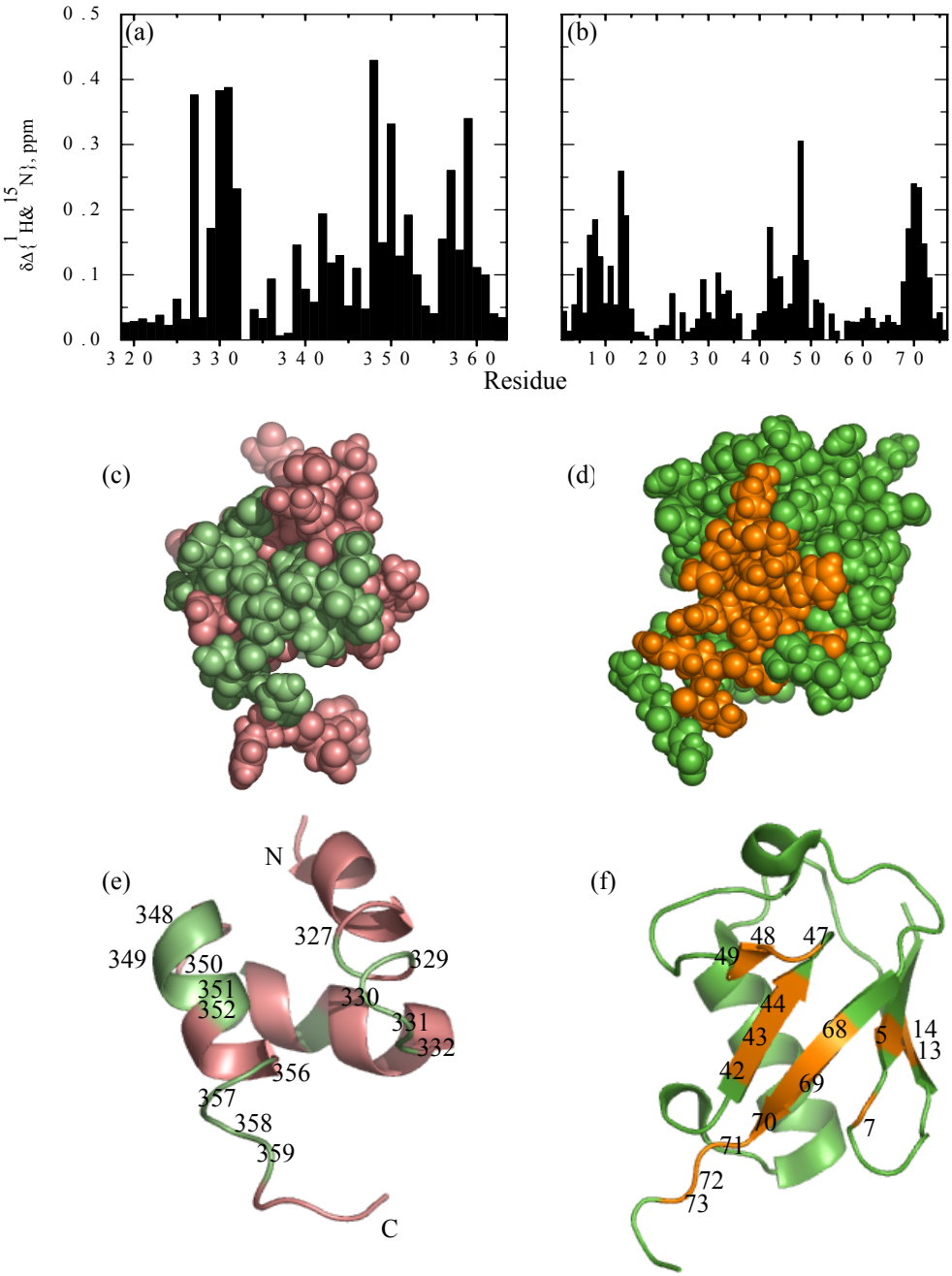

Figure 6.1 Mapping the UBA-monoUb interface Chemical shift perturbations observed in the backbone NH groups of (a) UBA(2) domain and (b) monoUb at final points in titration experiments. The perturbed residues are mapped on the surfaces of (c) UBA(2) and (d) monoUb. UBA(2) is colored in pink, and perturbed residues are in lime, monoUb is shown in green and perturbed residues are shown in orange. Panels (e) and (f) show ribbon representations of the two proteins in the same orientation as in panes (c) and (d) for reference. Coordinates of UBA(2) and Ub are from 1DV0.pdb and 1D3Z.pdb respectively.

6.2.2 Stoichiometry and affinity of binding

Knowledge of the stoichiometry of the UBA(2)-monoUb complex is necessary to characterize the complex, and to estimate the affinity of binding. Determination of the molecular weight of the complex by methods such as native gel electrophoresis and analytical ultracentrifugation were not successful due to aggregation of the proteins in solution. However, the observation of a contiguous binding site on both UBA(2) and monoUb, and comparable surface areas of the binding surfaces on both proteins (254.5 $Å^2$ for UBA(2) and 255.2 $Å^2$ for Ub) suggests a 1:1 stoichiometry of binding. A more accurate estimate of the molecular weight of the complex was made using ^{15}N longitudinal relaxation experiments. The longitudinal relaxation time (T_1) is a sensitive indicator of the overall tumbling rate, which is directly related to the size of the molecule under observation. A molecular weight calibration curve was plotted using measured ^{15}N T_1 values for free monoUb, Ub_2 and Ub_4 constructs (figure 6.2a). The average ^{15}N T_1 value for the UBA(2)-monoUb complex was 547 ± 42 ms corresponding to a molecular weight of 13 ± 1 kDa (compared to 14.3 kDa expected for a 1:1 UBA:Ub complex), consistent with the formation of a 1:1 (UBA(2):Ub)complex.

The apparent dissociation constant (K_d) of the binding event was calculated from the titration curves (representative curves shown in figure 6.3). The chemical shift perturbations observed as a function of increasing ligand concentration were fit to a 1:1 binding model (procedure described in Section 3.5), yielding an average K_d of 0.4 (±0.1) mM from perturbations in UBA(2). In experiments with ^{15}N-labeled monoUb, into which UBA(2) was titrated, the fit yields an average K_d of 0.3 (± 0.3)

mM. These K_d values indicate a relatively weak interaction, and are similar to those reported by other groups: 0.36 mM for Ub binding to UBA(2) from hHR23B [37] and 0.5-0.6 mM for yeast Ub interaction with UBA(2) from hHR23A [55].

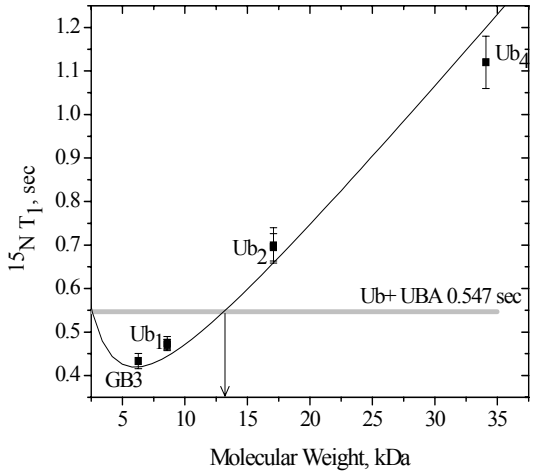

Figure 6.2 Estimation of molecular weight from ^{15}N relaxation times The solid curve represents the theoretical dependence of ^{15}N T_1 on molecular weight, calculated as described in section 3.5.From the measured value of ^{15}N T_1 of 547 ± 42 ms, the molecular weight of the monoUb-UBA(2) complex was estimated to be 13 kDa.

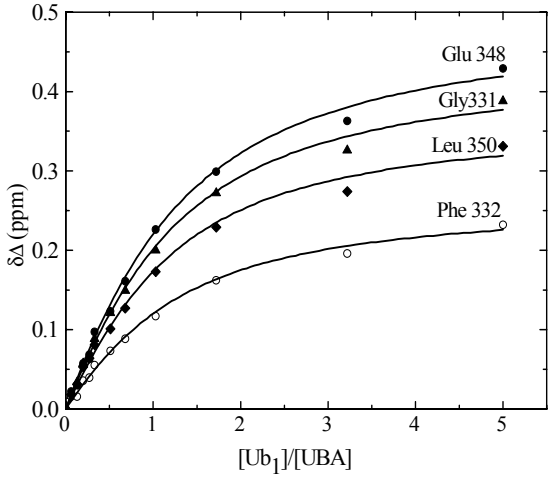

Figure 6.3 Titration curves for the UBA(2) domain Combined amide chemical shift perturbations observed in residues 331, 332, 348 and 350 in UBA(2) during titrations with monoUb, plotted as a function of [Ub]/[UBA] molar ratios. The solid lines represent the data fit to a 1:1 model of binding.

6.2.3 Spin-labeling studies on the UBA-monoUb complex

While chemical shift mapping gives an accurate description of the binding interfaces, it does not provide information about the pair-wise interactions or the relative orientation of the proteins in the complex. In a recent study, Mueller and coworkers[21] proposed structures for the UBA-monoUb complex based on chemical shift perturbations–driven protein docking and homology modeling based on the NMR structure of a related CUE-Ub complex [27] (reviewed in Chapter 2). The docked structure of the monoUb-UBA(2) complex differs from the homology model by a 45^{o} rotation in the relative orientation of the proteins. Although both structures appear to be generally consistent with the chemical shift perturbations, neither has been validated experimentally.

In the present study, site-directed spin labeling was used to asses the modeled structures of the UBA(2)-monoUb complexes. A paramagnetic spin label (methane thiosulfonate nitroxide radical, MTSL) was covalently attached to a Cys residue on one of the two proteins, and its effect on both Ub and UBA(2) was measured. Both UBA(2) and Ub contain a single Cys (Cys^{344} in UBA(2) and Cys^{48} in the K48C Ub mutant), and hence are ideally suited for these studies. Attachment of MTSL to either Ub or UBA(2) resulted in attenuation in signal intensities in both proteins. A comparison of the positions of amide resonances in the absence and in the presence of the spin label (both in the oxidized and in the reduced state) indicated that MTSL moiety did not significantly perturb the UBA-Ub interaction. The pattern of attenuation observed in both UBA(2) and Ub was mapped onto both the modeled structures of the UBA(2)-Ub complex (figure 6.4). Although the location of the

attenuated sites in both proteins in the presence of MTSL is generally consistent with both proposed structures, the docked structure (figure 6.4(a)) appears in a better qualitative agreement with the data.

Since the effect of paramagnetic relaxation enhancement is distance-dependent, the observed attenuation in signal intensities can be used to derive structural information on the complex. Signal attenuations were converted into distance constraints between the amides and the spin label, which were then used to reconstruct the position of the spin label (described in section 3.7). The results for the case when MTSL was attached to Ub are shown in figure 6.4. As control, the position of the spin label on Ub was calculated from the signal attenuations observed in spin-labeled Ub to be 4.75Å from C_β of residue Cys^{48} (the site of MTSL attachment), in very good agreement with its expected location. The signal attenuations in UBA(2) were then used to determine the position of the same spin label as "seen" by UBA(2). This analysis was done for both docked and homology-modeled structures of the Ub-UBA(2) complex. A comparison of the location of the same spin label "seen" by both domains (figure 6.4) indicates that the docked structure is in better agreement with the experimental data. Although the agreement is not perfect, the 5.6 Å distance between the MTSL positions "seen" by Ub and UBA(2) (versus 10 Å for homology modeled structure) could reflect the precision of the SL positioning due to its inherent flexibility, the on-off dynamics in the complex, and the experimental errors. It is also possible that the relative orientation of the proteins in the docked structure slightly deviates from their actual orientation.

(a)

(b)

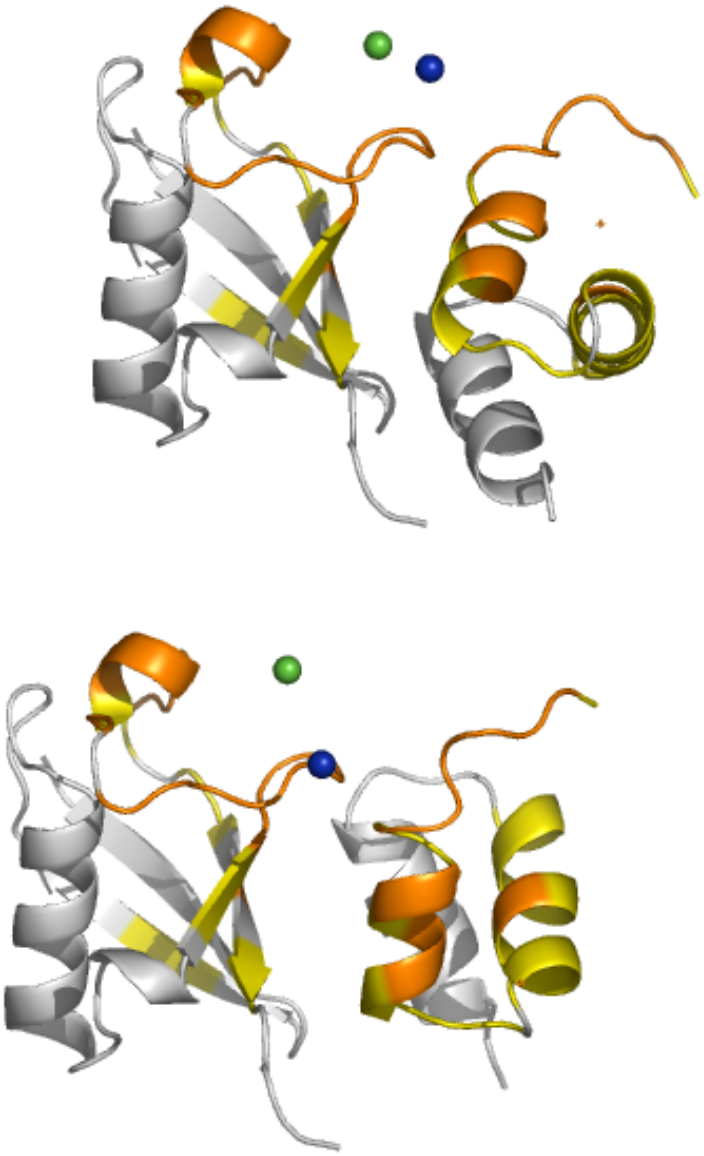

Figure 6.4 Spin labeling experiments to validate models of the UBA-monoUb interaction The paramagnetic spin label MTSL was attached to Cys^{48} on Ub. The pattern of attenuation observed on both the proteins is shown in the following color scheme: residues that experience >50% signal attenuation are colored in orange, and those that experience up to 30% attenuation are shown in yellow. The position of the spin-label as 'seen' by Ub and the UBA(2) domain are shown as green and blue spheres respectively. Panel (a) shows mapping the results of the spin-labeling experiments on the docked structure [20] of the UBA-monoUb complex. Mapping of the results on the structure based on the structural homology of UBA and CUE domains [20] is shown in panel (b). The results of the spin-labeling experiments are in better agreement with the structure of the complex modeled by docking (panel(a)) than the homology-based model (in panel (b)).

A similar analysis was also performed when UBA(2) was spin-labeled. The results were also consistent with the structure Ub-UBA(2) complex but less definitive in terms of discriminating between the docked and homology-modeled structures. This is because Cys^{344} on UBA(2) is located farther away from Ub and in a position which makes the attenuation pattern observed in Ub less sensitive to the two orientations of the UBA(2) domain proposed in the modeled structures.

Thus, the UBA(2)-monoUb complex is characterized by a weak 1:1 complex (K_d~0.3-0.4 mM). Although the docked model of Mueller and coworkers is in better agreement with the spin-labeling data discussed above, determination of the exact structure of the complex will require more extensive experiments that will provide information (for example NOEs) on pair wise interacting residues in the two proteins. However, since this study was principally aimed at understanding the interactions of differently linked polyUb chains with UBA(2) domains, the structure of the UBA(2)-monoUb complex was not rigorously determined.

6.3 Interaction of Lys^{63}-linked Ub_2 with UBA(2) domains

6.3.1 Mapping the UBA(2)-Ub_2 interaction sites

In the preceding chapter, Lys^{63}-linked Ub_2 chains were shown to adopt an extended conformation in solution. The extended conformation allows the hydrophobic surfaces on the two Ub domains to be readily accessible for ligand binding, such that the two Ub domains might be expected to bind ligands independently, and in a mode similar to that of monoUb. To verify this model, the interaction of UBA(2) with Lys^{63}-Ub_2 was characterized.

The binding sites on UBA(2) and Lys^{63}-linked Ub_2 were identified by chemical shift perturbation mapping. Backbone amide chemical shifts were monitored in a series of ^{15}N-^{1}H HSQC spectra recorded on samples with ^{15}N labeled protein (UBA(2), Ub_2-D or Ub_2-P) with increasing amounts of the binding partner (Ub_2 or UBA(2)) in solution. Significant backbone amide perturbations were observed in both domains of Ub2 and the UBA(2) domain, suggesting the formation of a specific complex (figure 6.5 a and b). In Ub_2, both domains showed an increase in perturbations with increasing UBA(2) concentrations, and saturation in the changes was observed at a molar ratio [UBA/Ub_2] >5. Chemical shift changes in both Ub domains are clustered around Leu^{8}-Ile^{44} and Val^{70}, suggesting that as expected, the interaction is mediated by the hydrophobic patch on Ub. In addition to chemical shift changes, several residues (marked in figure 6.5 a,b) in the proximal Ub exhibited line broadening, suggesting the binding occurred in the intermediate exchange regime on the NMR timescale. On the other hand, although the magnitude of chemical shifts was slightly higher in the distal Ub, no line broadening was observed upon titration of UBA(2). The onset of intermediate exchange observed in the proximal Ub could be caused by slower off-rates of UBA(2), and suggests a tighter association of UBA(2) with the proximal Ub (see also determination of binding affinities below). Nevertheless, considering both chemical shift perturbations and signal attenuation, the sites involved in UBA(2) binding, directly or indirectly, are similar for both Ub domains. Moreover, the perturbation maps for both Ub domains are similar to that observed for monoUb binding to UBA(2). In addition, the directions of peak shifts in the HSQC spectra acquired during the titration were compared between the distal and

proximal Ub domains and monoUb. Since shifts in the ^{15}N and ^{1}H coordinates reflect changes in the local environments of the ^{15}N and ^{1}H nuclei, they are sensitive indicators of local perturbations in protein structure due to binding. The directions of peak shifts observed on addition of UBA(2) were almost identical in both the Ub domains and in monoUb, suggesting that each of the Ub domains binds UBA(2) similarly, and in a mode similar to the monoUb-UBA(2) binding.

Mapping of the Ub_2 binding site on UBA(2) is shown in figure 6.5(c). The residues perturbed on Ub_2 binding include Leu^{327}, Ala^{329}-Phe^{332} (in loop1 connecting helices 1 and 2), and Glu^{348}-Ala^{352}, and Leu^{356} in helix 3 of UBA(2), forming an epitope shown in figure 6.5(e). Chemical shift perturbations were also observed in Phe^{342}, Gln^{339} and Leu^{336} in helix 2, as in the case of monoUb-UBA(2) binding. The perturbed residues in helix 2 lie on the "back side" of UBA(2), therefore, the perturbations could be caused by an indirect effect of structural rearrangements in UBA on binding Ub. A comparison of the chemical shifts observed in UBA(2) on binding monoUb and Lys^{63}-linked Ub_2 shows no additional residues in UBA(2) to be involved in binding. This observation rules out the possibility that one UBA(2) domain binds to both the distal and proximal Ubs at the same time, forming an Ub-UBA-Ub "sandwich" complex.

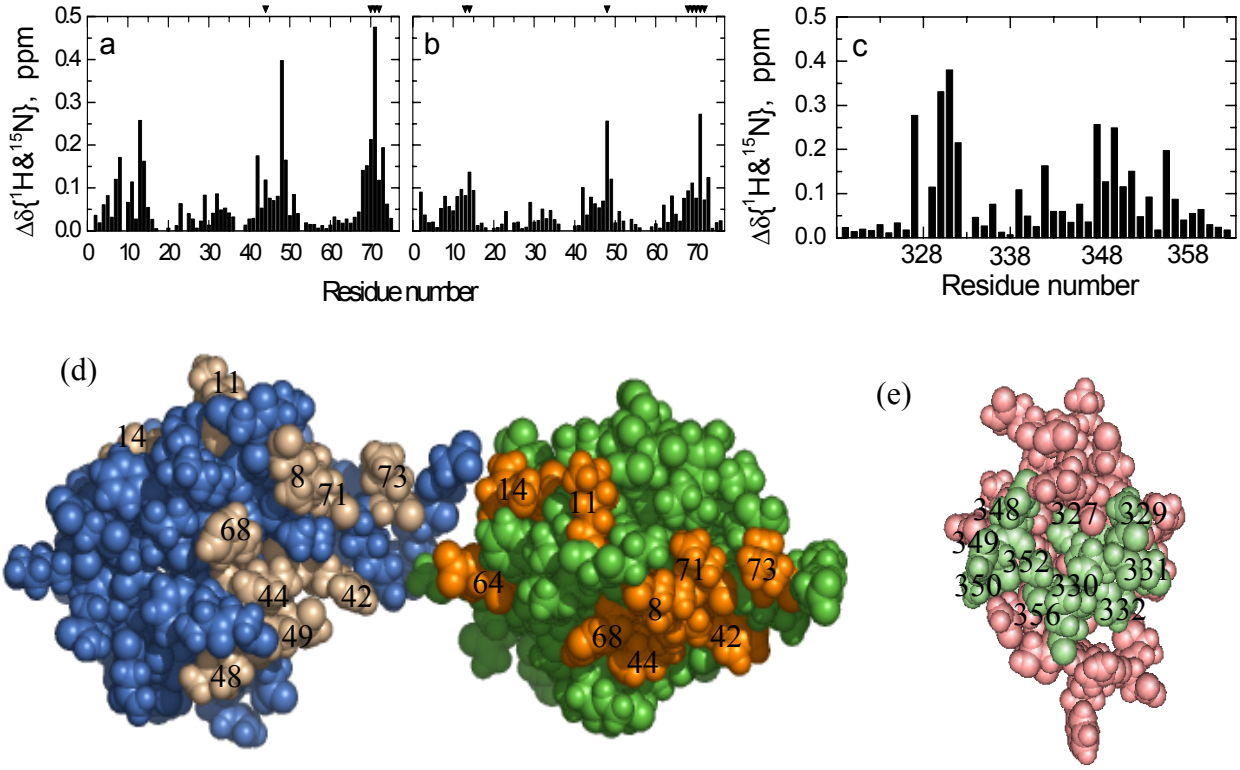

Figure 6.5 Mapping the UBA-Ub$_2$ (Lys^{63}-linked) interaction sites Chemical shifts observed in the backbone amide groups in the (a) distal (b) proximal Ub domains of Lys^{63}-linked Ub$_2$, and (c) in UBA(2) domain. Panels (d) and (e) show the proteins in surface representations with the following color scheme: distal Ub in blue, proximal Ub is in green, and UBA(2) domain is in pink. Perturbed sites on the proteins are colored in wheat, orange and lime. The structure of the Lys^{63}-linked chain is the same as shown in figure 5.2c, coordinates of UBA(2) are from 1DV0.pdb. Residues marked with triangles in panels (a) and (b) show signal attenuation >30% on binding UBA(2).

6.3.2 Stoichiometry and affinity of binding

The molecular weight of the Lys^{63}-linked Ub$_2$-UBA(2) complex was estimated from ^{15}N longitudinal relaxation experiments. ^{15}N longitudinal relaxation times (T_1) in Ub$_2$ were measured at the last points of the titration, when a saturating amount of UBA(2) was present in solution, and an average ^{15}N T_1 was obtained by excluding residues in the flexible loops and C-terminus of Ub. The apparent molecular weight of the complex was then determined from the calibration curve

(figure 6.6). For the Lys^{63}-linked Ub_2-UBA(2) complex, an average ^{15}N T_1 value of value of 956 ± 7 ms was measured, corresponding to an apparent molecular weight of ~26 kDa. This molecular weight is slightly larger than what is expected for a 1:1 Ub_2:UBA complex (23 kDa) and slightly smaller than that expected for a 1:2 Ub_2:UBA complex (29 kDa), and therefore represents a partitioning between 1:1 and 1:2 complexes in solution. In addition, the average ^1H transverse relaxation times (^1H T_2) measured at high Ub_2:UBA ratios (1:6 and 1:10) were measured to be in the range of 14-16 ms. This value is in good agreement with the 15 ms expected for a 1:2 complex and shorter than 19 ms expected for a 1:1 complex based on the inverse dependence of T_2 on molecular weight seen in monoUb, Ub_2 and Ub_4 in Chapter 4. These results suggest the stoichiometry of the Lys^{63}-linked Ub_2-UBA(2) complex is 1:2 (Ub_2:UBA).

The titration curves (figure 6.7) were used to extract the apparent dissociation constant (K_d) as described in section 3.6. Titration curves in both Ub domains were observed to be hyperbolic, suggesting the binding of UBA(2) to each domain was a independent, non-cooperative event. With a 1:2 stoichiometry (Ub_2:UBA) of the complex, assuming that the two UBA(2) molecules bind independently to a Ub domain each, microscopic dissociation constants of 0.28 ± 0.1 mM for the distal Ub, and 0.18 ± 0.08 mM for the proximal Ub were obtained, comparable with the monoUb-UBA(2) interaction (0.3-0.4 mM). The predicted macroscopic binding constant, $K_d/2$, is therefore in the range 0.14-0.09 mM, slightly lower than that observed for the monoUb-UBA(2) interaction. These results agree well with GST-pull down experiments[27, 54] that suggest a detectable preference of UBA(2)

domain for Lys^{63}-linked Ub_2 over monoUb. The K_d was also determined from titration curves for UBA(2) when Ub_2 was added into solution. Fitting the data assuming a 1:2 (Ub_2:UBA) model resulted in an average K_d of 0.21± 0.1mM, in good agreement with the values obtained from the Ub domains in the complex.

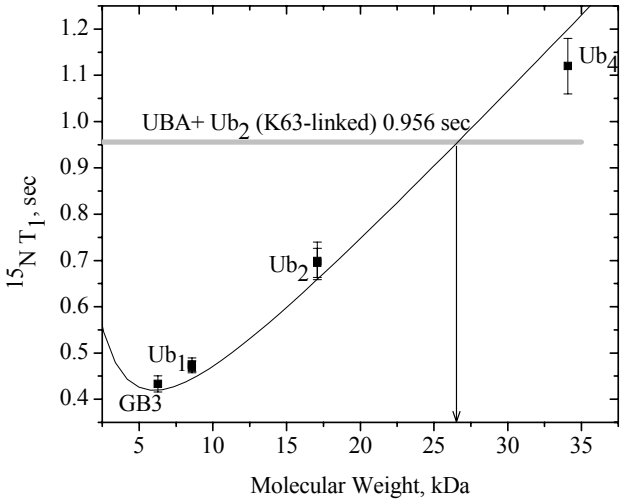

Figure 6.6 Molecular weight estimation of the UBA-Ub_2 (Lys^{63}-linked) complex The solid curve represents the theoretical dependence of ^{15}N T_1 on molecular weight, calculated as described in section 3.5.From the measured value of ^{15}N T_1 of 956 ± 7 ms, the molecular weight of the UBA(2)-Ub_2 complex was estimated to be 26 kDa, corresponding to a 2:1 UBA:Ub_2 complex

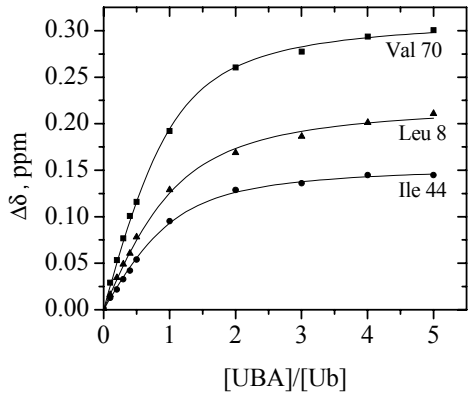

Figure 6.7 Titration curves for the UBA-Lys^{63}-linked Ub_2 interaction Combined amide chemical shift perturbations in residues 8,44 and 70 in the distal Ub in Lys^{63}-linked Ub_2 on titration of UBA(2) plotted as a function of increasing UBA(2) concentrations. The solid curves represent the data fit to a 2:1 UBA:Ub_2 mode of binding.

6.3.3 Modeling the UBA-Ub_2(Lys^{63}-linked) complex

The results discussed above show that the UBA(2)-Lys^{63}-linked Ub_2 interaction occurs via the hydrophobic patches on the surfaces of the Ub domains, and in a mode similar to that of the UBA(2)-monoUb interaction. The results also suggest that the hydrophobic surfaces on the two Ub domains present non-interacting binding sites for UBA(2) domains, such that two UBA(2) domains could bind the chain. The Ub_2-UBA(2) interaction was modeled to understand if simultaneous binding of two UBA(2) domains to Ub_2 was sterically feasible. The docked structure of the UBA(2)-monoUb complex, from Mueller and coworkers [21], was used to model the interaction of the individual Ub domains with UBA(2). As shown in figure 6.8, the extended conformation of the Lys^{63}-linked Ub_2 chain allows each of the two UBA(2) domains to simultaneously bind the chain. The model is consistent with the chemical shift perturbations observed in Gln^{2} and Glu^{64} (figure 6.5(a)), and >50% line broadening observed for Ile^{13} and Thr^{14}, only in the proximal Ub on addition of UBA(2). These residues are located close to the Gly^{76}-Lys^{63} linkage site and the site of UBA(2) binding on the distal Ub, and therefore could likely be affected by a dynamic effect of the proximal Ub "bumping" into the UBA bound to the distal Ub.

The modeled UBA-Ub_2 complex was also validated using a spin label (MTSL) attached to the single Cys (Cys^{344}) on the UBA(2) domain, and monitoring its effect on the two Ub domains in Ub_2. Significant signal attenuation (>60%) was observed in residues 8-11, 44-49 and 68-75 in both Ub domains. This is consistent with the model of both Ub domains binding to one UBA(2) domain each, as the same residues were attenuated when spin-labeled UBA(2) binds monoUb. In addition,

residues 2-7, 11-15 and 60-67 were attenuated only in the proximal Ub. As shown in figure 6.8, these residues are located facing the UBA(2) bound to the distal Ub. These results are therefore in very good agreement with the proposed model of the UBA-Ub_2 complex. Interestingly, the results of the spin-labeling experiments also favor the Ub_2 conformation shown in figure 5.2(a) over that shown in figure 5.2(b).

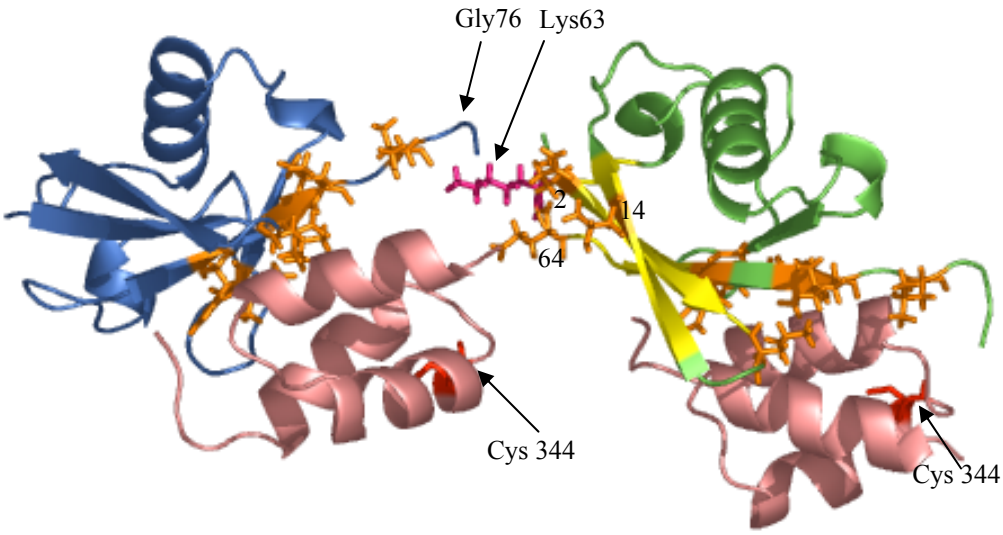

Figure 6.8 Model of the UBA(2) complex with Lys^{63}-linked Ub_2 The UBA(2) domains were modeled on the Lys^{63}-linked Ub_2 structure (from figure 5.2a) according to the docked model of the UBA-monoUb complex. The UBA(2) domains are colored in pink, and perturbed residues are shown in violet sticks. The proximal and distal Ubs are colored in blue and green respectively, with corresponding perturbed residues shown in orange sticks. Residues 2, 14 and 64, perturbed specifically in the proximal domain are marked to show their positioning facing the distal Ub. Cys^{344} on UBA(2) modified with MTSL in spin-labeling experiments is shown in red. The residues that are specifically attenuated in the proximal Ub and not in the distal Ub on addition of spin-labeled UBA(2) are shown in yellow.

6.4 Interaction of Lys^{48}-linked Ub_2 with UBA(2)

6.4.1 Mapping the UBA(2) interaction sites on Ub_2

From the results of studies on the UBA(2)-monoUb and UBA(2)-Lys^{63}-linked Ub_2 complexes, it is apparent that the interaction of UBA(2) with polyUb chains is a

predominantly hydrophobic interaction, involving the Leu^{8}-Ile^{44}-Val^{70} patch on the surface of Ub. In Lys^{48}-linked Ub_2, these residues are sequestered at the inter-Ub interface. However, as seen in section 4.2, the interdomain interface in Lys^{48}-linked Ub_2 is not rigid, such that the Ub_2 is in dynamic equilibrium between "open" and "closed" states. As a result, the hydrophobic residues sequestered at the interface could become available for interactions with other Ub-binding proteins, such as UBA(2) domains. In order to understand why UBA(2) domains bind Lys^{48}-linked Ub_2 chains with higher affinity than Lys^{63}-linked Ub_2 or monoUb, it is necessary to determine if the UBA-Ub_2(Lys^{48}-linked) interaction is mediated by a direct interaction with the hydrophobic surfaces on Ub, or if it involves recognition of a conformational determinant unique to Lys^{48}-linked Ub_2 chains.

The sites on Lys^{48}-linked Ub_2 involved in binding UBA(2) were identified using chemical shift perturbation analysis in ^{15}N-^{1}H HSQC spectra of Ub_2-P and Ub_2-D on titration of unlabeled UBA(2). The chemical shift changes and signal attenuation observed in the two Ub domains are shown in figure 6.9(a-c). The perturbations (shifts and/or attenuations) are clustered in the same regions on both the Ub domains. Specifically, the largest perturbations were observed in the Leu^{8}-Ile^{44}-Val^{70} hydrophobic region, as in the case of monoUb-UBA binding. Strong perturbations were also observed in Ile^{13} and Thr^{14}, located on the β2 strand facing the α-helix; these perturbations were also observed in binding studies with monoUb and Lys^{63}-linked Ub_2, and since they are away from the main binding site, likely reflect rearrangements in the protein core. The data therefore suggest that the interaction with UBA(2) domains involves the same sites in both Ub domains in

Lys^{48}-linked Ub_2 as in monoUb. The presence of specific signal attenuations (in addition to broadening caused by an increase in molecular weight), in contrast to minor attenuations observed in monoUb and Lys^{63}-linked Ub_2, suggests that the binding occurs in the slow exchange regime on the experimental timescale. The shift from fast exchange behavior observed in monoUb and Lys^{63}-linked Ub_2, to the slow exchange regime indicates the formation of a tighter complex, consistent with the tighter binding of UBA(2) to Lys^{48}-linked Ub_2. Detailed analysis of the titrations is discussed in the following sections.

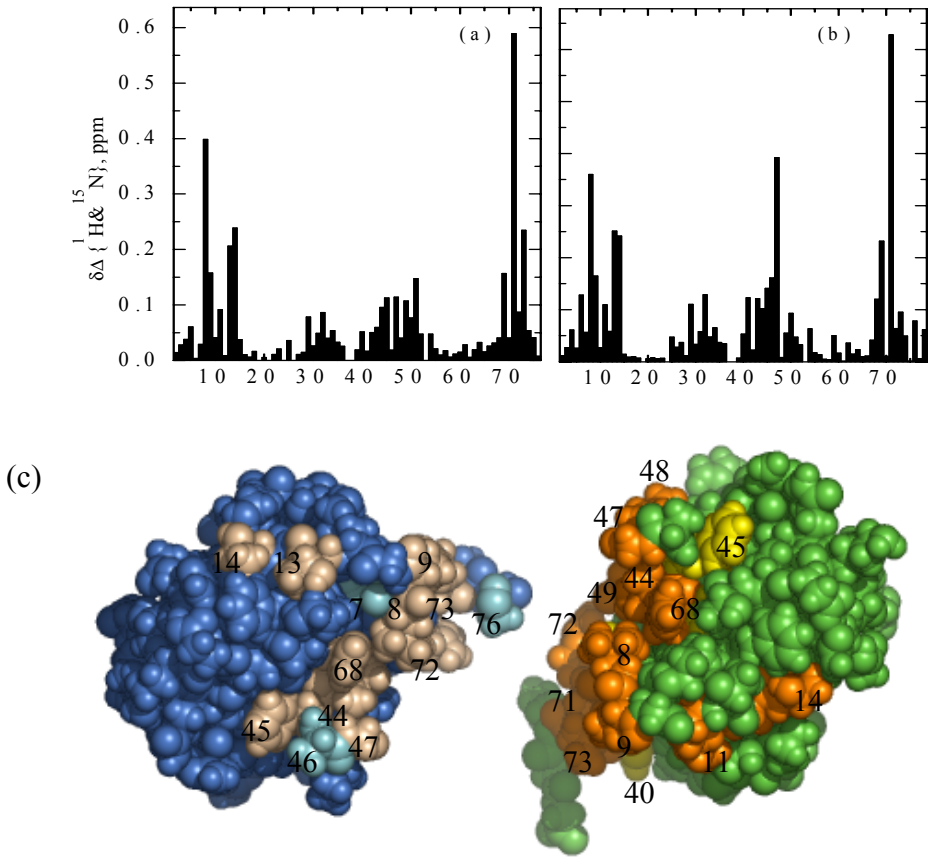

Figure 6.9 Chemical shift perturbation mapping of the UBA(2) interaction sites on Lys^{48}-linked Ub_2 Combined amide chemical shifts in the (a) distal Ub and (b) proximal Ub domain on addition of UBA(2). Panel (c) shows mapping of the perturbed sites on the solution conformation of the Lys^{48}-linked Ub_2. The distal and proximal Ubs are colored in blue and green respectively. The residues on the corresponding domains that show chemical

shifts are colored in wheat and orange, and those that experience signal attenuation (>50%) are shown in cyan and yellow respectively.

Because Lys^{48}-linked Ub_2 exists in equilibrium between "open" and "closed" conformations, it is possible that the observed chemical shift perturbations are caused by an indirect effect of UBA(2) binding a different epitope on Ub_2 that results in a destabilization of the Ub-Ub interface. However, no additional residues are perturbed in either the distal or the proximal Ub in Lys^{48}-linked Ub_2 on addition of UBA(2), compared to monoUb- and Lys^{63}-linked Ub_2. The perturbations are therefore likely a result of direct binding of UBA(2) to these sites. In addition, the directions of shifts of the amide resonances in the HSQC spectra were used as an indicator of the changes in the local electronic environment of the ^{1}H and ^{15}N nuclei. The directions of unit shift-vectors were compared in each Ub unit upon Ub_2-UBA binding with those associated with the transition between the "closed" and "open" conformations of Lys^{48}-linked Ub_2. The latter perturbations were assessed as the difference in chemical shifts between Ub_2 and monoUb. The differences in the shift-vector orientations indicate that the observed changes in Ub_2 are not consistent with a simple shift in the equilibrium towards an open conformation, thus supporting the conclusion that UBA(2) interacts with the hydrophobic patches on the Ub units directly.

Most of the perturbed residues in Ub_2 are located at the interdomain interface in the "closed" conformation of Ub_2 (figure 6.9e). Since these perturbations are caused by the direct binding of UBA(2), the binding event is accompanied (and possibly controlled by) an "opening" of the Ub_2 "closed" conformation that would expose the hydrophobic residues on Ub buried at the interface.

Perturbations in UBA(2) domain were monitored by changes in the ^{1}H-^{15}N HSQC spectra upon titration of unlabeled Ub_2(Lys^{48}-linked) into solution. Saturation in perturbations was observed at molar ratios Ub_2/UBA >1.5. In addition to chemical shift changes, attenuation in signal intensities was also observed, indicative of association-dissociation events in the intermediate exchange regime on the NMR timescale. As pointed out above, transition to the intermediate exchange regime indicates the UBA(2)-Ub_2(Lys^{48}-linked) complex is tighter than the UBA-monoUb and UBA-Ub_2 (Lys^{63}-linked) complexes. The perturbation map of UBA(2) (figure 6.10) shows that, as in the case of binding to monoUb and Lys^{63}-linked Ub_2, perturbed sites are located on loop1 and helix 3. However, significant perturbations are also seen in residues Phe^{342}-Glu^{345} (helix 2). Although smaller perturbations were observed in helix2 in binding studies with monoUb and Lys^{63}-linked Ub_2 (figure 6.5(c)), these residues also experience strong signal attenuation, disappearing at the end of the titrations with Lys^{48}-linked Ub_2. From the titration data alone it is unclear if these perturbations in helix 2 represent sites that directly bind Ub_2, or if they are an indirect result of structural rearrangements in the UBA(2) core (see however, NOE data below).

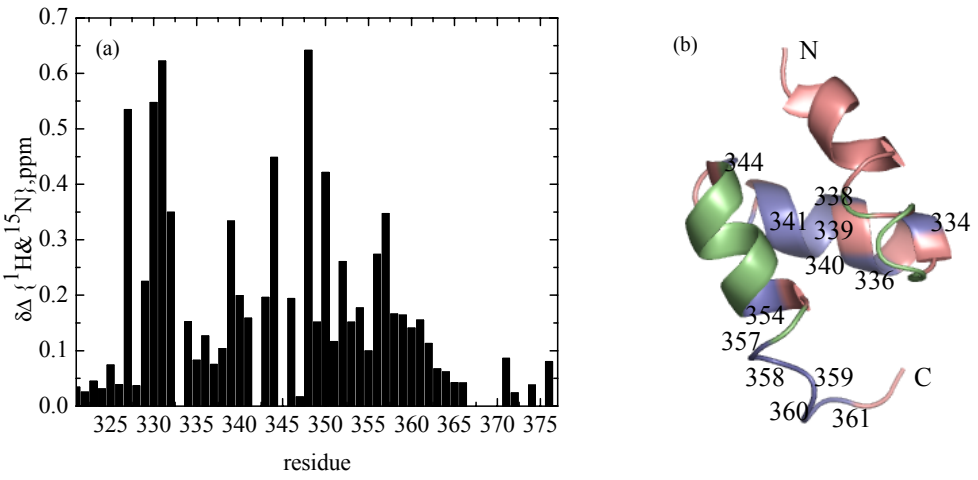

Figure 6.10 Chemical shift perturbation mapping of Ub_2 binding site on UBA(2) domain
Panel (a) shows the combined amide chemical shifts observed in UBA(2) on binding Lys^{48}-linked Ub_2. The perturbed residues are mapped on the surface of the UBA(2) molecule in panel (b). The UBA(2) molecule is shown in pink, the residues perturbed in interactions with monoUb, Lys^{63}- and Lys^{48}-linked Ub_2 are colored green. Residues in blue show chemical shift perturbations only on binding Lys^{48}-linked Ub_2. Coordinates of UBA(2) are from 1DV0.pdb.

6.4.2 Binding of the individual Ub domains to UBA(2)

The chemical shift perturbations suggest that both domains in Ub_2 interact with UBA(2) via their hydrophobic surfaces, as might be expected. Examination of the individual resonances in the two Ub domains during the course of the titration, however, reveals striking differences in the response of the two domains to the addition of UBA(2). In the proximal Ub, almost all residues with significant chemical shift perturbations exhibit slow exchange with the appearance of a second peak corresponding to the bound state starting at a molar ratio Ub_2:UBA of 1:0.4. The original (unbound) resonances of Lys^{48}, Gln^{49}, and Val^{70} completely disappeared by the end of the titration. Thr^{7} and Lys^{11} exhibited an intermediate exchange behavior with signal attenuation >60%, in addition to the attenuation caused by the increased molecular weight of the complex. On the other hand, in the distal domain, the

corresponding residues were observed to be in fast to intermediate exchange. Interestingly, in the distal Ub, these resonances displayed an initial plateau phase and started to shift significantly later in the titration, at molar ratio Ub_2:UBA of 1:1 (or 1:0.8 in some residues). As an example, Figure 6.11 shows a comparison of the behavior of residue 14 in the two Ub domains during the titrations (see also figure 6.16). At the end of the titration (Ub_2:UBA = 1:5) signal attenuations of more than 60% were observed in Thr^{7}, Lys^{11}, Ile^{13}, Thr^{14}, Ile^{44}, Phe^{45}, Leu^{69}, Val^{70}, Arg^{72}, and the C-terminal Gly^{76}, suggesting the onset of an intermediate exchange. Comparison of the behavior of peaks in the two Ub domains (slow exchange in the proximal *vs* fast to intermediate exchange in the distal Ub) therefore suggests that the proximal Ub binds UBA(2) tighter than the distal Ub. This behavior is strikingly different from UBA(2) binding to Lys^{63}-linked Ub_2, where the extended conformation of the chain allows both Ub units to bind UBA(2) independently and in a mode similar to monoUb. Combined with the spectroscopic indication of a tighter binding in the case of the Lys^{48}-linked Ub_2 (intermediate or slow exchange *versus* fast or intermediate exchange in Lys^{63}-linked Ub_2), the data suggest that the conformation of the Lys^{48}-linked Ub_2 might be critical to their higher affinity-binding to UBA(2) domains.

Interestingly, in both Ub domains the signal of Val^{70} was observed to experience perturbations (shift and signal attenuation) at the very early steps in the titration, at UBA:Ub_2 molar ratio as low as 0.4. A similar tendency was also present in the studies of UBA binding to monoUb and to Lys^{63}-linked Ub_2. These observations suggest that Val^{70} might be the primary recognition/binding site for UBA(2). The preference of the UBA(2) domain for the proximal Ub could be

explained by the relative positioning of Val^{70} in the two Ub domains: inspection of the average solution conformation of Lys^{48}-linked Ub_2 shows that the region around Val^{70} is more readily accessible in the proximal than in the distal Ub.

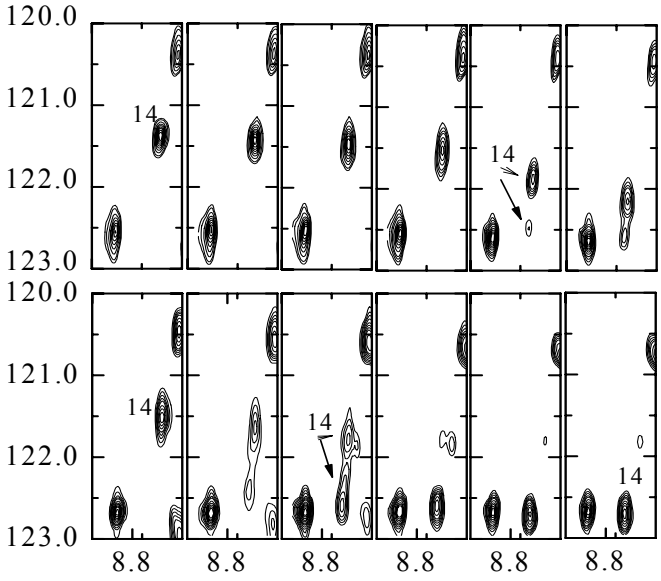

Figure 6.11 Difference in behavior of the distal and proximal Ub on titration with UBA(2) Expanded regions of the ^{15}N-^{1}H HSQC spectra showing behavior of residue 14 on addition of UBA(2). The top panels show the resonance of residue 14 in the distal domain at 1:0, 1:0.4, 1:0.6, 1:1, 1:3 and 1:5 Ub_2:UBA molar ratios during the course of the titration. The bottom panels show the position of residue 14 in the proximal Ub at the same points in the titrations.

6.4.3 Stoichiometry and affinity of binding

The stoichiometry of the UBA-Ub_2(Lys^{48}-linked) complex was determined from an estimation of the molecular weight of the complex using ^{15}N longitudinal relaxation experiments. Early in the titration, at a molar ratio UBA(2):Ub_2 = 0.5, when only the proximal Ub shows chemical shift perturbations, the ^{15}N T_1 values, averaged over residues belonging to Ub core, were measured to be 801 ± 43 ms and 805 ± 35 ms for the distal and proximal Ubs respectively. This corresponds to

molecular weight range from 21-23 kDa, consistent with 23 kDa expected for a 1:1 UBA-Ub_2 complex (figure 6.12). In samples with saturating amounts of UBA(2), the average ^{15}N T_1 values were measured to be 1095 ± 41 ms (distal Ub) and 1118 ± 89 ms (proximal Ub), corresponding to a molecular weight range of 28-34 kDa. These ^{15}N T_1 values are slightly higher, but within experimental errors, from 1030 ms expected for a 2:1 UBA:Ub_2 complex (29 kDa). These results suggest that the stoichiometry of the UBA-Ub_2 complex is 1:1, when only one UBA(2) domain is primarily bound to the proximal Ub, and changes to 2:1 UBA:Ub_2 when UBA(2) is in excess in solution, and a second UBA(2) domain occupies the binding site on the distal Ub.

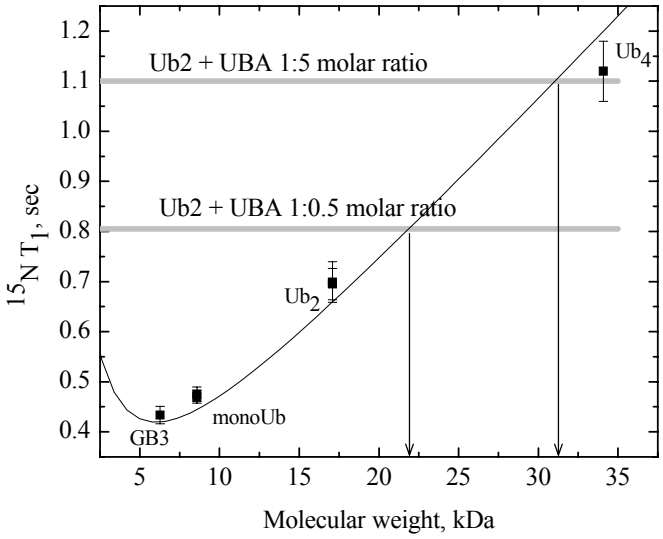

Figure 6.12 Estimation of molecular weight of the UBA-Ub_2 complex The solid curve represents the theoretical dependence of ^{15}N T_1 on molecular weight, calculated as described in section 3.5.From the measured values of ^{15}N T_1 the molecular weight of the UBA(2)-Ub_2 complex was estimated to correspond to a 1:1 UBA:Ub_2 complex. At the end points of the titrations, however, formation of 2:1 UBA:Ub_2 complexes was also observed.

A recent study by Raasi et al [27], using cross-linking experiments and surface plasmon resonance (SPR), suggested that Lys^{48}-linked Ub_2 and Ub_4 chains

bind a single UBA(2) domain, forming a 1:1 UBA:Ub_2 (or Ub_4) complex. The observation of a 1:1 UBA:Ub_2 complex at low molar ratios in the experiments discussed above is in agreement with the results of the cross-linking and SPR experiments performed at identical UBA:Ub_2 ratios. However, the detection of 2:1 UBA:Ub_2 complexes in the longitudinal relaxation experiments at later stages of the titration suggests that mode of UBA(2) binding to Lys^{48}-linked Ub_2 may not be a simple 1:1 interaction. This is also supported by the observations that the proximal Ub appears to bind UBA(2) early in the titration, and significant perturbations in the distal Ub are observed only in the later stages of the titration. It is possible that steric factors associated with immobilization, and lower concentrations (100-300 μM compared to ~3mM UBA(2) at end points of titrations in this study) preclude the detection of larger complexes in the cross-linking and SPR experiments. On the other hand, it is also possible that the relatively high protein concentrations ([UBA(2)] ~ 3mM in solution at end points of the titration) in the NMR experiments force the formation of 2:1 complexes.

The affinity of UBA(2) domains for the Lys^{48}-linked Ub_2 was determined from an analysis of the slow exchange behavior exhibited by residues in the proximal Ub. In the slow exchange regime, the populations of the 'free' and 'bound' species are proportional to the volumes of the resonance peaks; therefore, the titration data can be used to estimate the binding affinity of UBA to the proximal Ub (as described in section 3.6). The signals corresponding to 'free' and 'bound' protein were integrated, and the ratio of the peak volumes was used to calculate the K_d for the UBA-proximal Ub interaction, assuming that a 1:1 UBA:Ub_2 complex is formed up

to molar ratios of 1:1 (UBA:Ub_2) in the titration, and a 2:1 UBA:Ub_2 complex is formed at later stages of the titration. Using this method, the K_d for the UBA-proximal Ub interaction was estimated to be in the range 50-150 μM (Table 6.1).

Table 6.1 Dissociation constants for the UBA(2)-proximal Ub interaction

Residue	K_d (mM)
8	0.1 (0.05)
14	0.05 (0.02)
50	0.14 (0.03)
68	0.18 (0.01)

Mean values of dissociation constants calculated for different residues in the proximal Ub during the titrations are shown above. The numbers in parantheses represent standard deviations.

6.4.4 Intermolecular NOEs in the UBA-Ub_2 complex

In order to detect close contacts between hydrogen atoms in UBA(2) and Ub_2, ^{15}N-filtered NOESY experiments were performed. Unlabeled Ub_2 was added to fully perdeuterated and ^{15}N-labeled UBA(2) at a 1:1 molar ratio in a buffer containing >90% H_2O, thus allowing all amide deuterons in UBA(2) to be exchanged with hydrogens. In these experiments, the intramolecular NOEs between the side chains and the amides in UBA(2) were suppressed by deuteration, and the NOEs within Ub_2 were removed by ^{15}N filtering. As a result, only intermolecular signals originating on hydrogen atoms in Ub_2 and ending on amides in UBA(2) could be detected. The intramolecular amide-to-amide NOEs in UBA were also observed; the latter however did not interfere with the intermolecular side chain to amide NOEs and could be

separated from the intermolecular amide-to-amide NOEs based on the symmetry of the signal pattern. Clear NOE signals were observed between methyl groups in Ub and Leu^{336}, Ile^{338} and Asn^{339} (helix 2), Asn^{349}, Leu^{350}, Ala^{351}, Ala^{352}, Asn^{353} (helix 3), and Asp^{362}, Glu^{363} (C-terminus) of UBA(2). All these residues show chemical shift perturbation in the presence of Ub_2. To verify that these signals are not intra-UBA(2) NOEs due to a less than perfect deuteration, a control NOESY experiment was performed on UBA domain alone prior to adding Ub_2.

The above experimental setup cannot discriminate between the two domains in Ub_2. To determine if these NOEs originated from the proximal or the distal Ub, the same experiment was performed when the Ub_2 construct added to UBA(2) was perdeuterated on the distal Ub (1:1 molar ratio UBA:Ub_2). In such an experiment, the only detectable intermolecular NOEs are those originating from the proximal Ub. Only the side chain-to-amide NOEs to helix 2 listed above, and to Ala^{352} and Asn^{353} on helix 3 were observed, providing evidence for direct interactions between these residues of UBA(2) and the proximal Ub. In order to assign these NOEs, a ^{15}N-edited TOCSY experiment that allows observation of connectivities in side-chains in the proximal Ub, was performed on the same sample. The NOEs observed to amides of Leu^{336}, Ile^{338} and Asn^{339} (helix2 of UBA(2)) were thus assigned as originating from side chain of Val^{70} (γ-methyl protons) in the proximal Ub, and NOEs to amide groups of Ala^{352} and Asn^{353} (helix3 of UBA(2)) were assigned as originating from Ala^{46} (β-methyl protons) of the proximal Ub.

In a complementary set of similar experiments, Ub_2 perdeuterated on the proximal Ub was added to ^{15}N and ^{2}H labeled UBA(2) to detect NOEs originating

from the distal Ub. NOEs to the residues in helix 3 of UBA(2) (to amides of Asn^{349}, Ala^{351}, Ala^{352}, Asn^{353}) were observed, indicating direct interaction of helix 3 with the distal Ub.

The observation of NOEs thus provides evidence for the direct contacts of UBA(2) with Lys^{48}-linked Ub_2. It also confirms that the chemical shift perturbations observed in residues in helix 2 of UBA(2) are a result of direct interaction with the proximal Ub, and not an indirect effect of structural rearrangements in the UBA(2) core. The interaction of the proximal Ub with helix 2 of UBA(2) is very surprising since UBA binds monoUb via helices 1 and 3. The titration data suggest that the proximal Ub binds UBA tighter than the distal Ub, therefore, if binding to the proximal Ub occurred in the 'UBA(2)-monoUb' mode, helices 1 and 3 would be expected to interact with the proximal Ub. The results therefore suggest that UBA(2) binding to Lys^{48}-linked Ub_2 does not involve the simple recognition of the proximal Ub by UBA(2) in a 'monoUb-UBA(2)' mode. The UBA(2) domain binds the proximal Ub via a novel binding site formed by hydrophobic residues on helix 2 that are not involved in the UBA(2)-monoUb interaction (and residues Ala^{352} and Asn^{353} on helix 3 that also form contacts with the distal Ub). The residues on helix 3 and the C-terminus of UBA(2) contact the distal Ub, as in the monoUb-UBA(2) complex. The reason why UBA(2) binds the proximal Ub via helix 2 is not immediately clear, and could be a result of steric factors when UBA(2) first interacts with Val^{70} and its neighboring residues on the proximal Ub.

The results bring out the important difference between the mode of binding of UBA(2) to Lys^{63}-linked Ub_2 and Lys^{48}-linked Ub_2 chains. Binding to Lys^{63}-linked

Ub_2 occurs in a mode where each Ub unit binds one UBA(2) domain independently in a mode similar to the UBA-monoUb interaction. Because the only difference between Lys^{48}- and Lys^{63}-linked chains is in the relative positioning of the Ub units, this difference in the mode of interaction suggests that the conformation of Lys^{48}-linked Ub_2 might be important for their high affinity mode of binding to UBA(2). Although the isopeptide bond in Lys^{48}-linked Ub_2 is involved in the binding of UBA(2) to Lys^{48}-linked Ub_2, it does not appear to be the predominant site of interaction: UBA(2) binds the Leu^{8}-Ile^{44}-Val^{70} hydrophobic patch tighter (slow exchange) than it binds the isopeptide bond (fast exchange). Hence, direct recognition of the Gly^{76}-Lys^{48} linkage is unlikely to be the cause for higher affinity of UBA(2) to Lys^{48}-linked chains.

6.4.5 Docking the UBA-Ub_2 complex

In order to model the UBA(2)-Ub_2 complex using the titration data and the observed side chain-to-amide NOEs, the UBA(2) domain was docked on Ub_2 using HADDOCK [56]. The docking protocol uses the knowledge of interacting sites on the proteins identified by chemical shift perturbations, or mutational analyses, as restraints to drive the docking process that optimizes the geometric complementarities at the interface. The docking algorithm allows side chains of residues at the interacting sites to move to optimize interface packing. Energy minimization is achieved using refinement with water, and the resulting structures are ranked on the basis of intermolecular energy.

The docked model was calculated in two steps. In the first step, the UBA(2) was docked on monoUb, to model the tighter UBA(2)-proximal Ub interaction. Residues in the proximal Ub that were perturbed on addition of UBA(2), and residues

on helices 2 and 3 of UBA(2) that showed chemical shift perturbations on addition of Ub_2 in titrations, and have >50% of main chain solvent accessible were used to define ambiguous interaction restraints (AIRs). NOEs observed between amides of Leu^{336}, Ile^{338}, Asn^{339} of UBA(2) and the side chain of Val^{70} of the proximal Ub, and Ala^{352}, Asn^{353} of UBA(2) and Ala^{46} of the proximal Ub were defined as unambiguous distance restraints for the docking process. In the second step, the lowest energy structure from refinement of this UBA(2)-Ub complex (figure 6.13(a)) was used to dock the distal Ub to model the UBA(2)-Ub_2 interaction. Again, residues in the distal Ub that showed perturbations on addition of UBA(2) and residues of helix 3 of UBA(2) that showed chemical shift perturbations on titration with Ub_2, were used together with solvent accessibility criteria to define AIRs. The chemical bonds for the Gly^{76}-Lys^{48} isopeptide linkage in Ub_2 and the NOEs observed between Asn^{349}, Ala^{351} (UBA(2)) and Val^{70} (distal Ub), Leu^{350} (UBA(2)) and Leu^{73} (distal Ub), and Asp^{361}, Asp^{362}, Glu^{363} (UBA(2)) and Ala^{46} of the distal Ub were used to define unambiguous distance restraints for the docking procedure. In both steps of the docking routine, 2000 initial structures were generated, and the 200 lowest energy structures were then used for energy minimization with water. Figure 6.13(b) shows the docked model of the UBA(2)-Ub_2 complex.

(a)

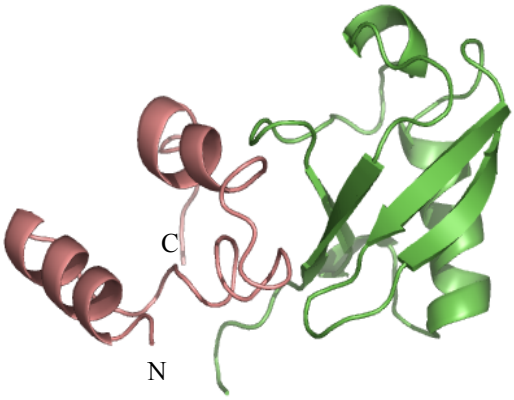

(b)

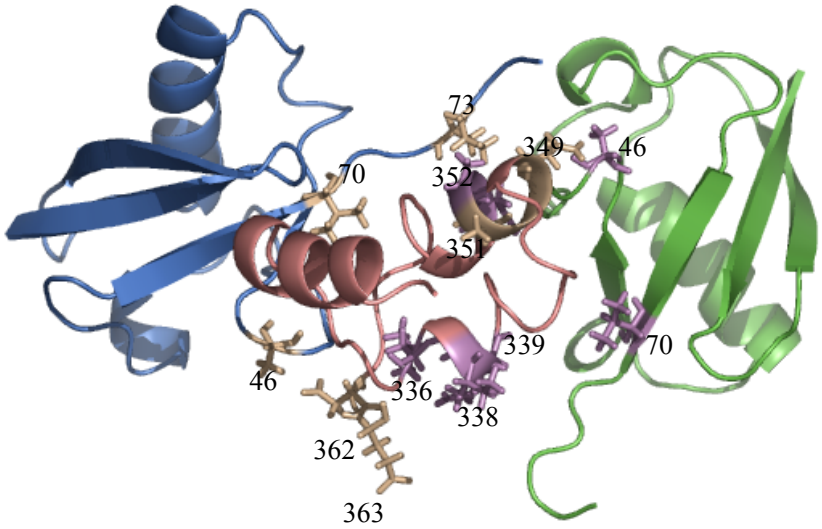

Figure 6.13 Docked model of the UBA-Ub$_2$ (Lys^{48}-linked) complex The UBA(2) domain was docked on the Lys48-linked Ub2 in two steps. In the first step, the higher affinity UBA-proximal Ub interaction was modeled (panel (a)). The distal Ub was docked on this complex to generate the 1:1 UBA-Ub2 complex. The lowest energy structure obtained from this process is shown in panel (b). The distal and proximal Ubs are colored in blue and green respectively, and the UBA(2) is shown in pink. Residues in UBA(2) showing intermolecular NOEs with the proximal and the distal Ub are represented as violet and wheat sticks respectively. Corresponding residues on Ub are shown in violet and wheat also.

Site-specific spin labeling experiments were used for validation of the docked model of the UBA-Ub2 complex. Experiments were performed with the paramagnetic spin label, methanethiosulfonate nitroxide (MTSL), covalently attached to the single

Cys residue (Cys^{344}) on UBA(2), and the effect of paramagnetic relaxation rate enahancement was measured on the proximal and distal Ubs in Ub_2 in 1:0.5 UBA:Ub_2-P or UBA:Ub_2-D samples. In a complementary experiment, the Cys^{48} on the distal Ub was modified with MTSL, and its effect was measured on UBA(2) in a 1:0.5 ^{15}N UBA:Ub_2 mixture. Attenuations in signal intensities observed in the HSQC spectra indicate residues in Ub_2 that are in close proximity to the Cys^{344}-MTSL on UBA(2), and residues in UBA(2) that are spatially close to the Cys^{48} of the distal Ub. Mapping the residues experiencing relaxation rate enhancement on the docked structure shows that the pattern of attenuation on UBA(2) is consistent with the position of the SL on the distal Ub (figure 6.14a). Spin-labeling of the UBA(2) molecule gives rise to attenuations in both the distal and the proximal Ub domains. Although the pattern of residues experiencing signal attenuation on the proximal Ub is consistent with the position of the spin-label (figure 6.14b), attenuations are also observed in residues 46-48 of the distal Ub that appear to be farther away from Cys^{344} on UBA(2) in the docked structure. It is possible that the UBA(2) might actually bind Ub_2 with a slightly different orientation than that shown in figure 6.14(b), while still maintaining direct contacts observed as NOEs. Therefore, although the docked structure does not represent an exact structure, it provides a reasonable working model of the UBA(2)-Ub_2 complex. More extensive experiments to determine side-chain contacts between UBA(2) and Lys^{48}-linked Ub_2 using ^{13}C and ^{15}N labeled proteins will be required in order to determine a more accurate structure of the complex.

(a)

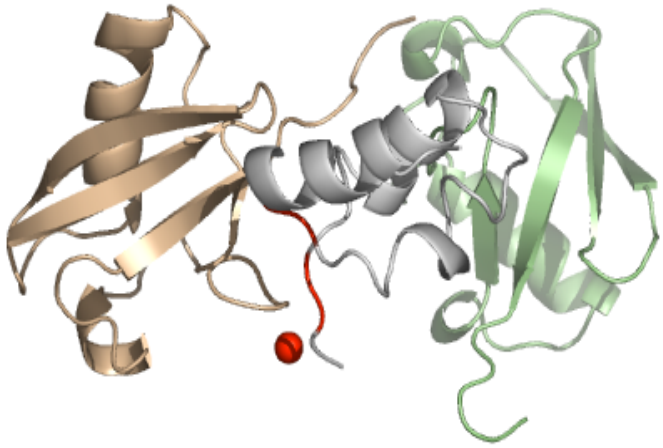

(b)

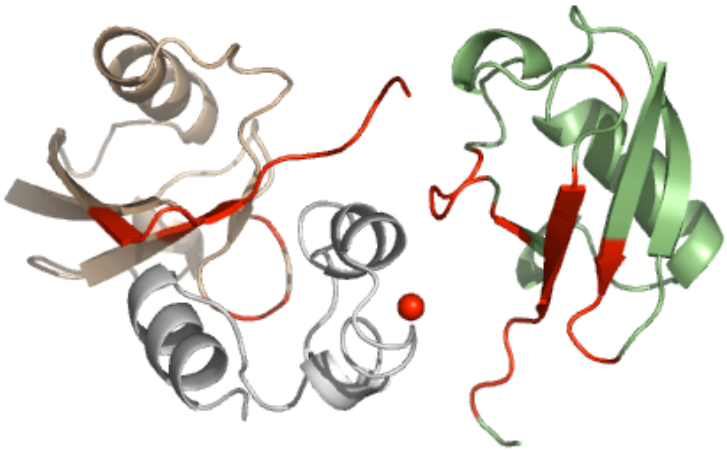

Figure 6.14 Spin labels to test the docked structure of the complex Pattern of signal attenuation observed in spin-labeling experiments mapped onto the structure of the UBA-Ub_2 complex modeled using HADDOCK. The distal and proximal Ubs are in wheat and green respectively. UBA(2) is shown in grey. Panel (a) shows the position of the spin-label attached to Cys^{48} on the distal Ub as a red sphere. The residues 329, 330, 360, 361 on UBA(2) that experience signal attenuation are colored red. The complex is rotated compared to the position shown in figure 6.13(b), for better visualization of the spin label and the affected residues. Panel (b) shows the pattern of signal attenuation observed in the two Ub domains when Cys^{348} on UBA(2). The position of the spin-label is marked by a red sphere, and the attenuated residues on Ub are colored in red. Residues attenuated in Ub_2 include 8-11, 46-49 and 68-76 in the distal Ub, and 6-9, 43-50, 63, 66-74 on the proximal Ub.

6.5 Probing the role of Ub_2 conformation with Leu8Ala, Ile44Ala Ub mutants

6.5.1 Binding of UBA(2) to Ub Leu8Ala, Ile44Ala double mutants

In the same study that showed that Lys^{48}-linked polyUb chains bind a single UBA domain, Raasi et al [27] also probed the effect of Leu8Ala mutations in Ub on polyUb-UBA interactions. The study used SPR to show that Ub_4 chains, with mutant Ub units at any two positions in the chain, bound the UBA(1) domain weaker than wild-type Ub_4. The positioning of the mutant Ub at different positions in the chain was shown to decrease the binding affinity to different extents. The authors suggested that this positional inequivalence of the mutations to UBA(1) binding implied that all Ubs in the Ub_4 did not make identical interactions with the UBA, as would be predicted if one UBA bound each Ub domain.

In order to probe the effect of similar mutations on binding of UBA(2) to Lys^{48}-linked Ub_2, Ub_2 molecules carrying Leu8Ala and Ile44Ala double mutations in the proximal (mutP) Ub were synthesized. In a control experiment, the UBA(2) domain was titrated with monoUb(Leu8Ala, Ile44Ala). The magnitude of chemical shift perturbations observed in the UBA(2) domain was smaller than in titrations with wild-type monoUb, suggesting that the mutations weakened the UBA-Ub interaction. The effect of the mutations in the proximal Ub in Ub_2 on the interaction with UBA(2) domains was studied by titrating UBA(2) into Ub_2 (proximal Ub mutated and ^{15}N labeled, henceforth referred to as Ub_2-mutP) and Ub_2 (proximal Ub mutated, distal Ub ^{15}N labeled, henceforth referred to as Ub_2-DmutP). Addition of UBA(2) to Ub_2-Pmut resulted in chemical shift changes in the amide resonances in the HSQC spectra. The same residues as those involved in the Ub_2-UBA(2) interaction showed

perturbations, suggesting that the same surface of Ub was still involved (figure 6.15). However, these residues experienced signal attenuation indicating that the binding event occurred in the intermediate exchange regime (in contrast to a slow exchange regime in 'wild-type' Ub_2-P). The shift in the time scale of the binding event, from slow to intermediate, suggested a weakening of the interaction of UBA(2) with the proximal Ub. The effect of mutating the proximal Ub on the binding of UBA(2) to the distal Ub was probed in experiments with Ub_2-DmutP construct. Upon titration of UBA(2), all residues on the distal ubiquitin that involved in the 'wild-type' Ub_2-D:UBA(2) interaction in were perturbed and displayed fast exchange behavior. In contrast to the Ub_2-D:UBA titrations, these residues did not display the initial 'plateau' phase in binding (figure 6.16), suggesting that unlike in the case of the 'wild-type' Ub_2, binding of the distal Ub to UBA(2) does not require the proximal Ub to be bound to UBA(2).

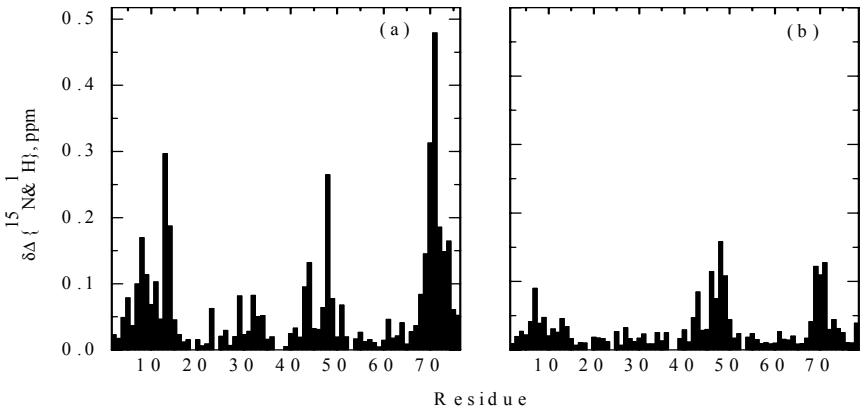

Figure 6.15 Chemical shift perturbations in Ub_2-proximal mutants Backbone amide chemical shift perturbations observed in the Ub_2-proximal mutated constructs in (a) the distal Ub and (b) the proximal Ub on addition of UBA(2). Although the magnitude of chemical shift perturbations appears larger in the distal Ub than in the proximal Ub domain, it should be noted that residues in the latter were in the intermediate exchange regime, compared to fast exchange observed in the distal domain.

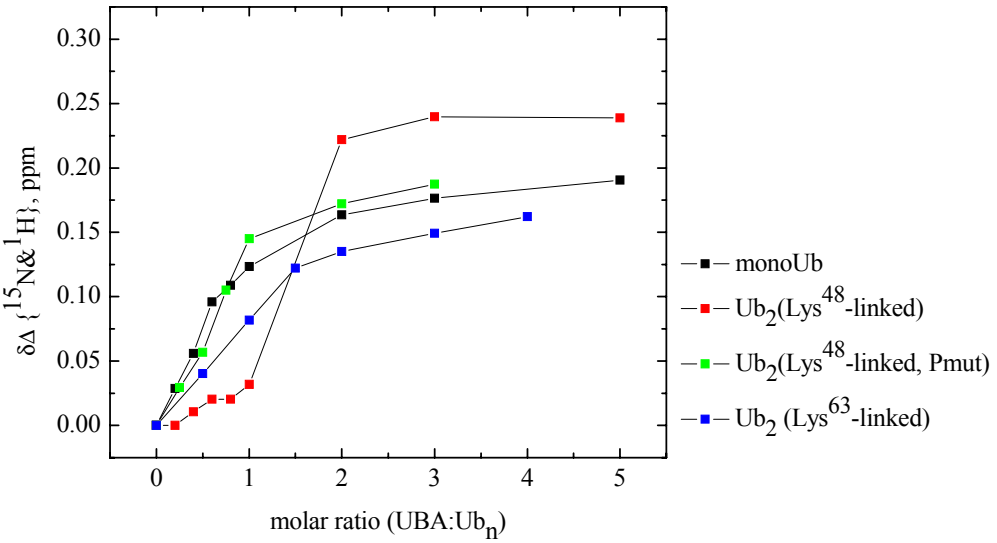

Figure 6.16 Comparison of titration curves in distal Ub Overlay of combined amide chemical shift perturbations observed in residue 13 in monoUb, Lys^{63}-linked Ub_2, Lys^{48}-linked Ub_2, and Lys^{48}-linked Ub_2 (proximal mutant) plotted as a function of increasing UBA(2) concentrations during the titrations. The data plotted in red represents shifts in residue 13 in the 'wild-type' Lys^{48}-linked Ub_2: as is apparent from the curve, only minor changes are observed in the distal Ub, up to [UBA]/[Ub_2] ratios of 1:1. The behavior of the same residue approaches that in the monoUb (black) in the Ub_2-proximal mutant construct (green).

It should be noted that in spite of mutations in the hydrophobic residues Leu^8 and Ile^{44}, the proximal Ub in the Ub_2-proximal mutants still binds UBA(2) tighter than the distal Ub. Thus, consistent with the observations with 'wild-type' Ub_2, the proximal Ub appears to be the primary site of UBA(2)-Ub_2 interaction. It is possible that weakening the proximal Ub-UBA(2) interaction might require a mutation at Val^{70} that appears to form the main interacting pocket (along with Leu^{69}, Leu^{71} and Leu^{73}) on the proximal Ub.

6.5.2 Effect of mutations on the Ub_2 interface

The destabilizing effect of the mutations on the UBA(2)-Ub_2 interactions could potentially arise from either a change in the conformation of Ub_2 (change in the

interface between the two Ub units in Ub_2) that presents a unique conformational determinant for UBA(2) recognition and/or a direct weakening of the UBA(2)-Ub interaction due to the double mutations. The control experiments with mutant monoUb show weaker binding to UBA(2) compared to wild-type monoUb. However, the effect of the mutations in the proximal Ub on the formation of the Ub_2 interface was also investigated. The chemical shift mapping data (figure 6.17) revealed only minor perturbations in the proximal and distal Ub in the proximal mutant Ub_2 constructs, except at the sites of the Gly^{76}-Lys^{48} isopeptide linkage. Therefore, the Leu8Ala and Ile44Ala mutations in the proximal Ub appear to destabilize the hydrophobic interface in Ub_2, shifting the conformational equilibrium towards 'open' states. The absence of the 'plateau' phase in the titration curves observed for Ub_2D-Pmut suggests that the destabilization of the 'closed' conformation allows the distal Ub to bind UBA(2) independent of the proximal Ub. The results therefore suggest that the 'closed' Ub_2 conformation is important for the tight binding to UBA(2) domains.

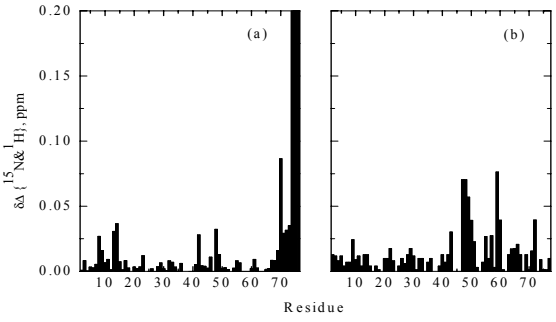

Figure 6.17 Chemical shift mapping of interface in Ub_2-proximal mutants Combined amide chemical shifts observed in the distal (a) and proximal (b) Ub domains in the Ub_2-proximal mutant construct in comparison with monoUbs (K48C Ub and (L8A,I44A,D77) Ub respectively).

6.6 Discussion

The experiments discussed in this chapter were aimed at elucidating the mode of interaction of Lys^{63}- and Lys^{48}-linked Ub_2 chains with UBA(2) in order to understand the structural basis of linkage-specific recognition of polyUb chains. The interaction of UBA(2) with monoUb and Ub_2 is mediated by the Leu^{8}-Ile^{44}-Val^{70} hydrophobic patch on the surface of Ub. In Lys^{48}-linked Ub_2, the same hydrophobic patch on Ub is involved in both the formation of the Ub_2 interface and interaction with UBA(2); therefore, the UBA(2) has to compete with the Ub-Ub interaction for binding Ub_2. Because the two hydrophobic surfaces are readily exposed in the Lys^{63}-linked Ub_2, one might expect that UBA(2) will bind these chains with higher affinity than Lys^{48}-linked Ub_2. However, biochemical studies have shown that this is not the case, and UBA(2) domains preferentially associate with Lys^{48}-linked chains [27, 54]. It has been speculated that in binding Lys^{48}-linked Ub_2 chains, UBA(2) domains either recognize conformational determinants unique to these chains, or the Gly^{76}-Lys^{48} linkage itself. It has also been suggested that binding to longer chains, that potentially present multiple binding sites, could invoke cooperative mechanisms that could give rise to higher affinity interactions.

A recent surface plasmon resonance (SPR) study showed that Lys^{48}-linked polyUb chains up to Ub_6 bind a single UBA(2) domain, thereby suggesting that a simplistic 'one-UBA-per-Ub' model might not apply to Lys^{48}-linked chains[27]. Consistent with the SPR data, the results presented here show that UBA(2) binds Lys^{48}-linked Ub2 in a 1:1 stoichiometry. Also consistent with such a mode of binding are chemical shift perturbations observed in both the 2^{nd} and 3^{rd} helices of UBA(2). In

addition, the NOE data indicate direct interactions between helix 2 of UBA(2) and the proximal Ub, and helix 3 and the distal Ub. The results presented here suggest that UBA-Ub_2(Lys^{48}-linked) interaction involves the association of one UBA(2) molecule primarily with the proximal Ub. The binding at the proximal site also allows for the simultaneous association of the distal domain with the UBA(2) in a 1:1 UBA:Ub_2 complex.

The striking decrease in the cooperative nature of UBA(2) binding of the distal Ub in Ub_2-proximal mutants suggests that the Ub_2 'closed' conformation is critical for the cooperative effect. Destabilization of the 'closed' Ub_2 conformation causes the two Ub domains to move farther apart, thus decreasing the ability of the distal Ub to cooperatively bind UBA(2) bound to the proximal Ub. At the limit of the open conformation are the Lys^{63}-linked Ub_2 chains that adopt an extended conformation with no contact between the two Ub domains. The positioning of Lys^{63} on the Ub surface precludes the formation of the hydrophobic interface between the two Ub domains as seen in the Lys^{48}-linked Ub_2. Hence, both Ub domains in Lys^{63}-linked Ub_2 can independently bind UBA(2) domains via their hydrophobic surfaces without a cooperative effect. The higher affinity of UBA(2) domains for Lys^{48}-linked Ub_2 chains is therefore a result of both Ub domains cooperatively binding one UBA(2) molecule, and decreased entropic costs associated with the independent binding of both Ub domains to a UBA(2) molecule each. The results also imply that the conformation of Lys^{48}-linked Ub_2 is important not for the recognition of a quaternary conformational determinant *per se;* it is the proper positioning (spatial and orientational) of the distal Ub conferred by the linkage that allows for co-operativity

in binding UBA(2) which renders the conformation critical to binding UBA(2) with high affinity.

6.7 Unresolved issues

The results presented in this chapter provide valuable insights into the structural basis of specific recognition of Lys^{48}-linked Ub_2 over Lys^{63}-linked Ub_2 and monoUb by UBA(2) domains. However, certain observations in the binding studies of UBA(2) to Lys^{48}-linked Ub_2 still remain unexplained. For instance, the binding of the UBA(2) domain to the Lys^{48}-linked Ub_2 requires an opening of the Ub_2 interface, but only very small chemical shift perturbations are observed in the distal Ub until the proximal Ub shows saturation in binding. It is somewhat surprising that changes at the Ub_2 interface (opening of interface and binding of UBA(2) to the proximal Ub) do not appear to cause significant chemical shift perturbations in the distal Ub. It is also not entirely clear why the UBA(2) binds the proximal Ub via helix 2, and not via helices 1 and 3 as in the case of monoUb. It is possible that this is a result of steric factors associated with binding the hydrophobic surface on the proximal Ub in the context of the Lys^{48}-linked Ub_2. In addition, the mode of UBA(2)-Ub_2 (Lys^{48}-linked) association modeled in section 6.4.5 represents the 1:1 UBA:Ub_2 interaction. However, ^{15}N T_1 measurements on Ub_2 samples saturated with UBA(2) suggests the formation of a 2:1 (UBA:Ub_2) complex. It therefore appears that saturating amounts of UBA(2) force the formation of 2:1 UBA:Ub_2 complexes. Surface plasmon resonance (SPR) data and cross-linking experiments [27] have suggested that polyUb chains up to Ub_6 bind only one UBA(2) molecule. Therefore, it is unclear if the 2:1 UBA:Ub_2 interaction observed here is physiologically relevant, or if it is an artifact of

saturating amounts of UBA(2) in solution. Alternatively, as pointed out in section 6.4.3, it is also possible that the steric factors associated with protein immobilization and the lower protein concentrations used in the SPR and cross-linking experiments do not allow formation of larger complexes. Finally, it also remains to be seen how the mode of UBA-Ub_2 interaction described here will propagate to longer Lys^{48}-linked chains. UBA(2) binding to longer Lys^{48}-linked chains will most likely involve binding by multiple Ub domains; however, whether such interactions will involve multiple UBA(2) domains and how these interactions involve co-operative mechanisms will need further investigation.

Chapter 7: Summary and Concluding Remarks

7.1 Summary of results

Using a combination of several NMR methods, the conformations adopted by Lys^{48}- and Lys^{63}-linked Ub_2 chains were characterized in this study. Lys^{48}-linked Ub_2 molecules were shown to exist in equilibrium between 'open' and 'closed' conformations, with the 'closed' state becoming increasingly populated with higher pH conditions. The 'closed' conformation of the Lys^{48}-linked Ub_2 is characterized by the formation of an Ub-Ub interface that involves the Leu^{8}-Ile^{44}-Val^{70} hydrophobic patch on the surface of both Ub domains. The interface was observed to be dynamic in solution, such that functionally important residues sequestered at the interface may be accessible for interaction with polyUb recognition factors. It was also shown that in spite of significant flexibility inherent in polyUb chains, Lys^{48}-linked Ub_4 chains are structured in solution. Preliminary data suggest the distal two Ub units in Ub_4 might adopt an Ub2-like 'closed' conformation. Further studies will be required to determine the average conformation of Ub_4 chains in solution.

In contrast, Lys^{63}-linked Ub_2 chains are characterized by an extended conformation, with no definitive interface between the two Ub domains. This is the first experimental evidence that alternatively linked Ub chains adopt distinct conformations in solution. The extended conformation is most likely a steric effect associated with the location of Lys^{63} on the surface of Ub, such that formation of the Gly^{76}-Lys^{63} isopeptide bond occludes direct contact between the hydrophobic surfaces of the Ub domains. It is possible that the hydrophobic interfaces involving

remote Ub units might be formed in longer Lys^{63}-linked chains, however, resulting in a pattern of Ub-Ub interactions that will be distinct from that in Lys^{48}-linked chains.

In order to understand how polyUb chain conformation modulates their interaction with different polyUb-recognizing proteins, the interaction of monoUb, Lys^{48}- and Lys^{63}-linked chains with the UBA(2) domain from hHR23a was investigated. hHR23A functions in proteasome-mediated proteolysis of substrates, by possibly delivering polyubiquitinated (Lys^{48}-linked) substrates to the proteasome, and, in some cases, by inhibiting proteasomal degradation. The UBA(2) domain of hHR23A has been shown to preferentially associate with Lys^{48}-linked polyUb chains in pull-down assays and surface plasmon resonance experiments. Previous structural investigation of the monoUb-UBA(2) complexes has shown that UBA(2) binds the hydrophobic surface on monoUb, in an orientation that allows helices 1 and 3 of UBA(2) to contact Ub. The results presented in this study show that the extended conformation of the Lys^{63}-linked Ub_2 allows both Ub domains to independently bind one UBA(2) domain each, and in a mode similar to the monoUb-UBA(2) interaction. Binding to the Lys^{48}-linked Ub_2, however, appears to involve the association of the UBA(2) domain primarily with the proximal Ub. Somewhat surprisingly, however, this interaction with the proximal involves a different epitope (formed by helices 2 and 3) on the UBA(2) surface. In addition, due to the positioning of the distal Ub conferred by the Gly^{76}-Lys^{48} linkage, the distal Ub is also able to associate with the same UBA(2) domain (at helix 3) in a 'sandwich'-like complex. Destabilization of the Ub_2 interface by Leu8Ala, Ile44Ala double mutations reduces this 'co-operative' effect, suggesting that the conformation of Lys^{48}-linked Ub_2 is critical to the high

affinity binding of these chains to UBA(2) domains. In addition, the results suggest that the preferential association of UBA(2) domains to Lys^{48}- over Lys^{63}-linked Ub_2 chains is not due to the direct recognition of the isopeptide linkage, or the recognition of conformational determinant unique to these chains. It is the unique relative positioning of the two Ub domains conferred by the Gly^{76}-Lys^{48} linkage, that allows both the Ub domains to bind and more effectively sequester the same UBA(2) molecule.

Thus, the results provide experimental evidence in support of the model that specificity in polyUb-mediated signaling depends on specific conformations adopted by differently linked Ub chains.

7.2 Scope for future studies

Signaling by (poly)ubiquitination represents an elegant cellular mechanism in which substrate modification by the different polymers of the same protein (ubiquitin) can result in diverse outcomes. The standing question in the field of ubiquitin-mediated signaling is how polyUb chains achieve specificity in signaling. The results presented here support the idea that differently linked polyUb chains represent structurally distinct signals to Ub-binding proteins that are involved in the various signaling events. Lys^{48}- and Lys^{63}-linked Ub_2 chains were shown to adopt distinct conformations in solution. Studies of interactions of UBA(2) domains with these chains suggest that the tighter binding to Lys^{48}-linked Ub_2 arises from the formation of a Ub-UBA-Ub 'sandwich'-like complex, that is formed because the specific conformation of the Lys^{48}-linked Ub_2 allows both Ub domains to bind the same UBA(2) molecule. It is likely that linkages in polyUb via other Lys residues will also

result in different relative positioning of the Ub domains that will result in preferential association of these chains with certain Ub-binding proteins over others. Structural studies on alternatively linked polyUb chains will be needed to verify this experimentally. In addition, an increasing number of Ub-binding domains that are specific towards different polyUb chain linkages are being discovered, for example, zinc finger motifs have been shown to prefer Lys^{63}-linked chains over Lys^{48}-linked chains [57]. Study of the interactions of polyUb chains with such Ub-binding motifs will provide valuable insights into how chain structure modulates their specific recognition.

References

1. Hershko, A. and A. Ciechanover, The ubiquitin system. *Annu Rev Biochem*, 1998. **67**: p. 425-480.
2. Pickart, C.M., Ubiquitin enters the new millennium. *Mol Cell*, 2001. **8**(3): p. 499-504.
3. Pickart, C.M., Mechanisms underlying ubiquitination. *Annu Rev Biochem*, 2001. **70**: p. 503-33.
4. Pickart, C.M., Back to the future with ubiquitin. *Cell,* 2004. **116**(2): p. 181-90.
5. Pickart, C.M. and R.E. Cohen, Proteasomes and their kin: proteases in the machine age. *Nat Rev Mol Cell Biol*, 2004. **5**(3): p. 177-87.
6. van Nocker, S., et al., The multiubiquitin-chain-binding protein Mcb1 is a component of the 26S proteasome in Saccharomyces cerevisiae and plays a nonessential, substrate-specific role in protein turnover. *Mol Cell Biol*, 1996. **16**(11): p. 6020-8.
7. Schauber, C., et al., Rad23 links DNA repair to the ubiquitin/proteasome pathway. *Nature*, 1998. **391**(6668): p. 715-8.
8. Chen, L., et al., Ubiquitin-associated (UBA) domains in Rad23 bind ubiquitin and promote inhibition of multi-ubiquitin chain assembly. *EMBO Rep*, 2001. **2**(10): p. 933-8.
9. Bloom, J. and M. Pagano, To be or not to be ubiquitinated? *Cell Cycle*, 2004. **3**(2): p. 138-40.
10. McCracken, A.A. and J.L. Brodsky, Evolving questions and paradigm shifts in endoplasmic-reticulum-associated degradation (ERAD). *Bioessays*, 2003. **25**(9): p. 868-77.
11. Muratani, M. and W.P. Tansey, How the ubiquitin-proteasome system controls transcription. *Nat Rev Mol Cell Biol*, 2003. **4**(3): p. 192-201.
12. Aguilar, R.C. and B. Wendland, Ubiquitin: not just for proteasomes anymore. *Curr Opin Cell Biol*, 2003. **15**(2): p. 184-90.
13. Osley, M.A., H2B ubiquitylation: the end is in sight. *Biochim Biophys Acta*, 2004. **1677**(1-3): p. 74-8.
14. Matunis, M.J., On the road to repair: PCNA encounters SUMO and ubiquitin modifications. *Mol Cell*, 2002. **10**(3): p. 441-2.
15. Nishikawa, H., et al., Mass spectrometric and mutational analyses reveal Lys-6-linked polyubiquitin chains catalyzed by BRCA1-BARD1 ubiquitin ligase. *J Biol Chem*, 2004. **279**(6): p. 3916-24.
16. Hicke, L. and R. Dunn, Regulation of membrane protein transport by ubiquitin and ubiquitin-binding proteins. *Annu Rev Cell Dev Biol*, 2003. **19**: p. 141-72.
17. Hartmann-Petersen, R., et al., UBA domain containing proteins in fission yeast. *Int J Biochem Cell Biol*, 2003. **35**(5): p. 629-36.
18. Bertolaet, B.L., et al., UBA domains of DNA damage-inducible proteins interact with ubiquitin. *Nat Struct Biol*, 2001. **8**(5): p. 417-22.
19. Mueller, T.D. and J. Feigon, Solution structures of UBA domains reveal a conserved hydrophobic surface for protein-protein interactions. *J Mol Biol*, 2002. **319**(5): p. 1243-55.

20. Mueller, T.D., M. Kamionka, and J. Feigon, Specificity of the interaction between ubiquitin-associated domains and ubiquitin. *J Biol Chem*, 2004. **279**(12): p. 11926-36.
21. Mueller, T.D. and J. Feigon, Structural determinants for the binding of ubiquitin-like domains to the proteasome. *Embo J*, 2003. **22**(18): p. 4634-45.
22. Buchberger, A., From UBA to UBX: new words in the ubiquitin vocabulary. *Trends Cell Biol*, 2002. **12**(5): p. 216-21.
23. Swanson, K.A., et al., Solution structure of Vps27 UIM-ubiquitin complex important for endosomal sorting and receptor downregulation. *Embo J*, 2003. **22**(18): p. 4597-606.
24. Schnell, J.D. and L. Hicke, Non-traditional functions of ubiquitin and ubiquitin-binding proteins. *J Biol Chem*, 2003. **278**(38): p. 35857-60.
25. Prag, G., et al., Mechanism of ubiquitin recognition by the CUE domain of Vps9p. *Cell*, 2003. **113**(5): p. 609-20.
26. Kang, R.S., et al., Solution structure of a CUE-ubiquitin complex reveals a conserved mode of ubiquitin binding. *Cell*, 2003. **113**(5): p. 621-30.
27. Raasi, S., et al., Binding of polyubiquitin chains to ubiquitin-associated (UBA) domains of HHR23A. *J Mol Biol*, 2004. **341**(5): p. 1367-79.
28. Sloper-Mould, K.E., et al., Distinct functional surface regions on ubiquitin. *J Biol Chem*, 2001. **276**(32): p. 30483-9.
29. Cook, W.J., et al., Structure of a diubiquitin conjugate and a model for interaction with ubiquitin conjugating enzyme (E2). *J.Biol.Chem.*, 1992. **267**: p. 16467-71.
30. Lam, Y.A., et al., Specificity of the ubiquitin isopeptidase in the PA700 regulatory complex of 26 S proteasomes. *J.Biol.Chem*., 1997. **272**: p. 28438-46.
31. Cook, W.J., et al., Structure of tetraubiquitin shows how multiubiquitin chains can be formed. *J.Mol.Biol.*, 1994. **236**: p. 601-609.
32. Phillips, C.L., et al., Structure of a new crystal form of tetraubiquitin. *Acta Cryst D*, 2000. **57**: p. 341-4.
33. Walters, K.J., et al., Structural studies of the interaction between ubiquitin family proteins and proteasome subunit S5a. *Biochemistry*, 2002. **41**(6): p. 1767-77.
34. Walters, K.J., et al., DNA-repair protein hHR23a alters its protein structure upon binding proteasomal subunit S5a. *Proc Natl Acad Sci U S A*, 2003. **100**(22): p. 12694-9.
35. Wang, Q., et al., Ubiquitin Recognition by the DNA Repair Protein hHR23a. *Biochemistry*, 2003. **42**(46): p. 13529-35.
36. Raasi, S. and C.M. Pickart, Rad23 ubiquitin-associated domains (UBA) inhibit 26 S proteasome-catalyzed proteolysis by sequestering lysine 48-linked polyubiquitin chains. *J Biol Chem*, 2003. **278**(11): p. 8951-9.
37. Ryu, K.S., et al., Binding surface mapping of intra and inter domain interactions among hHR23B, ubiquitin and poly ubiquitin binding site 2 of S5a. *J Biol Chem*, 2003. **278**(38): p. 36621-7.
38. Piotrowski, J., et al., Inhibition of the 26S proteasome by polyubiquitin chains synthesized to have defined lengths. *J.Biol.Chem*., 1997. **272**: p. 23712-21.

39. Fushman, D., R. Xu, and D. Cowburn, Direct determination of changes of interdomain orientation on ligation: use of the orientational dependence of ^{15}N NMR relaxation in Abl SH(32). *Biochemistry*, 1999. **38**: p. 10225-30.
40. Tjandra, N. and A. Bax, Direct Measurement of Distances and Angles in Biomolecules by NMR in a Dilute Liquid Crystalline Medium. *Science*, 1997. **278**(5340): p. 1111-4.
41. Tolman, J.R., et al., Nuclear magnetic dipole interactions in field-oriented proteins: information for structure determination in solution. *Proc Natl Acad Sci U S A*, 1995. **92**(20): p. 9279-83.
42. Ruckert, M. and G. Otting, Alignment of biological macromoleculse in novel nonionic liquid crystalline media for NMR experiments. *J. Amer. Chem. Soc.*, 2000. **122**: p. 7793-7797.
43. Ottiger, M., F. Delaglio, and A. Bax, Measurement of J and dipolar couplings from simplified two-dimensional NMR spectra. *J Magn Reson*, 1998. **131**(2): p. 373-8.
44. Garrett, D.S., et al., A common sense approach to peak picking in two-, three- and four-dimensional spectra using automatic computer analysis of contour diagrams. *J Magn Reson*, 1991. **95**: p. 214-220.
45. Walker, O., R. Varadan, and D. Fushman, Efficient and accurate determination of the overall rotational diffusion tensor of a molecule from 15N relaxation data using computer program ROTDIF. *J. Magn. Reson.*, 2004. **168**: p. 336-345.
46. Ghose, R., D. Fushman, and D. Cowburn, Determination of the Rotational Diffusion Tensor of Macromolecules in Solution from NMR Relaxation Data with a Combination of Exact and Approximate Methods - Application to the Determination of Interdomain Orientation in Multidomain Proteins. *J.Magn.Reson.*, 2001. **149**: p. 214-217.
47. Woessner, D., Nuclear spin relaxaion in ellipsoids undergoing rotational brownian motion. *J.Chem.Phys*, 1962. **37**: p. 647-654.
48. Akerud, T., et al., Intramolecular dynamics of low molecular weight protein tyrosine phosphatase in monomer-dimer equilibrium studied by NMR: a model for changes in dynamics upon target binding. *J Mol Biol*, 2002. **322**(1): p. 137-52.
49. Fushman, D., S. Cahill, and D. Cowburn, The main chain dynamics of the dynamin pleckstrin homology (PH) domain in solution: Analysis of ^{15}N relaxation with monomer/dimer equilibration. *J. Mol. Biol.*, 1997. **266**: p. 173-194.
50. Fushman, D., N. Tjandra, and D. Cowburn, An approach to direct determination of protein dynamics from 15N NMR relaxation at multiple fields, independent of variable 15N chemical shift anisotropy and chemical exchange contributions. *J. Am. Chem. Soc.*, 1999. **121**: p. 8577-8582.
51. Kosen, P.A., Spin labeling of proteins. *Methods Enzymol*, 1989. **177**: p. 86-121.
52. Jain, N.U., et al., Distance mapping of protein-binding sites using spin-labeled oligosaccharide ligands. *Protein Sci*, 2001. **10**(11): p. 2393-400.
53. Pickart, C.M., Ubiquitin in chains. *TIBS*, 2000. **11**: p. 544-48.

54. Varadan, R., et al., Solution conformation of Lys63-linked di-ubiqutin chain provides clues to functional diversity of polyubiquitin signaling. *J Biol Chem*, 2004. **279**: p. 7055-7063.
55. Mueller, T.D., M. Kamionka, and J. Feigon, Specificity of the interaction between UBA domains and ubiquitin. *J Biol Chem*, 2004.
56. Dominguez, C., R. Boelens, and A.M. Bonvin, HADDOCK: a protein-protein docking approach based on biochemical or biophysical information. *J Am Chem Soc*, 2003. **125**(7): p. 1731-7.
57. Kanayama, A., et al., TAB2 and TAB3 Activate the NF-kappaB Pathway through Binding to Polyubiquitin Chains. *Mol Cell*, 2004. **15**(4): p. 535-48.